

Assessing Late Quaternary Activity along the Ute Pass Fault, El Paso County, Colorado Front Range

Program Element II: Evaluate Urban Hazard and Risk.

Final Technical Report

Contract G20AP00030
National Earthquake Hazards Reduction Program
U.S. Geological Survey

Principal Investigators:

Matthew Morgan
Colorado Geological Survey
Colorado School of Mines
1500 Illinois Street
Golden, CO 80401-1887
E-Mail: mmorgan@mines.edu
Phone:(303)384-2647

Co-PI:

James P. McCalpin
GEO-HAZ Consulting, Inc.
P.O. Box 837, 600 E. Galena Ave.
Crestone, CO 81131
E-Mail: mccalpin@geohaz.com
Phone:(719)588-4279

29-SEPT-2021

This report was prepared under contract to the U.S. Geological Survey and has not been reviewed for conformity with USGS editorial standards and stratigraphic nomenclature. Opinions and conclusions expressed herein do not necessarily represent those of the USGS. Any use of trade names is for descriptive purposes only and does not imply endorsement by the USGS.

TABLE OF CONTENTS

	Page
1. ABSTRACT	5
2. INTRODUCTION	6
2.1 Significance and Scope of Study	6
2.2 Seismotectonic Setting	8
2.3 Previous Work on Neogene Movement of the UPF	8
3. METHODS	9
3.1 Mapping	9
3.2 Geophysics.....	9
3.3 Geochronology	9
4. SPLAY FAULT SITE	10
4.1 Structural Setting.....	12
4.2 Surface Geology.....	14
4.2.1 The “Tilted Block of Alluvium”	14
4.2.2 Verdos Pediment Failed as a Lateral Spread, North End of Splay Fault	17
4.3 Possible Fault Geometries Below the Splay Scarp	18
4.4 Seismic Survey Line	19
4.4.1 Goals of the Seismic Survey	21
4.4.2 Results of the Seismic Survey.....	21
4.5 Reconciling Geophysical Interpretation with Surface Geology	25
5. FRENCH CREEK LANDSLIDE SITE	26
5.1 Structural Setting.....	26
5.2 Surface Geology.....	27
5.3 Seismic Survey Lines	29
5.3.1 Refraction Lines	29
5.3.1.1 Line V (Refraction Calibration Line)	29
5.3.1.2 Line A	31
5.3.2 Reflection Lines	32
5.3.2.1 Line A	34
5.3.2.2 Line B	35
5.3.2.3 Line C.....	36
5.4 Reconciling Geophysical Interpretation with Surface Geology	38
6. CONCLUSIONS	41
7. ACKNOWLEDGMENTS.....	42
8. REFERENCES	42
9. APPENDICES	45

List of Figures	Page
Fig. 1. Location map of the UPF (purple lines) and its three sections as defined by Harza Engineering Company (1985).....	6
Fig. 2. Peak ground acceleration predicted for an M7.0 scenario earthquake on the Ute Pass fault.....	7
Fig. 3. Clip from Scott and Wobus’ 1973 1:62,500 geologic map of the Colorado Springs 15’ quadrangle	10
Fig. 4. Clip from Rowley et al. 1:24,000 geologic map of the Colorado Springs 7.5’ quad	11
Fig. 5. Topographic profile along the splay fault, as it crosses two deep gullies	12
Fig. 6. Oblique Google Earth view of the splay fault (yellow), looking NE	12
Fig. 7. 10 m DEM of the southern end of the UPFZ (red lines).....	13

Fig. 8. Part of the geologic map of the Cheyenne Mountain 7.5' quadrangle (Rowley et al., 2002) around the NE-trending splay fault (at center)	14
Fig. 9a. Lidar DEM of the central Splay fault (red line), the wider scarp (pink polygons), and the location of the roadcut exposing "tilted alluvium."	15
Fig. 9b. Telephoto view of the roadcut cited by Kirkham and Rogers (1981), taken from 150 m south of the cut.....	16
Fig. 9c. Lidar oblique view to the SW of the northern end of the splay fault	17
Fig. 9d. Cartoon of a lateral spread, from Highland and Bobrowsky, 2018.....	18
Fig. 10a. Lidar DEM of the Splay Fault area	20
Fig. 10b. Close-up of fault (red) and associated SE-facing scarp crossing the central pediment remnant	20
Fig. 11. Refraction modeling for Line SP1.....	21
Fig. 12. Refraction modeling for Line SP2.....	22
Fig. 13. Refraction modeling Line SP1	23
Fig. 14. Refraction modeling for Line SP2.....	23
Fig. 15. Line SL: 15 m COG with forward shots	24
Fig. 16. Line SL: 15 m COG with forward shots on non-static-corrected, raw data	24
Fig. 17. Oblique lidar view to the NW up Fountain Creek, showing part of the Central section of the UPF, with the French Creek landslide (QIs) at upper center.....	26
Fig. 18. Streams (green) crossing the UPF between the French Creek landslide ("Old Slide") and the Town of Manitou Springs (lower right).	27
Fig. 19. Oblique lidar view to the NW up Fountain Creek, from just north of Manitou Springs	28
Fig. 20a. Oblique lidar DEM looking SE at the surface of the French Creek landslide (hummocky low-angle surface at left center) and the probable slide source area on the steep valley-wall escarpment to the right.....	28
Fig. 20b. Lidar DEM of the French Creek landslide, showing mapped strands of the UPF (red lines); lidar-interpreted lineaments (yellow dashed lines)	29
Fig. 21. Cross section of modeled velocity structure along Line V.....	30
Fig. 22. Observed and model predicted travel times for direct and refracted arrivals along Line V.....	30
Fig. 23. Photo looking N55E down the lower part of Line A, as it traverses an old borrow area adjacent to access road	31
Fig. 24. Observed and model predicted travel times for direct and refracted arrivals, Line A	32
Fig. 25. Static corrected shot gather for Line A with shot location at 95 m corresponding to the location of geophone 20	33
Fig. 26. Static corrected shot gather for Line B with shot location at 40 m corresponding to the location of geophone 9	33
Fig. 27. Static corrected shot gather for Line C with shot location at 35 m corresponding to the location of geophone 8	33
Fig. 28. Line A: 15 m COG with forward shots	34
Fig. 29. Line A: 15 m COG with reverse shots	34
Fig. 30. Line A: 20 m COG with reverse shots	35
Fig. 31. Line B: 15 m COG with reverse shots	35
Fig. 32. Line B: 15 m COG with forward shots	36
Fig. 33. Line C: 15 m COG with forward shots	36
Fig. 34. Line C: 15 m COG with reverse shots	37
Fig. 35. Line C: 20 m COG with forward shots	37
Fig. 36. Line C: 20 m COG with reverse shots	38
Fig. 37. Conceptual cross-sections of the French Creek slide deposit and the pre-slide valley of Fountain Creek.....	39

Fig. 38. Conceptual cross-sections of the French Creek slide deposit and the pre-slide valley of Fountain Creek.....	40
--	----

List of Appendices.....	Page
Appendix 1: Preliminary Luminescence Ages	45
Appendix 2A: Previous Work on the UPF- Kirkham and Rogers, 1981	46
Appendix 2B: Previous Work on the UPF- Allen, 1984.....	48
Appendix 2C: Previous Work on the UPF- text from Harza Engineering Company, 1985	49
Appendix 2D: Previous Work on the UPF- Annotated fault maps from Harza Engineering Company, 1985.....	53
Appendix 2E: Previous Work on the UPF- Text from Geotechnical Advisory Committee, 1985, Part 4	71
Appendix 2F: Previous Work on the UPF- Text from Geotechnical Advisory Committee, 1986 ...	72
Appendix 2G: Previous Work on the UPF- Text from Wm. Lettis & Assoc., 1994	74

1. ABSTRACT

In this project we examined two of the most promising localities for preserving evidence for Quaternary faulting on the UPF. The first site was the splay fault and accompanying scarp across a Verdos-age pediment at the southern end of the UPF. This site was cited by Kirkham and Rogers (1981) as having the best geomorphic & stratigraphic evidence for post-Verdos (<600 ka) but pre-Slocum (>250 ka) fault movement. We interpret Kirkham and Rogers' "tilted block of alluvium" as an unfaulted, post-Verdos paleochannel filled with dipping colluvial strata, underlain by horizontal Verdos channel gravels. Thus, it is not compelling evidence for post-Verdos faulting. The base of the pediment gravels was examined in the field across the mapped fault trace and did not appear to be faulted. Alluvium thickness was essentially identical on both sides of the fault. In contrast, the seismic lines do show some anomalies. The inferred alluvium-bedrock contact reflector cannot be traced beneath the center of the surface scarp, although it exists on either side. Disruption of this reflector could represent pre-Quaternary faulting of the Pierre Shale, however. Overall, there is no compelling evidence for Quaternary faulting at this site.

The second site was the massive rockslide at French Creek in the Central section of the UPF. The landslide deposit is full of house-sized boulders of Pikes Peak granite, which subsequent to the original deposit emplacement have raveled down the post-slide sideslopes many tens of meters. Due to a lack of good exposures, it was not possible to assess Quaternary faulting from surface mapping. Seismic lines did show some reflectors (probably the Qls/Ypp contact), and on four of the seismic lines breaks in reflectors occurred beneath mapped fault traces (Line A, Figs. 28, 29; Line B, Fig. 31; Line C, Fig. 34). On the other five lines there were either no breaks in reflectors, or if there were, they did not lie beneath mapped faults.

It was hoped that seismic sections might show shallow reflectors vertically offset at shallow (<5 m) depths, which could be then be exposed by a deep paleoseismic trench. But the only consistent reflector occurred at depths of 12 to 20 m, too deep to trench. Based on the height of the slide deposit above modern Fountain Creek (~100 m), we presumed it was old, perhaps half as old as the 600 ka Verdos pediments (i.e., ~300 ka). However, preliminary luminescence dates indicate the slide deposit is only 32-35 ka. In that case, we would not expect to see surface faulting evidence here, because we do not see such scarps anywhere else on widespread deposits of similar age (Pinedale equivalent).

It is just as important to note what we did NOT observe in this study. In all our lidar mapping, we never saw a linear scarp crossing a Holocene or late Pleistocene deposit (Pinedale or Bull Lake equivalent) that was not clearly erosional (such as a terrace riser). Even on the oldest geomorphic surfaces mapped in the area, such as the Miocene-Pliocene Divide paleovalley deposit, there are no surface scarps along the mapped faults crossing the paleochannel. This is true even where the fault traces offset paleovalley gravels. In places along these faults there is sometimes vertical relief, but half of the time the relief is opposite to the movement direction of the fault, which indicates the relief is from differential erosion, not from direct faulting.

Overall, we were not successful in finding compelling evidence for Quaternary surface faulting, even using 1-meter lidar DEMs, and even in areas where such faulting evidence had previously been interpreted. However, we understand that absence of evidence is not evidence of absence. One untried approach would be to trench the fault zone across a planar Quaternary surface down to bedrock, and document the fault exists in bedrock, but there are no faults in Quaternary deposits. Colorado Springs Utilities may own a site with those characteristics.

2. INTRODUCTION

2.1 Significance and Scope of Study

The Ute Pass fault (UPF) is the longest Quaternary fault in Colorado's fast-growing Front Range Urban Corridor (Fig. 1), with an end-to-end length of 71 km and a segmented length of 78 km. The UPF has been ranked by the Colorado Geological Survey within the top five priority faults for further study (Morgan, 2015, 2018). It traverses El Paso, Teller, and southern Douglas counties and lies partly within the city limits of Colorado Springs.

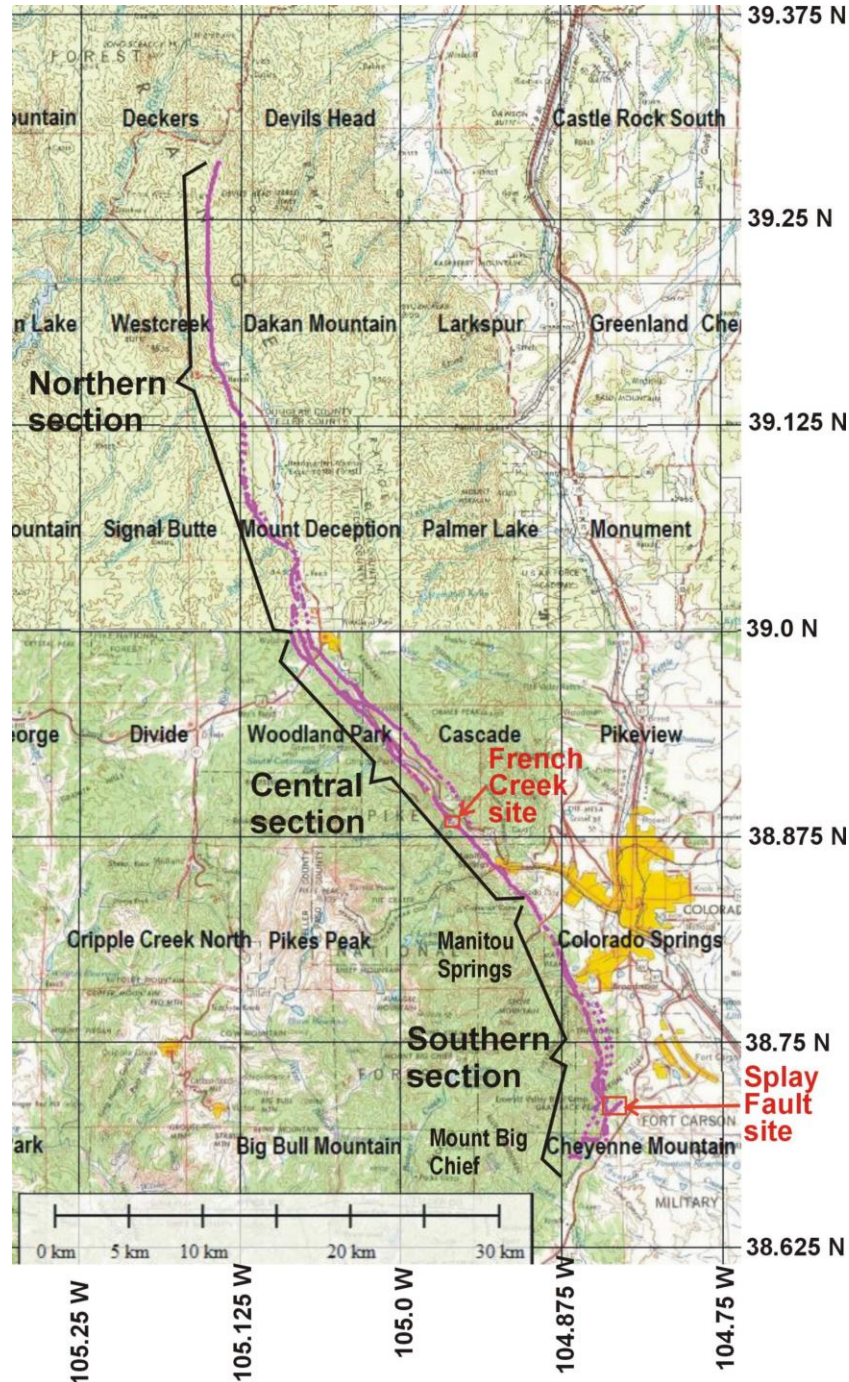


Fig. 1. Location map of the UPF (purple lines) and its three sections as defined by Harza Engineering Company (1985). Detailed study sites labeled in red. Grid shows 7.5' quadrangles.

The fault is composed of three geometric sections (Fig. 1). The northern section trends N10°W and is 32 km long. The middle section trends N40°W and is 23 km long. The southern section trends N15°E to N25°W and is 22 km long.

The UPF is the longest Quaternary fault in the South-Central Colorado Urban Area. This area is composed of the Colorado Springs Metropolitan Statistical Area, the Pueblo Metropolitan Statistical Area, and the Cañon City Micropolitan Statistical Area (population 851,500 in 2010 census; estimated at 954,000 in 2017). El Paso County itself has grown from a population of 622,263 in 2010 to 694,967 in 2017, an increase of 12%. Its 2017 population is essentially equal to that of Denver County, making Colorado Springs one of the densest population centers in Colorado. According to the Colorado State Demographer, by 2050 Colorado Springs is projected to top Denver in total population, making it the largest city in Colorado. Colorado Springs is also home to several facilities of critical national importance, including NORAD Headquarters, Fort Carson, and the U.S. Air Force Academy. The UPF trace lies just downslope from the entrance to NORAD Headquarters; its entrance road crosses the fault.

In 2013, Morgan and Fitzgerald (2013) performed a HAZUS damage analysis of a full-length rupture (71 km) on the UPF (Fig. 2), which equates to an M7.0 earthquake, based on rupture length scaling relationships established by Wells and Coppersmith (1994) and Leonard (2010). An M7 earthquake on the UPF would cause an estimated \$17B in damages and around 700 fatalities.

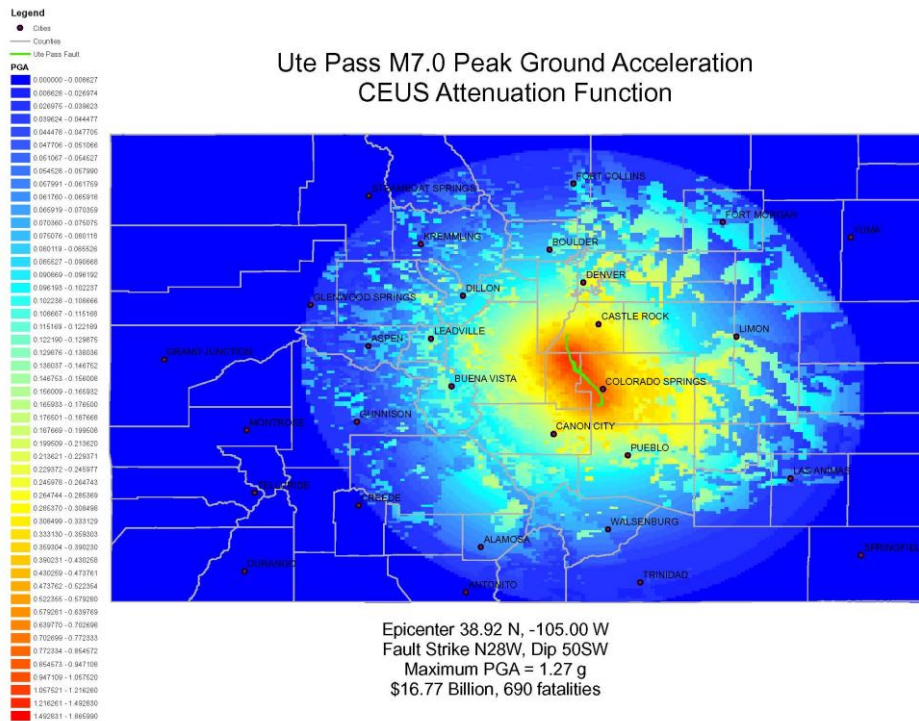


Fig. 2. Peak ground acceleration predicted for an M7.0 scenario earthquake on the Ute Pass fault. Monetary loss and fatality predictions are from Morgan and Fitzgerald (2013). Since the abandonment of the late Eocene erosion surface on Front Range basement rocks, the UPF has vertically offset the surface by 300 m in the present stress field (Epis and Chapin, 1975). This movement has created the largest topographic anomaly in the late Eocene surface, the Neogene Manitou Park-Woodland Park graben.

2.2 Seismotectonic Setting

Colorado is currently dominated by a weak east-west extension partly associated with the Neogene Rio Grande rift zone (Berglund et al., 2012; Murray et al., 2019). The present E-W extension of 1.2 nanostrains/yr spans the eastern Colorado Plateau, the Rio Grande rift, and the western edge of the Great Plains, including the Front Range Urban corridor. This is equivalent to 1.2 mm/yr extension over a 1000 km-long transect, or 0.12 mm/yr over a 100 km-long transect (the distance between the Urban Corridor and the Rio Grande rift). That this stress field can reactivate properly-oriented faults on the Great Plains has been proven by work on the Cheraw fault, which lies SE of Colorado Springs and even farther out on the Great Plains. Crone et al. (1997), Zellman and Ostenaar (2016), and Ostenaar and Zellman (2018) have confirmed three Holocene/Late Pleistocene reactivations of this old fault.

Considered in this light, the UPF has even a better chance of being reactivated in the present stress field:

- 1-the UPF is more favorably oriented (N-S) to accommodate E-W extension than is the Cheraw fault,
- 2-the UPF is a more mature fault with much more net displacement
- 3-the UPF is closer to the axis of the Rio Grande rift than is the Cheraw fault

2.3 Previous Work on Neogene Movement of the UPF (after Widmann et al, 1998)

Studies of the Neogene movement on the UPF began in the mid-1970s. By the mid-1980s late Cenozoic movement was supported on the UPF (e.g., Taylor, 1975; Scott and others, 1978; Kirkham and Rogers, 1981; Dickson, 1986), with strength of the evidence varying among the three sections. Appendices 2A through 2F cite the relevant data and conclusions from these studies.

Northern Section: Neogene fault activity is apparent based on offset of Pliocene and Miocene gravels (Scott and Wobus, 1973), and 300 m of throw on the fault since the Eocene was recorded by Epis and Chapin (1975). In contrast, Quaternary deposits do not appear to be offset across the northern section of the fault (Bryant and others, 1981; Dickson and others, 1986; Geotechnical Advisory Committee, 1986).

Central Section: The fault lies primarily in Precambrian bedrock. Scott and Wobus (1973) and Wobus and Scott (1977) mapped the fault as concealed by Quaternary deposits. Pliocene and Miocene gravel deposits were mapped by Scott and others (1978) as offset by the fault. Pleistocene fan alluvium abuts against the fault according to Bryant and others (1981).

Southern Section: Scarps developed in Quaternary (Yarmouth to Illinoian age) rockfall deposits are cited as evidence for recent fault activity on the south end of the fault by Scott and Wobus (1973) and Kirkham and Rogers (1981). The fault system is marked by subtle, discontinuous, anomalous lineaments, visible on aerial photos, that extend through rockfall deposits at the south end of the fault (Kirkham and Rogers, 1981). Scarps and lineations in rockfall deposits are believed to represent the second of two surface ruptures, while the rockfalls themselves are interpreted as resulting from an earthquake during the Yarmouth interglacial period (Scott and Wobus, 1973). Unruh and others (1994) however, found no evidence of offset in late Pleistocene to Holocene deposits along the south end of the fault.

A prominent scarp is present in Verdos Alluvium at the south end of the UPF, on a short, NE-trending splay fault (Scott and Wobus, 1973. This scarp is truncated by a younger (Slocum?)

terrace of Rock Creek, indicating the scarp formed before Slocum time (ca. 250 ka). Unruh et al. (1994) did not recognize any evidence to support mid-Pleistocene to Holocene displacement on this scarp, suggesting the scarp was probably erosional. However, Rowley et al. (2002) mapped both the Pierre Shale bedrock and the overlying Verdos alluvium as being faulted along the scarp.

Due to the discrepancies noted above, we studied two sites in detail where Quaternary deposits overlie the mapped trace of the UPF. The first site is the splay fault at the south end of the UPF, which Kirkham and Rogers (1981) cited as the strongest evidence for post-Verdos faulting. The second site is in the Central section between Manitou Springs and Cascade, where a Quaternary landslide overlies the UPF. The landslide surface contains several fault-parallel lineaments that may reflect subsequent fault movement. In addition, this large anomalous slide may have itself been triggered by ground shaking, as suggested for the scarps described by Kirkham and Rogers (1981) on the southern section rockfall deposits.

3. METHODS

3.1 Mapping

Mapping in the office and field utilized the 1-meter lidar DEMs of El Paso and Teller Counties. In the field this lidar was contained on Toughbook field computers so earlier desktop mapping could be revised and updated. We used Global Mapper GIS v.14 through v.22 for mapping and data recording.

3.2 Geophysics

Seismic refraction and reflection lines were surveyed on ~115 m-long lines utilizing 25 geophones with a spacing of 5 m, except for French Creek Line V, which used a 2.5 m spacing. The energy source for all surveys was a 16-lb sledgehammer. System equipment was loaned to CGS by the Department of Geosciences, Colorado State University, Ft. Collins. Our refraction model was developed using Refract 2.1.2 by Craig H. Jones. This software allows for multiple dipping interfaces, although all interfaces must be planar. Our model was parameterized to be a single layer over a half space representing the Quaternary deposits overlying pre-Quaternary bedrock.

3.3 Geochronology

All ages were derived by optically-stimulated luminescence (OSL) dating at the Luminescence Dating Research Laboratory, Baylor University, TX. Dated pure quartz separates ranged from 150 microns to 500 microns (fine sand to medium sand). Ultra-small aliquots with 20-80 grains/aliquot were analyzed under blue-light excitation (470 ± 20 nm) by Single Aliquot Regeneration protocols (SAR; Murray and Wintle, 2003; Wintle and Murray, 2006). Equivalent dose (D_e) was calculated by Minimum age model (Galbraith and Roberts, 2012). U, Th, Rb and K contents were analyzed by inductively-coupled plasma-mass spectrometry by ALS Laboratories, Reno, NV. Cosmic dose rate was calculated from parameters in Prescott and Hutton (1994) and includes soft components (Peng and Forman, 2019). Systematic and random errors were calculated in a quadrature at one standard deviation by the Luminescence Dating and Age Calculator (LDAC) <https://www.baylor.edu/geosciences/index.php?id=962356> (Peng and Forman, 2019). Datum year is AD 2010.

4. Splay Fault Site

According to previous mapping, the UPF contains an alleged fault scarp on the ~600 ka Verdos Alluvium, in the north-central part of the Cheyenne Mountain quadrangle (T15S, R66W, Sec. 25). Scott and Wobus (1973) mapped a 1.6 km-long NE-trending fault here, corresponding to part of a 75-125 m wide, SE-facing scarp with a vertical separation of 12-15 m. The fault was mapped as a dashed line across the Verdos Alluvium, but as a solid line across the Pierre Shale (Kp) in two gullies incised into the Verdos terrace (Fig. 3).

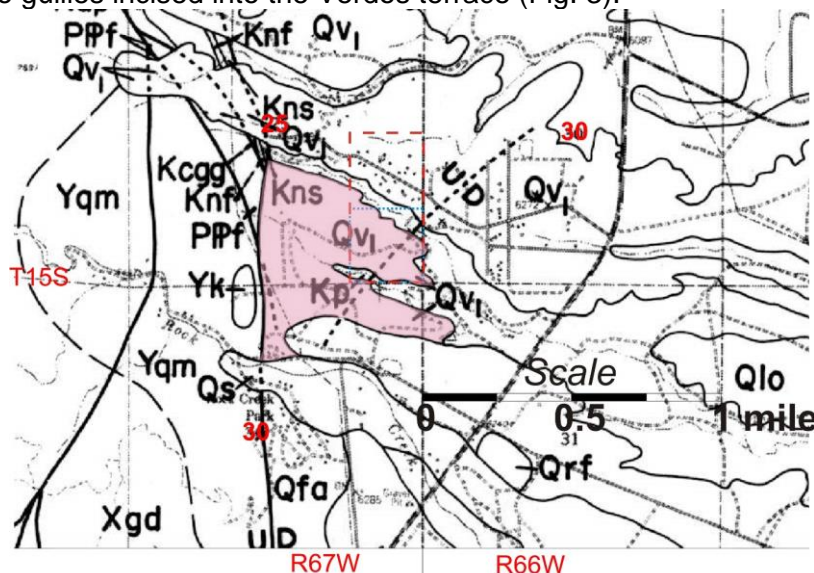


Fig. 3. Clip from Scott and Wobus' 1973 1:62,500 geologic map of the Colorado Springs 15' quad. At center is their 1 mile-long, NE-trending fault that is mapped as "approximately located" across the Verdos Alluvium (pink shading), but mapped as a solid line in in the Pierre Shale (Kp). Red dashed box is area the 1/8 section cited by Kirkham and Rogers (1981). Blue dotted box shows private 40-acre parcel.

Kirkham and Rogers (1978, 1981) described this short fault as one of two lines of evidence for Quaternary movement on the UPF; the other evidence being discontinuous, parallel topographic lineaments in the very southern part of the Colorado Springs quadrangle (T15S, R67W, Secs. 1, 12, and 13), described previously. On p. 56 they state: "A prominent scarp is developed in Verdos Alluvium along a bedrock fault in sec. 30, T. 15S., R.66W. (Scott and Wobus, 1973). The nature of this feature is not known with certainty, but a tectonic origin is supported by the tilted block of Verdos Alluvium exposed in a roadcut in E1/2 SE1/4 sec. 25, T.15S., R.67W., on strike with the prominent scarp." There is only one road shown crossing the scarp in Sec. 25, which is the private driveway to a 40-acre parcel (formerly part of the Colorado Springs to Canon City highway). [This roadcut was examined in the present study and is described in Section 4.]

Unruh et al. (1994) "confirm the presence of an abrupt east-facing bedrock scarp along the mapped fault trace, and small saddles along ridges that are crossed by the fault. Stream bank exposures show, however, that the top of the bedrock can be traced continuously across the mapped fault trace and is observed to underlie late Quaternary fluvial deposits at shallow depth east of the fault. We conclude that the bedrock scarp is a result of differential erosion between the bedrock and Quaternary fluvial deposits. The small ridge-crest saddles probably result from head ward erosion of small intermittent streams incised along the contact between the bedrock and Quaternary fluvial deposits. We observed no scarps or anomalous geomorphic features in the fluvial deposits east of the bedrock scarp."

Rowley et al. (2002) mapped the fault at 1:24,000 (Cheyenne Mountain quadrangle), but differently than Scott and Wobus (1973). As shown in Fig. 4, Rowley et al. map the fault as only 1.1 km long, omitting the northern 500 m mapped by Scott and Wobus. The central 600 m of the scarp is mapped as a solid line, even across the Verdos Alluvium, indicating they thought the Verdos was demonstrably faulted. The southernmost 200 m is mapped as concealed (dotted line) beneath a lower terrace of probable Slocum age (based on it lying 88 ft [27 m] above stream level; Rowley et al., 2002, p. 8). Thus, their mapping disagrees with the erosional interpretation of Unruh et al. (1994), published eight years earlier.

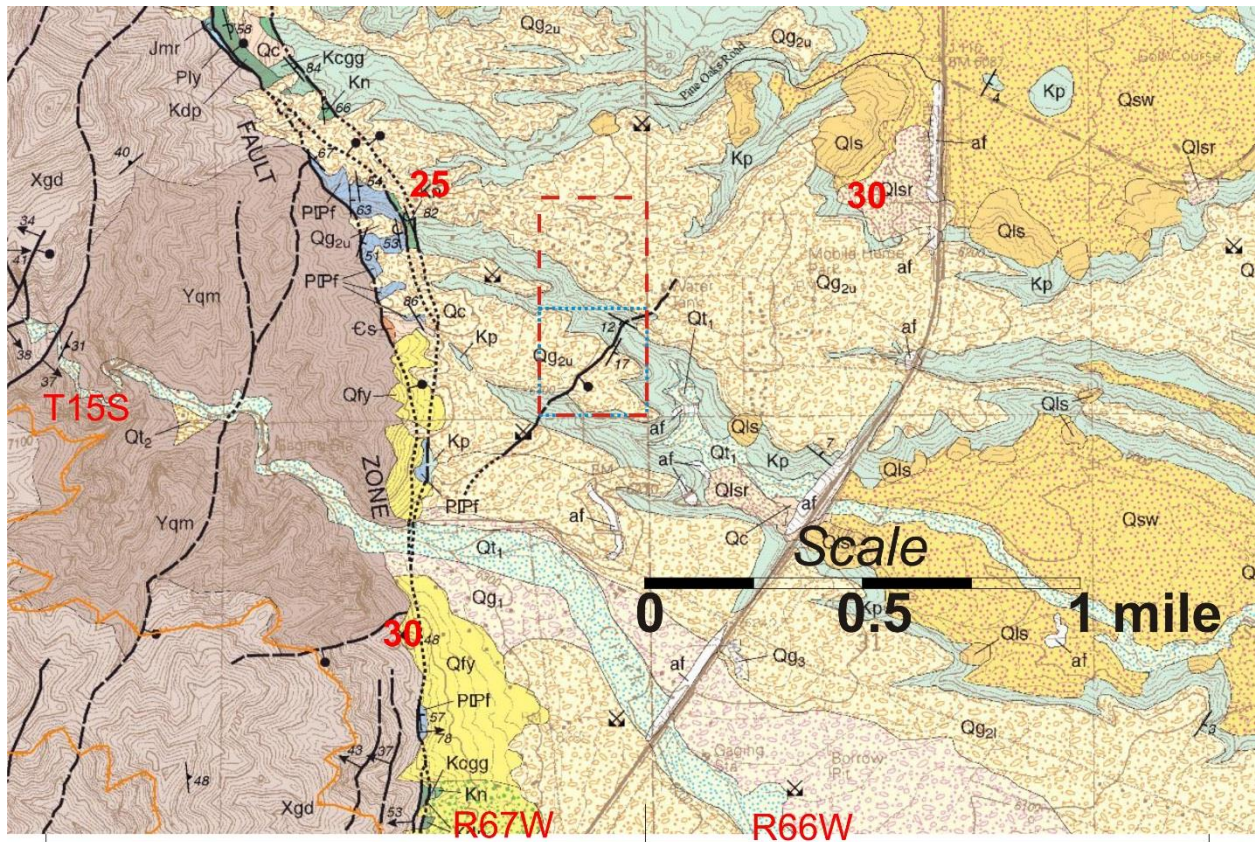


Fig. 4. Clip from Rowley et al. 1:24,000 geologic map of the Colorado Springs 7.5' quad. At center is their 1 km-long, NE-trending fault that is mapped as “definite” across the Verdos Alluvium and the Pierre Shale. Red dashed box is area the 1/8 section cited by Kirkham and Rogers (1981). Blue dotted box shows private 40-acre parcel.

A topographic profile along the non-concealed fault trace is shown in Fig. 5. Using the elevation of contacts mapped by Rowley et al., the Verdos Alluvium (Qg2u) ranges from 15 m thick on the southern end of the fault to 6 m thick on the northern end. It is underlain by Pierre Shale (Kp) with variable dips of bedding (17°SE to 12°SW). The former attitude strikes parallel to the scarp and dips in the same direction. In the two incised gullies 15 to 30 m of Pierre Shale is exposed in section (see Fig. 6).

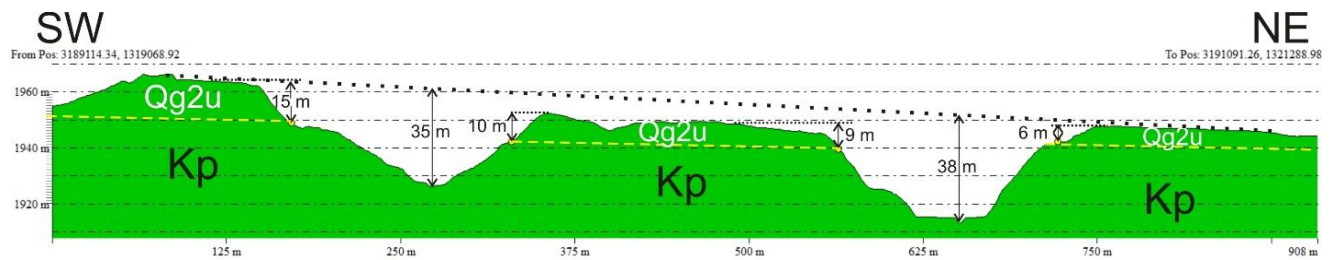


Fig. 5. Topographic profile along the splay fault, as it crosses two deep gullies.

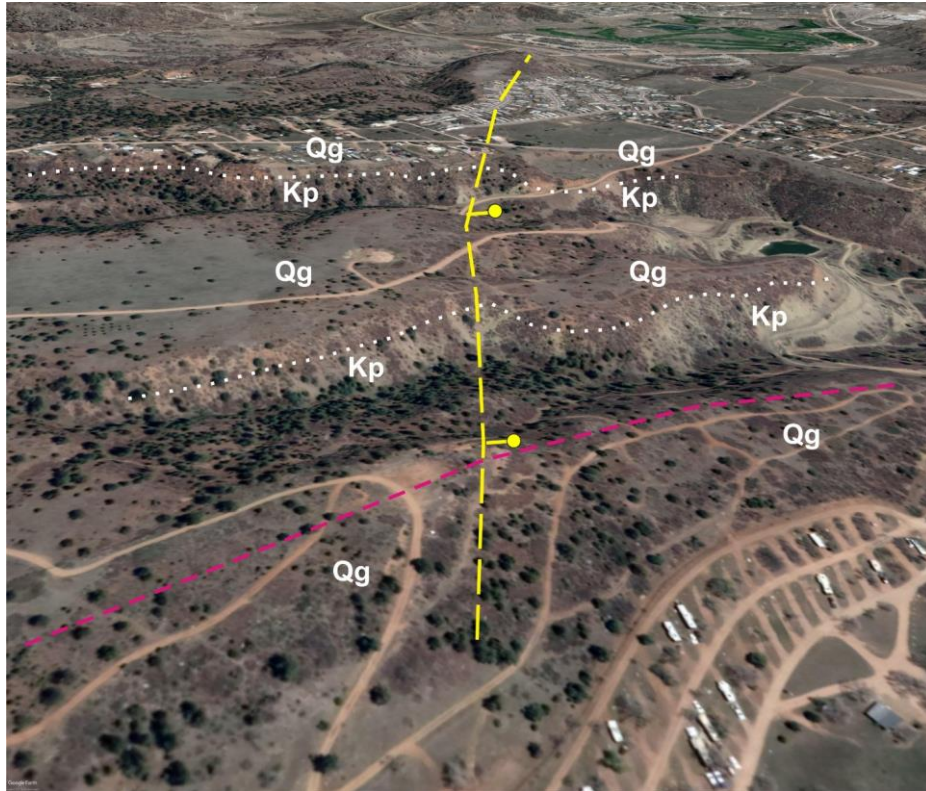


Fig. 6. Oblique Google Earth view of the splay fault (yellow), looking NE. Qg terrace gravels are reddish; underlying Kp bedrock (Pierre Shale) is gray. Red dashed line shows possible geophysics line down crest of southern Qg pediment remnant. However, our seismic survey was located on the central pediment remnant in the center of the photo. Golden Eagle RV Park at lower right.

4.1 Structural Setting

The splay fault lies on the downthrown block of the main UPF, and mimics the trend of the range front south of the UPF (Fig. 7). This is a geometry that might result if the splay fault was a continuation of a post-Verdos rupture that had originated to the SW on the N30-40E trending range front. In that case, the rupture would have propagated NE, and when the range front at Cheyenne Mountain turned N, the rupture kept going NE onto the downthrown side of the UPF.

We examined the 1m lidar DEM for traces of a post-Verdos rupture on the NE-SW trending range front into the Big Chief Mountain quadrangle. However, at the range front there were no preserved terraces as old as Qg2. The oldest terrace was Qg1 at Little Fountain Creek, but Qg1 was not faulted by the splay fault in the Cheyenne Mountain quad, so is younger than the latest movement on the splay fault. A Qg2 terrace does appear farther south in the Cheyenne

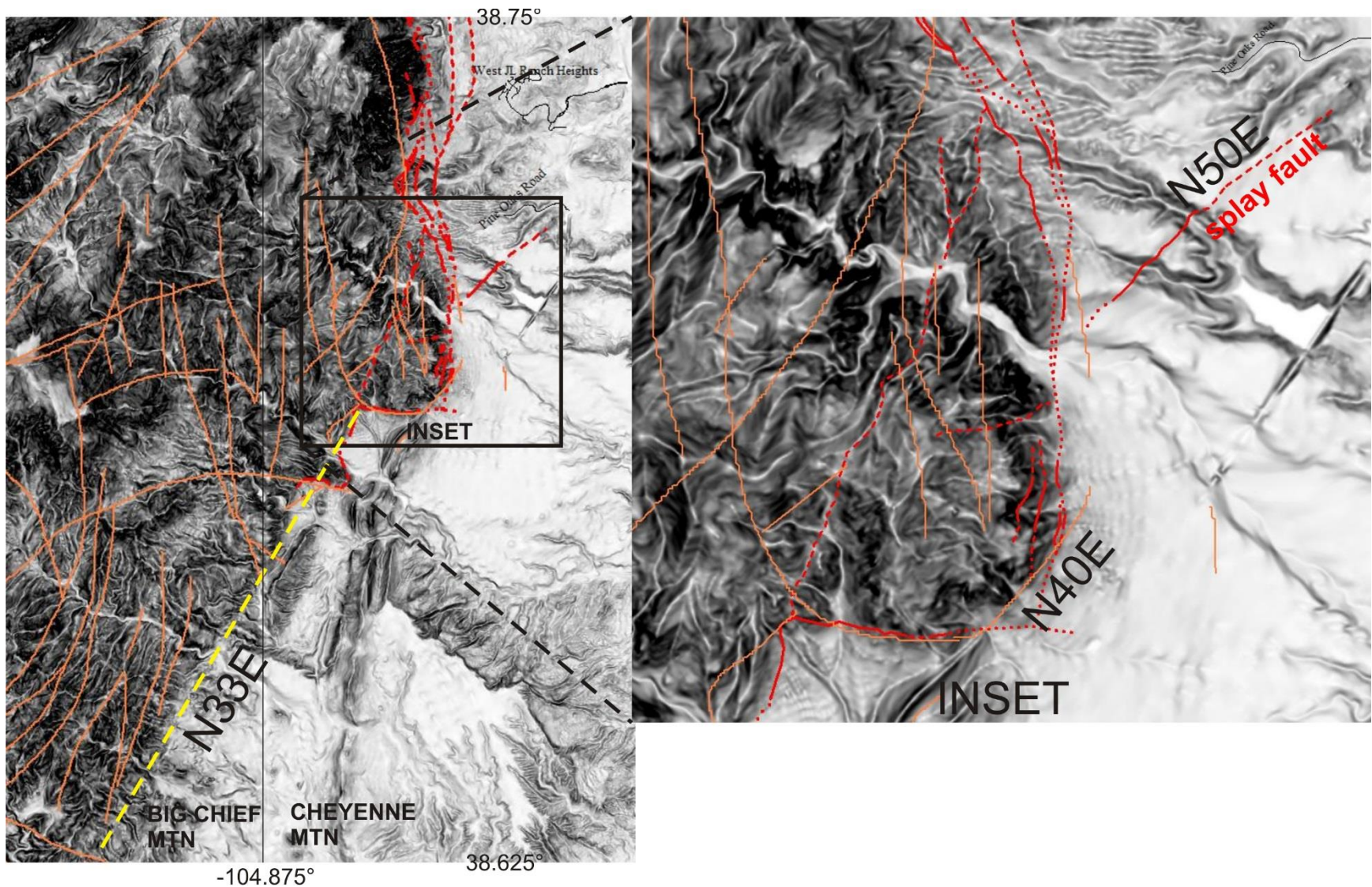


Fig. 7. Left, 10 m DEM of the southern end of the UPFZ (red lines). South of the UPFZ the Front Range escarpment bends to a SSW strike. Yellow line, general trend of range front south of the bend; orange lines, faults from the Boos-Boos 125k map. Right, Inset map showing the splay fault (upper right), and the farthest-north range front fault that trends NE, rather than N-S.

Mountain quad, but about 1 km E of the range front. That terrace may continue W to the range front in the Big Chief Mountain quad, but that quad has not been mapped at 1:24,000. Trimble and Machette's (1979) map I-857-F does cover the range front south to 38.625°, and shows six Verdos Alluvium remnants south of Little Turkey Creek, but none of them reach the range front and Precambrian rocks.

4.2 Surface Geology

Fig. 8 shows the geology of the Cheyenne Mountain quadrangle around the Splay Fault (NE-trending black line at center). Rowley et al. (2002) mapped the fault as a solid line across the Pierre Shale (Kp) and the Verdos alluvium (Qg2u). At its SW end the scarp is truncated by a lower terrace (Qg2l, Slocum). Rowley et al. dotted a fault trace across a lower inset terrace, but our field mapping shows there is no scarp there. Instead, there is a subtle slope break caused by the deposition of a small alluvial fan onto the west edge of the Slocum terrace. This small fan was not mapped by Rowley et al., but was obvious on the lidar and was conformed in the field. The fan surface is steeper than the terrace surface, and makes a subtle slope break at the toe of the fan. This slope break is apparently what Rowley et al. extended their dotted fault line to, but it is not a tectonic feature.

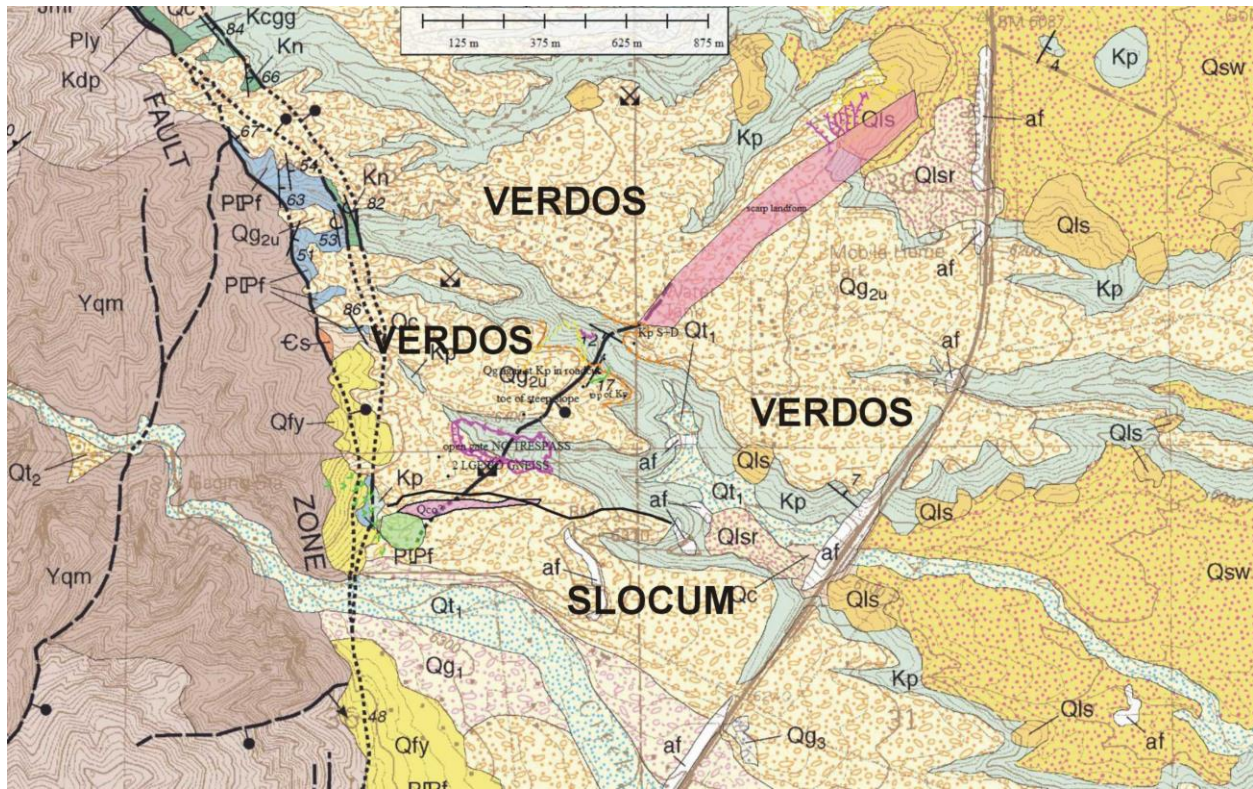


Fig. 8. Part of the geologic map of the Cheyenne Mountain 7.5' quadrangle (Rowley et al., 2002) around the NE-trending splay fault (at center). Pink polygon shows the continuation of the scarp NE of the fault mapped by Rowley et al. At the NE end of the polygon is a lateral spread landslide (Qls) described in the text.

4.2.1 The "Tilted Block of Alluvium"

Kirkham and Rogers (1981) described a "tilted block of Verdos Alluvium exposed in a roadcut in E1/2 SE1/4 sec. 25, T.15S., R.67W., on strike with the prominent scarp", and offered it as

evidence of post-Verdos faulting. We re-examined this roadcut and have the following comments:

1-the roadcut exposure is not exactly “on strike” with the scarp or the mapped fault. It’s closest approach to the mapped fault is 65 m (see Fig. 9a).

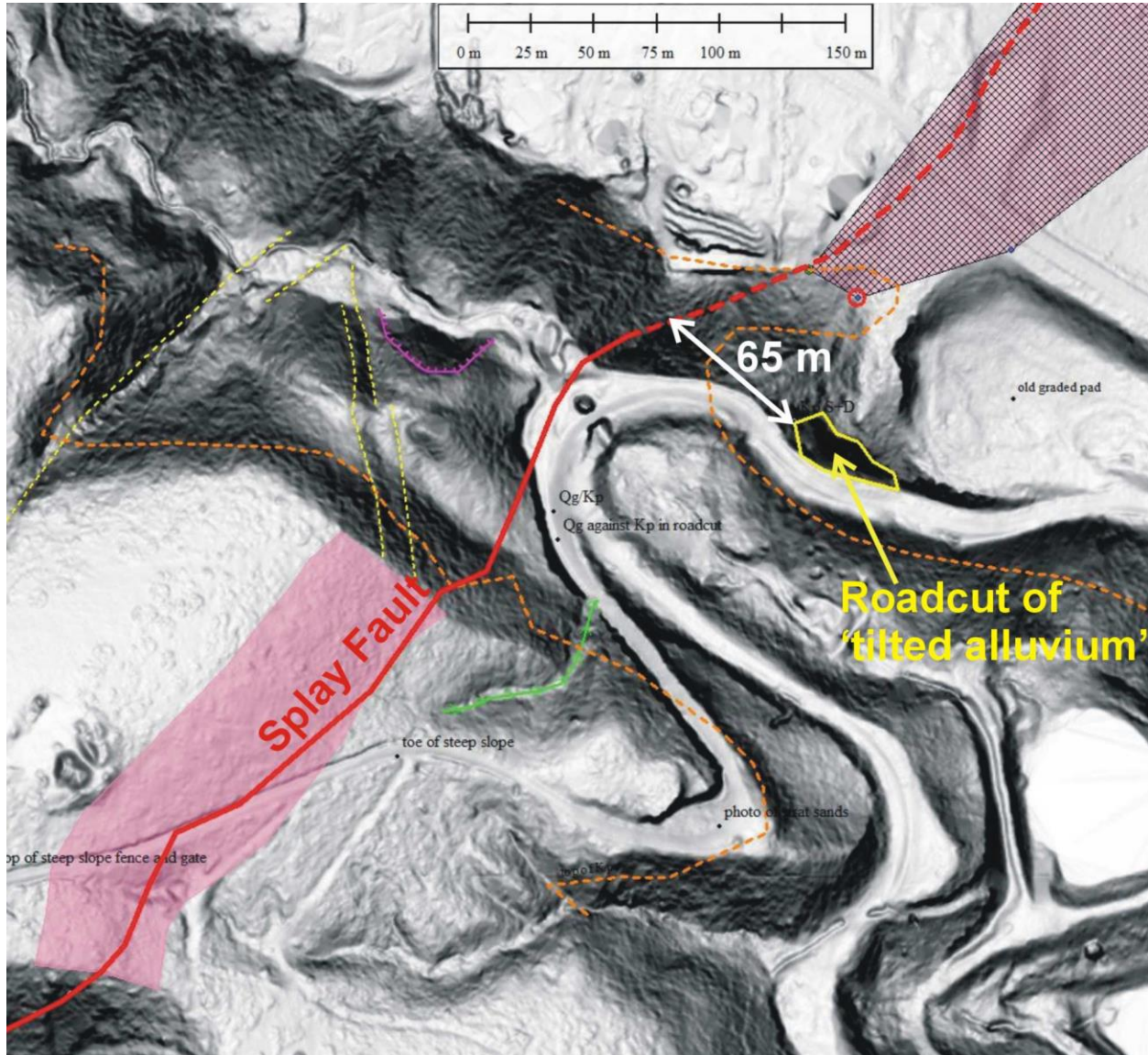


Fig. 9a. Lidar DEM of the central Splay fault (red line), the wider scarp (pink polygons), and the location of the roadcut exposing “tilted alluvium.” Orange line is the Qg2u/Kp contact from Rowley et al., 2002. Sinuous wide road below roadcut is the old Colorado Springs-to-Canon City Highway.

2-The deposit exposed in the roadcut is atypical of Qg2u alluvium, which is composed elsewhere of cobbly to boulder gravel. Only the lowest 1 to 1.5 m of alluvium atop the Pierre Shale looks like typical channel alluvium of Qg2u. The remaining 8.5 m is much finer grained and looks more like sideslope slopewash deposits (clast-free) and colluvium (gravelly sand). See Fig. 9b.

3-From a distance the finer deposits do look tilted, with the tilt increasing to the west, toward the splay fault. However, this is apparent steeper tilt to the west is caused mostly by the 3D geometry of the roadcut. The eastern 80% of the roadcut exposure trends N65°W, whereas the western 20% of the exposure trends N20°W, or 45° more northerly, so it strikes into the slope. When seen from a distance, as in Fig. 9b, the dips in the western 20% are “telescoped” to appear steeper than they really are.

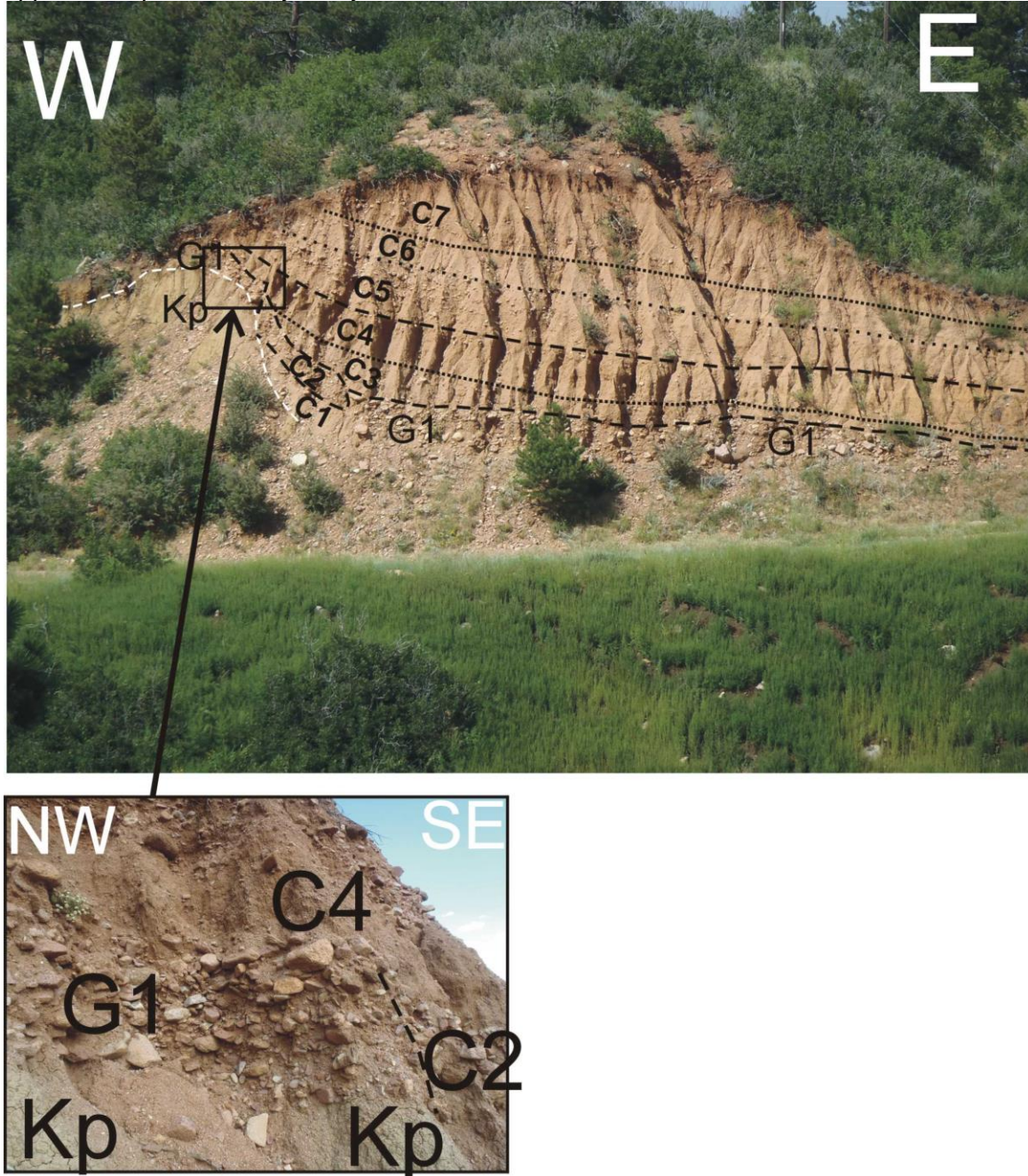


Fig. 9b. Top: Telephoto view of the roadcut cited by Kirkham and Rogers (1981), taken from 150 m south of the cut. Kp, Pierre Shale; G1, channel gravel facies of Qg2u, or of a post-Qg2u paleochannel; C1 through C7, locally-derived colluvium and slopewash that has filled the paleochannel. Bottom: close-up of units Kp, G1, and C2-C4 on the northwestern channel margin of the paleochannel. Note that the G1 gravels are imbricated to the left (NW) and into the slope (N), indicating either the direction of flow in the paleochannel, or some post-depositional backtilting of the section into the slope.

4-Deposit facies and sedimentary structures suggest the roadcut exposes a NE-trending paleochannel, with the western 20% exposing the NW channel margin. After channel abandonment the paleochannel filled with fine-grained, locally-derived colluvium and slopewash from the W and NW. These deposits had a primary, nonhorizontal dip to the E and SE, which increased toward the channel margin. Due to the shape of the exposure, dips in the western 20% are exaggerated when viewed from the south. At first glance, this gives the impression that a block of Qg2u pediment gravels have been tilted east. But note that basal unit G1 is not tilted.

In summary, we do not consider that the roadcut exposure shows compelling evidence for post-Verdos tectonic deformation.

4.2.2 Verdors Pediment Failed as a Lateral Spread, North End of Splay Fault

The north end of the splay fault is expressed as an east-facing scarp on the eastern margin of a flat Verdors pediment remnant (Fig. 8). The northern tip of the pediment has disintegrated into a lateral spread, making a topography of rectangular mounds 4-6 m high separated by shallow, flat-bottomed troughs (Fig.9c).

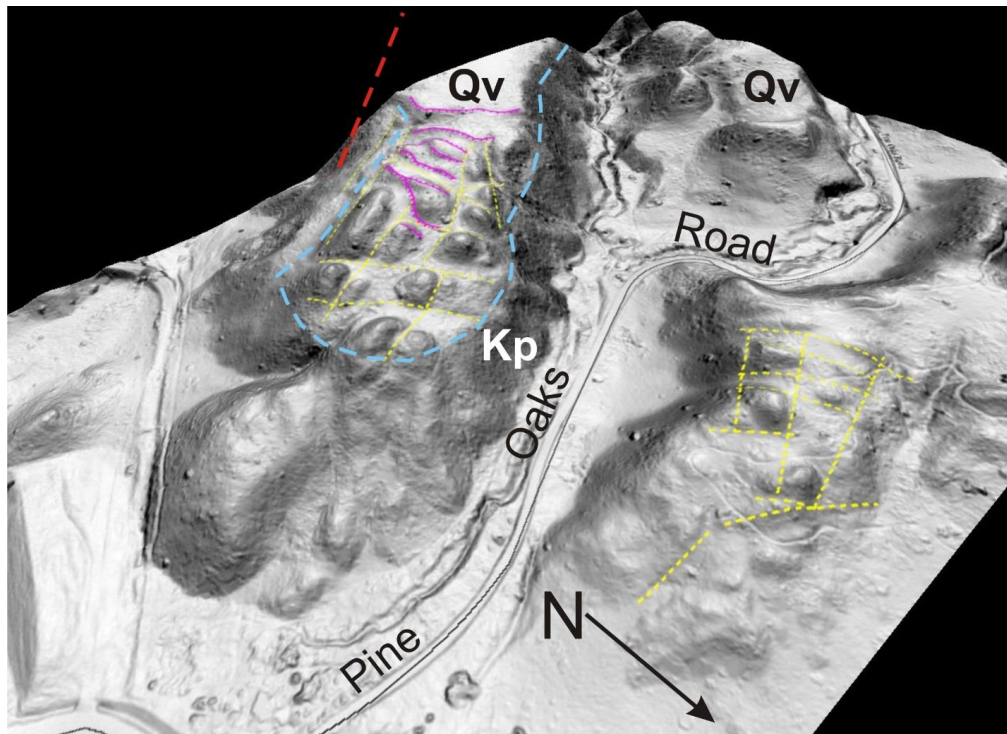


Fig. 9c. Lidar oblique view to the SW of the northern end of the splay fault (red dashed line at top). The Verdors alluvium has separated into rectangular blocks, apparently sliding and spreading on top of the Pierre Shale (Kp). The alluvium/bedrock contact (Qv/Kp) shown by dashed blue line. The overall morphology resembles a lateral spread (Fig. 9d).

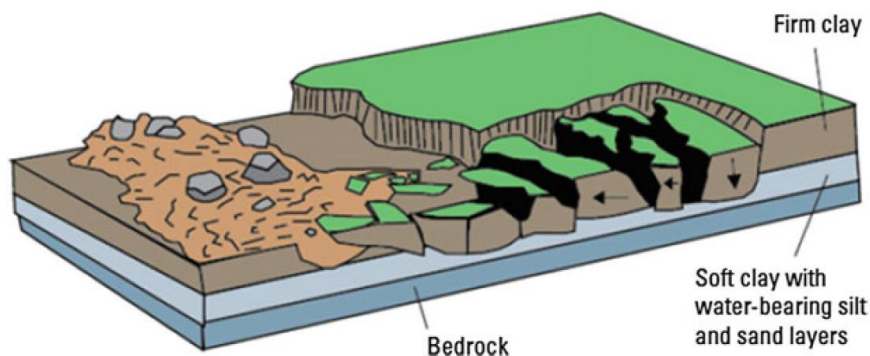


Fig. 9d. Cartoon of a lateral spread, from Highland and Bobrowsky, 2018. Lateral spread blocks in the source area in this drawing are elongated perpendicular to the spreading direction, whereas at the Splay scarp site they are nearly square.

This lateral spread is one of the few preserved and visible on lidar in the Cheyenne Mountain and Colorado Springs quadrangles. Lateral spreads require liquefaction of an underlying deposit overlain by an unsaturated, more firm, brittle deposit. When the saturated deposit liquefies it begins to flow downslope, stretching and fracturing the overlying brittle deposit, and eventually separating it into blocks which slide down a gentle slope. Such near-surface liquefaction is normally caused by earthquake shaking. Non-earthquake (static) liquefaction is quite rare, because it is difficult to raise near-surface pore pressures that high without earthquake shaking. In the near-surface, elevated pore pressures generated by high water tables are relieved simply by surface seepage at topographic breaks. Static liquefaction is only known to occur in rare instances, such as at the outside toe of artificial levees on the Mississippi River during extreme high flood events (Kolb, 1975). However, that model does not fit the current topography at the splay fault.

It is possible that the lateral spread formed long ago, soon after the deposition of the Qg2u pediment gravel ca. 600 ka. In that case the topography would have been different than that today's (but still, not a Mississippi River). However, the block topography looks too fresh to be a 600,000 year-old landslide, especially given the erodible nature of the Pierre Shale once exposed.

4.3 Possible Fault Geometries Below the Splay Scarp

We assume that the Verdos Alluvium is 6-15 m thick (Figs. 5 and 6) and overlies the Pierre Shale on an erosional unconformity parallel to the ground surface. Bedding in the Kp is assumed the strike parallel to the fault and dip SE at 17°. Given these data, there are numerous possible geometries for subsurface fault structure:

Geometry Option 1-A vertical to steeply-dipping fault which displaces the Kp and Qv deposits. The upper half of the scarp face has been eroded back from the fault. The lower half of the scarp face is a post-faulting colluvial wedge composed of retransported Qv. Colluvial thickness equals half the scarp height. Neither fault block has been rotated.

Geometry Option 2-Same as above, but the downthrown block has been rotated down towards the fault. This thickens the colluvial wedge at the fault (> half the scarp height).

Geometry Option 3-Downslope of the main fault there is a graben defined by one or more antithetic faults. This also thickens the colluvial deposits compared to Scenario 1.

Geometry Option 4-The scarp is underlain by a series of step-faults. Thickness of each wedge is half the vertical displacement of the step-fault, so each individual wedge is much thinner than half the scarp height.

In options 1-4 the fault(s) dip more steeply than 17° , so would be seen to cross-cut beds of the Pierre Shale in a geophysics line. However, at deeper depths the fault could remain planar, or curve in a listric fashion to subhorizontal. Planar fault options would be 1 through four, and listric options would be 1a through 4 a. If the fault is seen to go listric a relatively shallow depth, it could be interpreted as a landslide.

Geometry Option 5- The scarp is underlain by a shallow-dipping, bedding plane fault in the Pierre Shale. In this scenario there is a fault but it does not cross-cut bedding in Kp.

Geometry Option 6- Verdos Alluvium is draped depositionally over a pre-Quaternary fault or fold in Kp, or a post-Verdos channel ran along such a fault, creating a fault-line scarp by erosion. This is equivalent to the erosional origin proposed by Unruh et al. (1994). In the latter case, the pediment surface downslope of the scarp may be underlain by deposits of a post-Verdos paleochannel (such as exposed in the roadcut exposure), as well as by the normal thickness of Qg2u gravels.

There are discontinuous exposures of the Qg2u/Kp contact just below the southern rim of the central pediment remnant. In a traverse along this rim, we measured the thickness of Qg2u from its basal contact with Kp, up to the pediment surface in two places on either side of the mapped Splay fault. 5 m E of the fault, cobbly-bouldery Qg2u gravels were 7.6 m thick. 50 m W of the fault, cobbly-bouldery Qg2u gravels were 8.4 m thick. Given the natural irregularity of the contact, these thicknesses are essentially identical.

In relation to the six possible subsurface geometries described above, this uniform thickness of pediment gravels appears to eliminate all Options that require a colluvial wedge (Options 1-4). This leaves Option 6 (erosional origin of the scarp) the most likely. However, uniform gravel thickness does not tell us why there is a scarp here, or whether there is a fault in the Pierre Shale bedrock. To address that issue, we decided to measure a seismic line across the scarp, hoping to image the alluvium-bedrock contact in the subsurface, to see if it was vertically offset, and perhaps to see reflectors within the Pierre Shale that might be offset.

4.4 Seismic Survey Line

The landowner of the Golden Eagle Ranch LLC granted permission for a geophysical line in one of two locations. The first we proposed was the southern pediment remnant, which lies just north of the Golden Eagle Ranch RV Park (Fig. 10a). A road from the RV Park to the geophysics line was an advantage here, but there were three disadvantages. First, pediment gravels appear to be thickest there, according to Fig. 5. Second, the scarp is quite broad and has been disturbed by excavation. Third, movement of cars and campers within the RV park would induce a high level of background noise to the seismic survey.

The scarp across the central pediment remnant is actually better preserved, where the scarp has the narrowest, steepest scarp face (Fig. 10b). At this site our seismic line could be shorter,

but potentially could image the largest vertical displacement. So we chose that location for our 115 m-long seismic line.

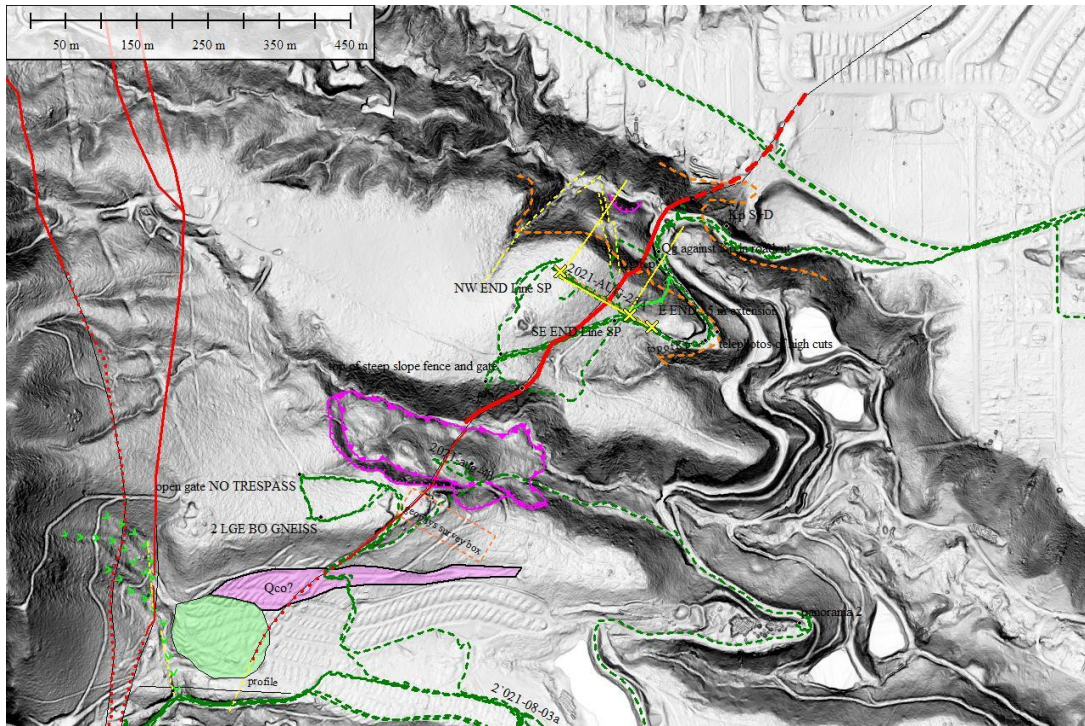


Fig. 10a. Lidar DEM of the Splay Fault area. Published fault traces in red (Splay fault at center, UPF main strand at left). Geophysics line (yellow line and X's) crosses splay fault at center. Green lines show 2021 field traverses. Purple outlines a landslide, which does not appear faulted.

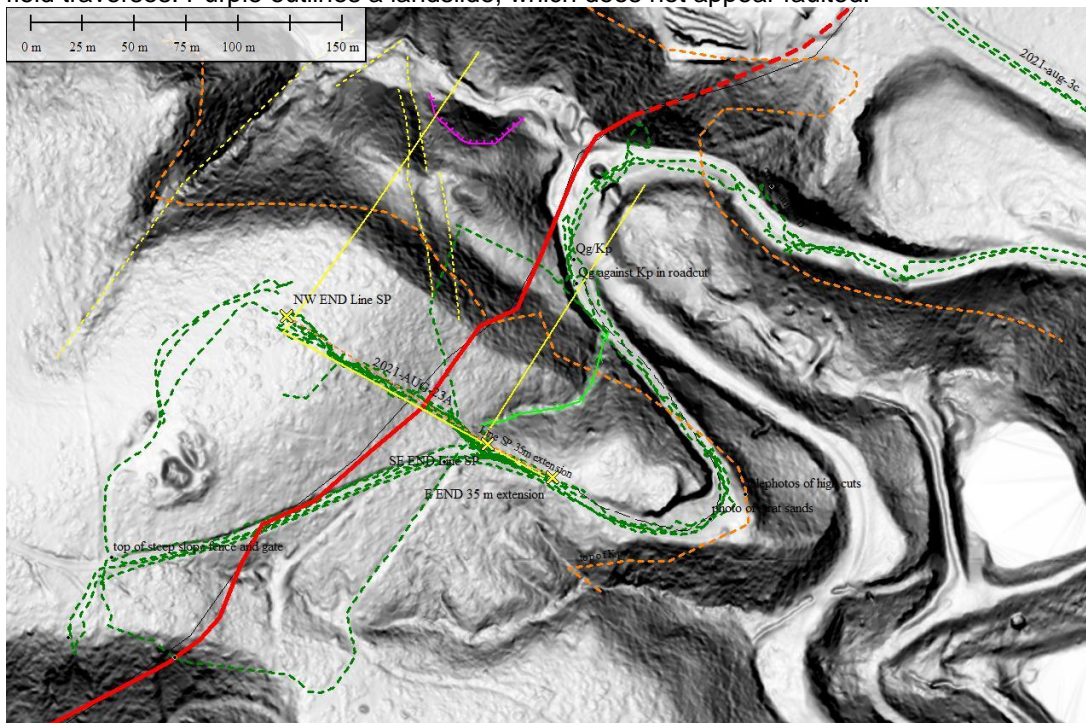


Fig. 10b. Close-up of fault (red) and associated SE-facing scarp crossing the central pediment remnant. Seismic Line SP is a thin yellow line across the fault, with yellow X's at each end. Green lines are field traverses. Orange lines are the Qg2u/Kp contact from Rowley et al. Purple lines outline a small slump

headscarp, which is cut into a larger slump block (not outlined). Lighter green line at center is a tributary incised below the scarp, which ends abruptly upslope and has no obvious catchment area. It may indicate spring sapping from emergent groundwater.

4.4.1 Goals of the Seismic Survey

- 1-Is the Verdos Alluvium faulted?
- 2-Is there a fault in the Pierre Shale beneath the scarp? If so, what is the dip of the fault? Can its displacement be measured?
- 3-Does the bedrock fault extend into or through the Verdos Alluvium?
- 4-If the answer to the above is yes (there is a fault that cuts the Verdos Alluvium), is it a tectonic fault or a landslide headscarp?
- 5-Conversely, if geophysics shows that neither Qv or Kp is faulted, then the erosional interpretation of Unruh et al. (1994) would be indicated.

4.4.2 Results of the Seismic Survey (by Kyren Bogolub, CGS)

On Line SP we did refraction modeling on two segments of the line, in part because the hammer source did not produce first arrivals clear enough for picking on the far ends of the total line, and in part because the topography has a steep break near the midpoint of the line. Splitting the line into two refraction lines makes each line a bit more planar, although still more topographically complex than is optimal. One section goes from 0 m to 57.5 m and is referred to as Line SP1 and the other section goes from 57.5 m to 115 m and is referred to as Line SP2 (Fig. 11 and 12).

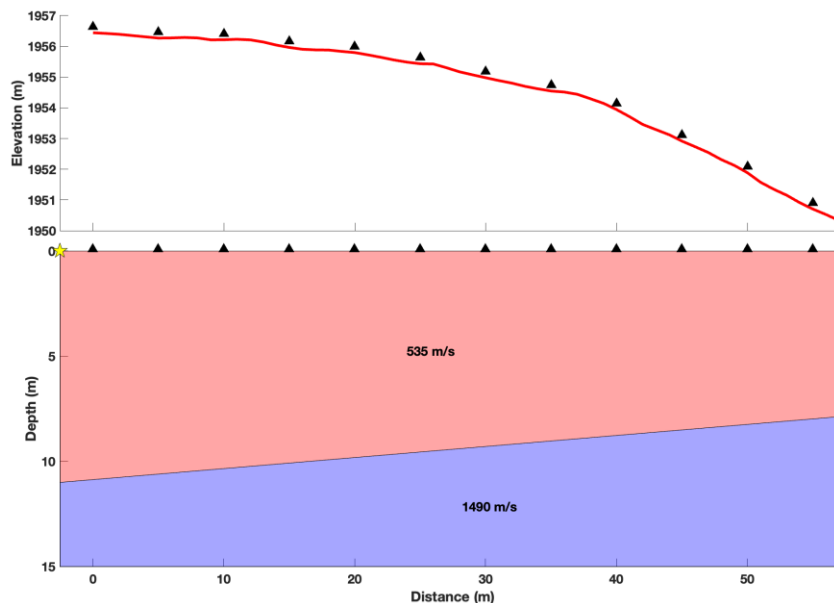


Fig. 11. Refraction modeling for Line SP1. Top: Elevation profile along geophone array for Line SP1. Black triangle mark geophone locations for geophones 1-12. Bottom: Cross section of modeled velocity structure alone Line SP1.

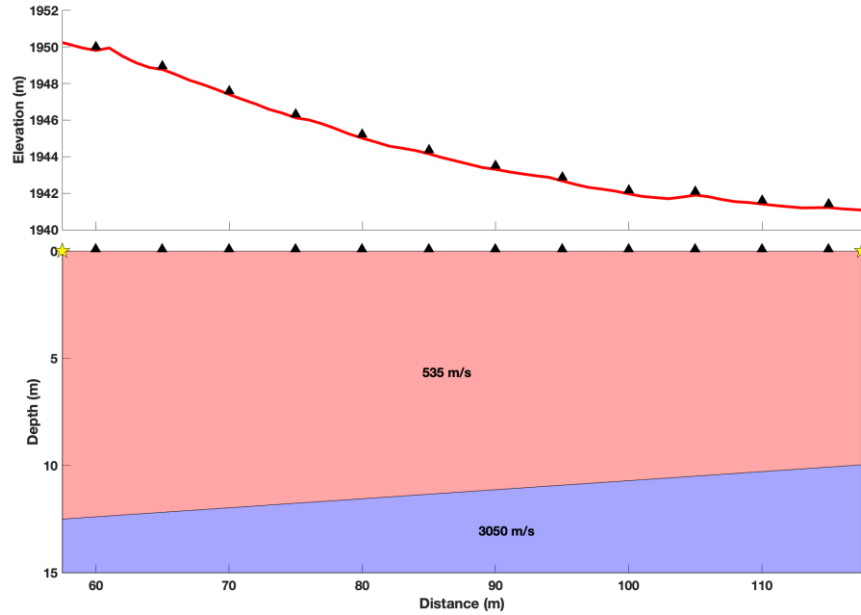


Fig. 12. Refraction modeling for Line SP2. Top: Elevation profile along geophone array for Line SP2. Black triangle mark geophone locations for geophones 13-24. Bottom: Cross section of modeled velocity structure alone Line SP2.

The cross sections produced from refraction modeling on two sections of Line SP are shown in Figs. 11 and 12. Again, these models were created with no corrections for topography or any subsurface heterogeneity aside from a dipping interface. The p-wave velocity for the upper Verdos Alluvium shale layer in both models is identical at 535 m/s. Again, because we have no correction for surface elevation, the dip of the interface between the two layers is largely meaningless.

The two segments of line provide drastically different values for the V_p of the shale. While not relevant for the reflection work, it's worth noting that the higher velocity for that shale given by the model from Line SP2 (Fig. 14) is likely more correct. Fig. 13 shows that the apparent velocity for the predicted arrival times from the model for Line SP1 are probably a good deal lower than the observed apparent velocities. It's likely that the topography is interfering with the observed times in such a way that the inversion could not fit the velocities of both layers properly. Fig. 14 shows the comparison of the modeled and observed arrival times for Line SP2. While the overall RMSE for this model is not much lower than Line SP1 (3.7 ms vs 3.9 ms) it seems that the slopes for the apparent velocity of the deeper layer more accurately fit the observations.

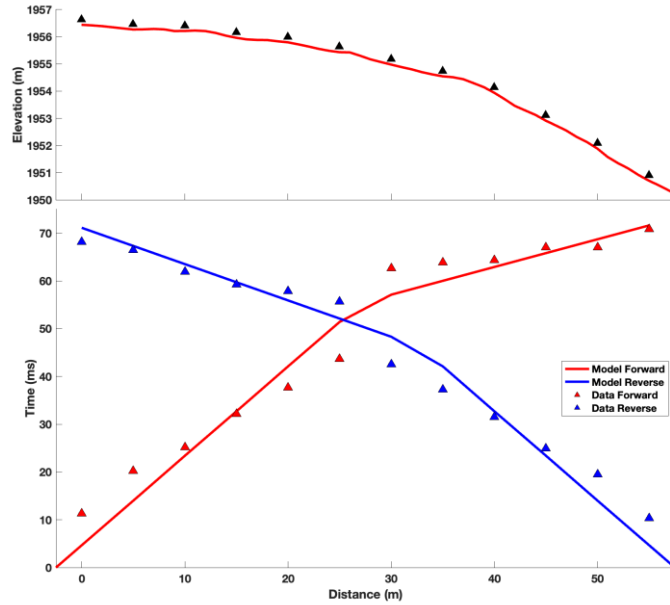


Fig. 13. Refraction modeling Line SP1. Top: Elevation profile along geophone array for Line SP1. Black triangle mark geophone locations for geophones 1-12. Bottom: Observed and model predicted travel times for direct and refracted arrivals along Line SP1.

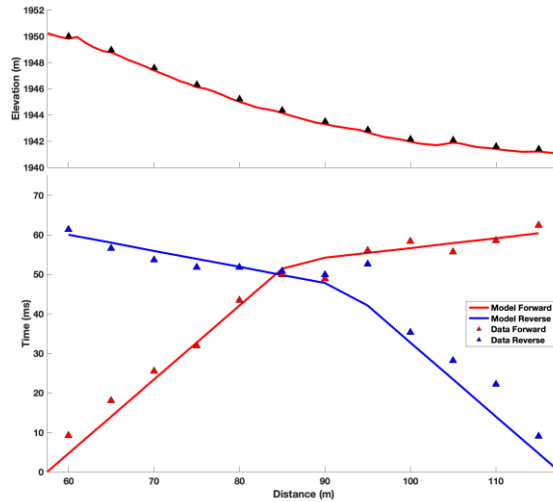


Fig. 14. Refraction modeling for Line SP2. Top: Elevation profile along geophone array for Line SP2. Black triangle mark geophone locations for geophones 13-24. Bottom: Observed and model predicted travel times for direct and refracted arrivals along Line SP2.

A static elevation correction was applied using a V_p of 535 m/s. However, instead of using the lowest elevation we use the elevation of the shot/receiver located at 5 m, a higher point on the line, simply for easier display. The relative delay times between arrivals is unaffected by the choice of reference elevation. Figure 15 shows the forward shots with 15 m offset for the full Line SL. At first glance, it seems quite apparent that the overall structure of arrivals is highly impacted by the static elevation correction. For this reason, we also include a 15 m offset forward shot COG for the raw, uncorrected data in Fig. 16. Without a more detailed analysis of the effect of topography, it's difficult to say which COG image is more accurate.

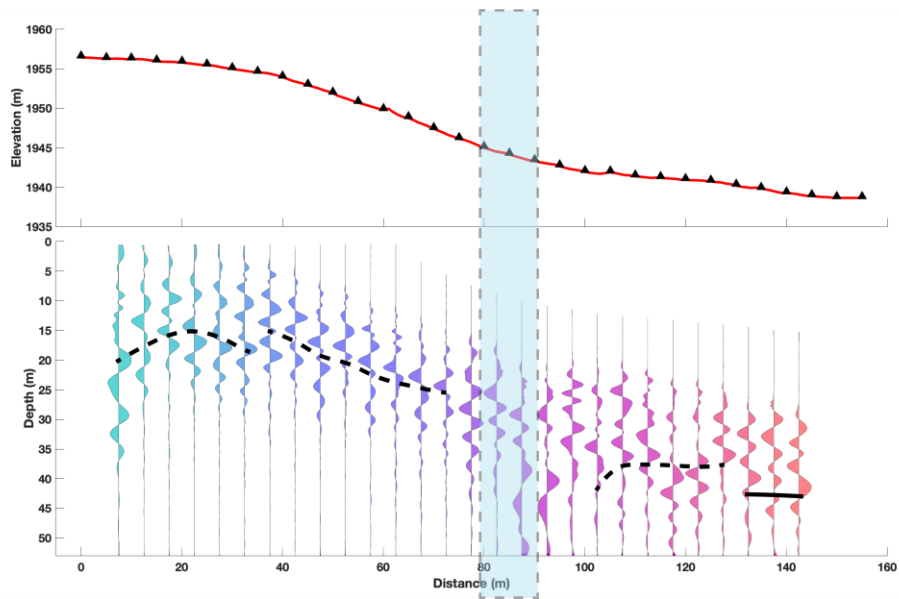


Fig. 15. Line SL: 15 m COG with forward shots. Blue shaded region represent approximate location of inferred Ute Pass Fault. Black lines show possible reflections.

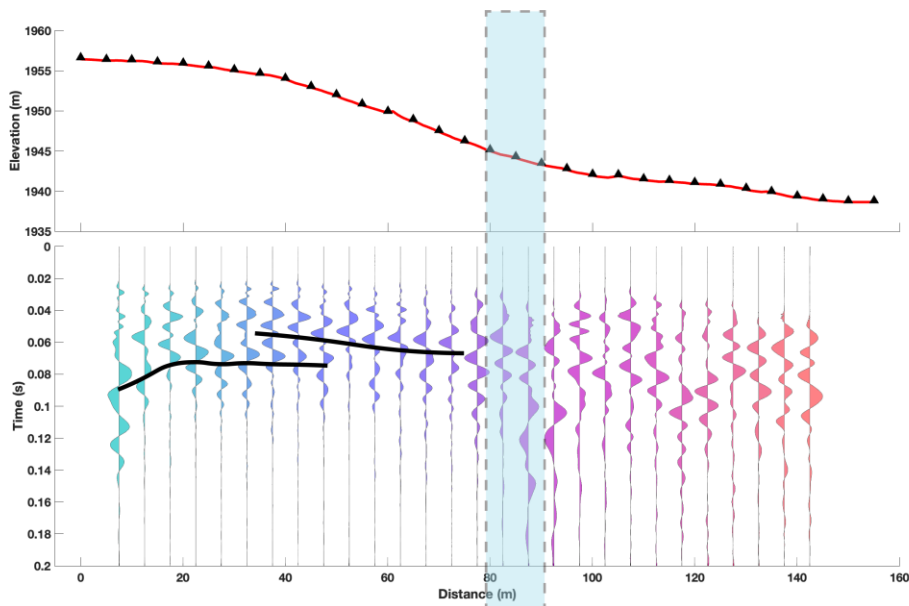


Fig. 16. Line SL: 15 m COG with forward shots on non-static-corrected, raw data. Blue shaded region represent approximate location of inferred Ute Pass Fault. Black lines show possible reflections. Note that the y-axis is time, not converted to depth

However, one feature can be observed clearly in both images. On the first ~ 80 m of the profile, there is one, or possible two fairly continuous signals. It's difficult to trace a them beyond 80 m distance in either Figures 15 or 66. Considering the two images together, it's difficult to say what the geometry of the reflector is, considering how sensitive its shape is to the topographic correction. It's entirely possible that the topography itself is dependent of the shape of the underlying bedrock layer and the reflector does indicate a curvature in the interface. It would be helpful to collect a line of refraction data going perpendicular to our existing line to better constrain the seismic velocities and thicknesses of the alluvium.

4.5 Reconciling Geophysical Interpretation with Surface Geology

Figs. 15 and 16 indicate two reflectors beneath the upper half of the survey line (SP1). The upper reflector on the depth section (Fig. 15) basically parallels the scarp ground surface at a depth of 10-12 m. While this depth is greater than the measured 7.6-8.4 m thickness of Qg2u gravels 175 m to the SW, it is likely that this upper reflector represents the Qg2u/Kp contact observed in the field. The lower reflector lies ~4 m below the upper reflector, but does not parallel the scarp surface or the upper reflector. It has an anticlinal shape suggestive of localized folding in ductile bedrock. We did not observe any pervasive folding in Kp exposed discontinuously on the southern rim. However, landslides are common in the Pierre Shale near the Splay fault, and local folding such as caused by landslide back-rotation might explain the lower reflector.

Reflectors beneath the lower half of the seismic line (SP2) also reflect the surface topography, which slopes more gently than on line SP1. However, the reflectors are deeper beneath the surface, with the upper reflector 12-17 m below the surface and the lower reflector 15-16 m below the surface. Beneath the center of the scarp reflections are incoherent, which would be expected if a fault zone had broken the top of Kp bedrock. In that case, the Qg2u/Kp contact might have been scoured out during initial Qg2u deposition, disrupting the clear reflector at the fault zone. Unfortunately, there are no internal reflectors within the Qg2u gravel deposit, so we cannot see if the gravel itself is faulted.

If the upper reflector on Lines SP1 (10-12 m deep) and on SP2 (12-17 m deep) represents the same Qg2u/Kp contact, then Qg2u alluvium is slightly thicker downslope of the scarp. However, thicker alluvium downslope of the scarp is predicted by all fault geometry options, including those where a fault exists (options 1-4) and the erosional option (option 6). However, the additional alluvium thickness below the scarp is small (0 to 5 m), on the same scale as the alluvium thickness change along strike between the south rim (7.6-8.4 m) and the seismic line (10-12 m), an increase of 2.4 to 3.6 m. So arguably, the thicker alluvium downslope of the scarp may simply reflect natural lateral variability.

5. French Creek Landslide Site

5.1 Structural Setting

The French Creek landslide lies in the Central section of the UPF, on the west side of Fountain Creek between the towns of Cascade and Manitou Springs (Fig. 17). The UPF in the Central section has a very linear trace regardless of topography, indicating a near-vertical dip. This has led past workers to infer mainly strike-slip motion on this fault section.

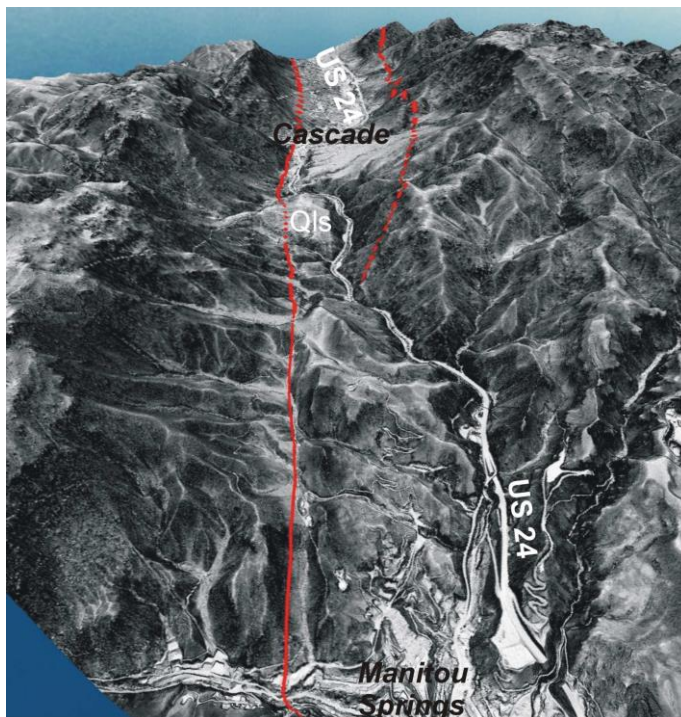


Fig. 17. Oblique lidar view to the NW up Fountain Creek, showing part of the Central section of the UPF, with the French Creek landslide (Qls) at upper center. Mapped traces of the UPF shown by red lines.

The strike-slip analogy is supported by the geomorphology of the UPF between the French Creek landslide and the Town of Manitou Springs (Fig. 18). The UPF is expressed as a linear, fault-controlled valley perched on the western sideslopes of the Fountain Creek valley. Roughly a dozen tributary streams cross the UPF as they flow NE toward Fountain Creek. In almost every case, the stream channel on the SW (upslope) side of the UPF is juxtaposed against a ridge crest at the fault trace, and is forced to deflect to the right or left. In other words, it looks like the UPF has laterally shifted the erosional topography. However, the deflections are not consistently in the same sense. The largest deflections (500 to 600 m) are in the center of this section, but have an opposite sense. That implies that the deflections may be erosional misalignments, not tectonic lateral displacements.

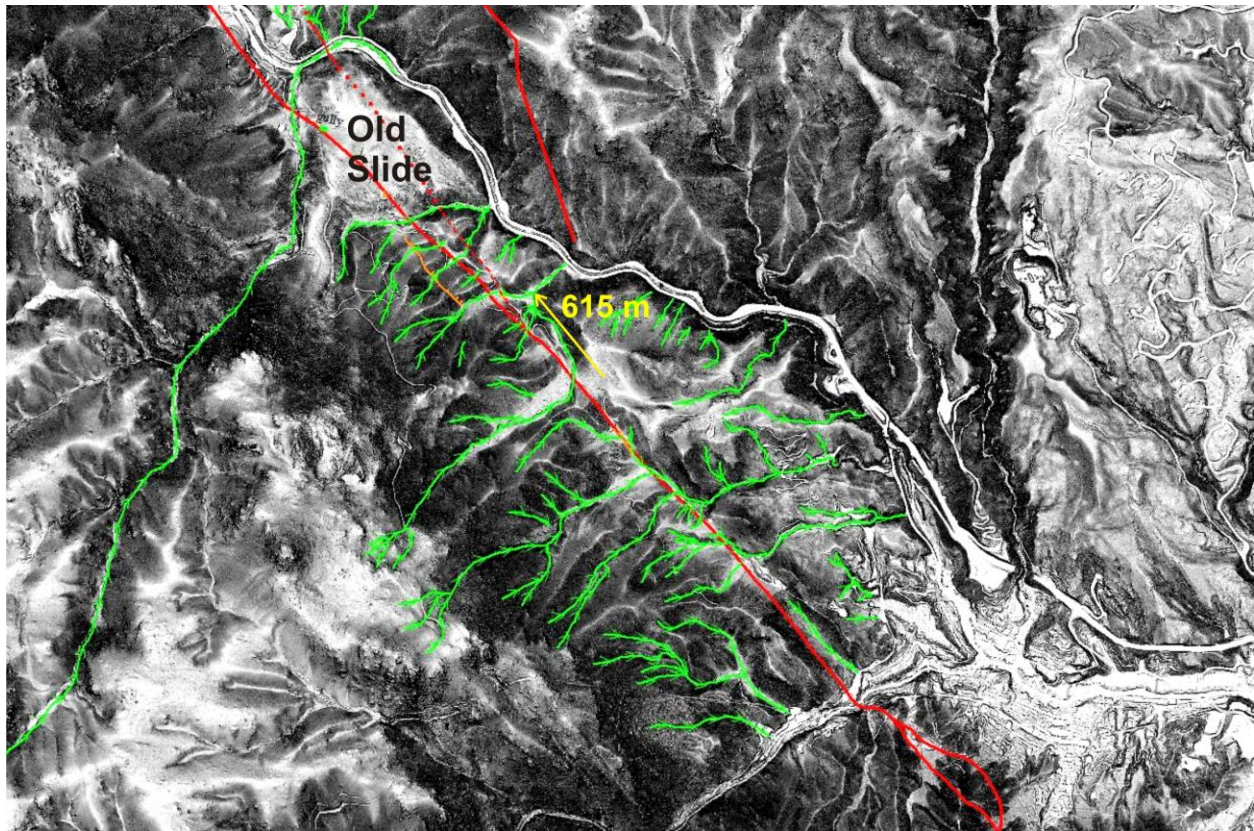


Fig. 18. Streams (green) crossing the UPF between the French Creek landslide (“Old Slide”) and the Town of Manitou Springs (lower right). Both right- and left-lateral stream deflections occur at the UPF, the largest of which is 615 m (left-lateral).

5.2 Surface Geology

At the landslide site Fountain Creek is incised about 100 m into the floor of an older, broad (850 m wide) pre-landslide paleovalley (Fig. 19). The paleovalley floor is well-expressed between the trace of the UPF and the west bank of Fountain Creek, as accordant, low-angle bedrock ridge crests between the tributary valleys. On the east side of Fountain Creek the preserved paleovalley is narrower, often expressed only as a bedrock bench.

Fig. 19 shows that the paleovalley floor west of modern Fountain Creek is bisected by the UPF. Every transverse topographic profile across the paleovalley floor shows that the floor is higher on the E side of the UPF (the downslope side) than W of the UPF. This anomalously reversed topography suggests that the paleovalley floor has been uplifted to the E by the UPF. A less likely explanation is that the Pikes Peak granite (Ypp) on the E side of the UPF is somehow more resistant to erosion than on the W side. However, such a relationship is not seen elsewhere along the UPF. In fact, on most of this fault strand in the Central section, the Ypp has been more deeply eroded on the E side than on the W side.

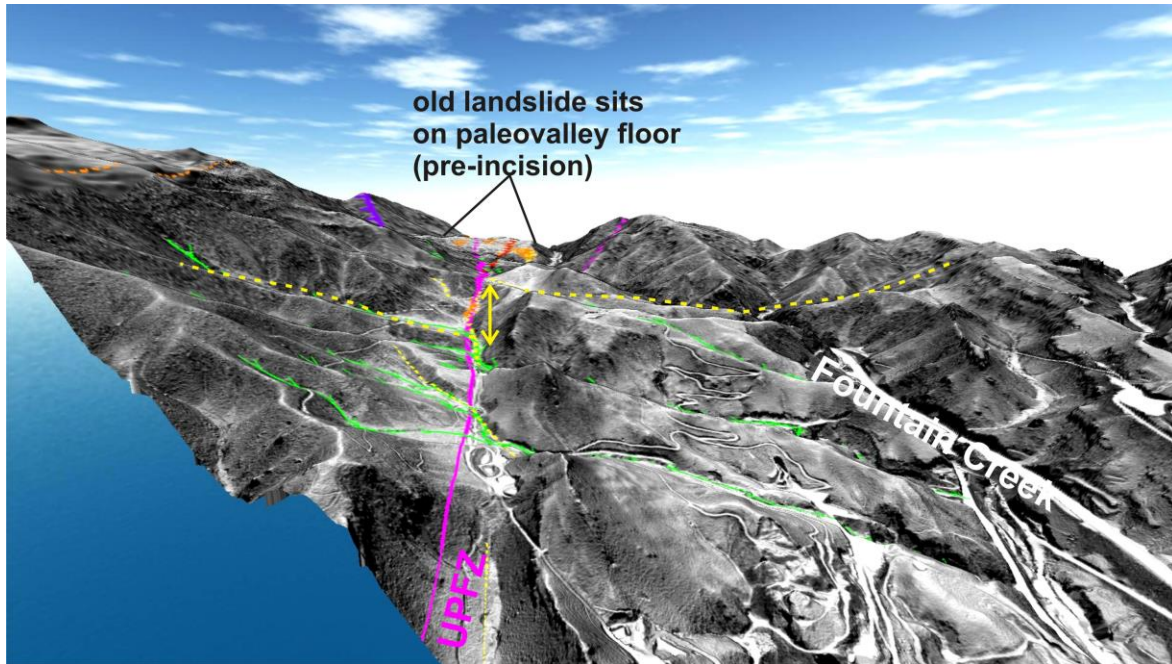


Fig. 19. Oblique lidar view to the NW up Fountain Creek, from just north of Manitou Springs. UPF in purple, tributary streams in green. The paleovalley floor is indicated by a dashed yellow line, which is offset vertically by about 50 m up-to-the E at the UPF.

The French Creek landslide deposit is derived from, and sits upon, the Pikes Peak granite (Fig. 20a). Its probable source area is a scooped-out section of the valley-wall escarpment of Fountain Creek, directly upslope from the slide mass. French Creek currently flows through this scooped-out area is a series of waterfalls, and then is slightly incised into the N margin of the slide down to its confluence with Fountain Creek. The hummocky topography contains some non-random elements such as fault-parallel gullies and slope breaks which are possibly the surface expressions of post-landslide strike-slip faulting (Fig. 20b). According to two luminescence dating samples (see Fig. 20b caption), the landslide deposit directly overlies stratified, sandy pre-slide alluvium dated at ca. 32-35 ka (see Appendix 1).

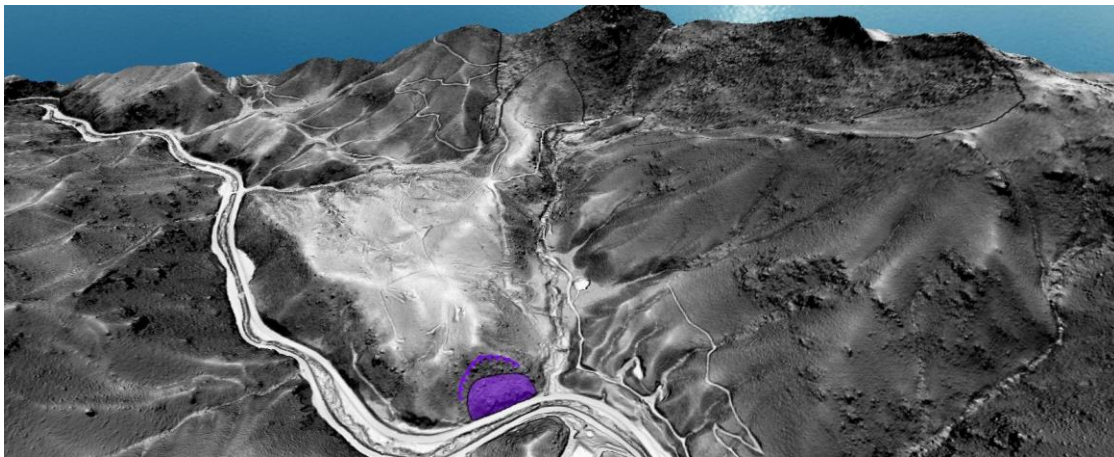


Fig. 20a. Oblique lidar DEM looking SE at the surface of the French Creek landslide (hummocky low-angle surface at left center) and the probable slide source area on the steep valley-wall escarpment to the right. Purple line and polygon are a secondary slump that postdates the main slide mass. Two

luminescence dating samples were collected from the steep roadcut into the landslide deposit just to the left of the secondary slump.

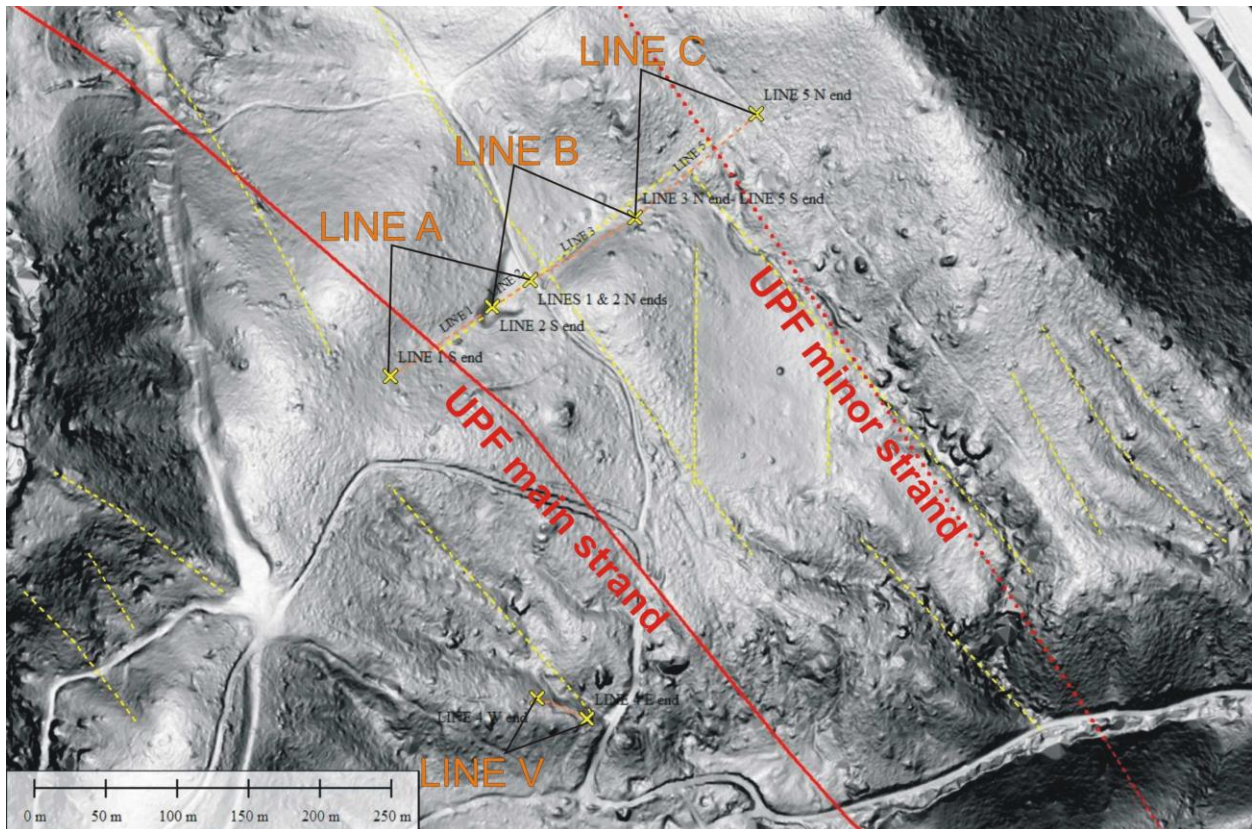


Fig. 20b. Lidar DEM of the French Creek landslide, showing mapped strands of the UPF (red lines); lidar-interpreted lineaments (yellow dashed lines); and geophysics lines (orange dashed lines between yellow X's).

5.3 Seismic Survey Lines

5.3.1 Refraction Lines

We used seismic refraction modeling to determine approximate seismic velocities for the landslide deposits which overlie the crystalline rock. Due to the varying topography in the study area as well as the unknown thickness of the landslide deposits, we positioned a refraction line 312 m south of our main line (Line V on Fig. 20b), where the landslide-crystalline rock contact is exposed in a roadcut. We measured the thickness of the slide deposit at this location as approximately 5-6 m. This thickness value informed the velocity structure modeling along this profile which is referred to as Line V.

5.3.1.1 Line V (Calibration Line for Refraction)

Our refraction model was developed using Refract 2.1.2 by Craig H. Jones. This software allows for multiple dipping interfaces, although all interfaces must be planar. Our model was parameterized to be a single layer over a half space representing the landslide deposits overlying crystalline bedrock. The resulting model is shown in Figure 21. There is considerable topographic variation along our profile however the surface is relatively planar. This leads us to believe our travel times are useful without a static elevation correction. We interpret the depth to the interface between our two layers to represent the depth from the surface.

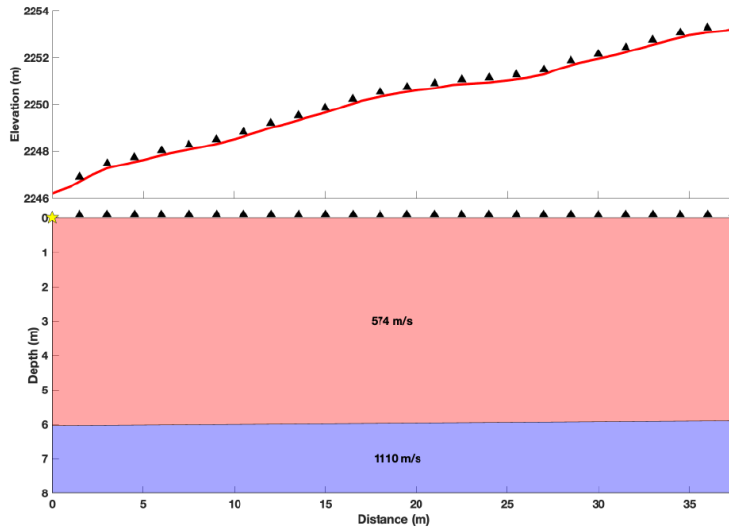


Fig. 21. Top: Elevation profile along geophone array for Line V. Black triangle mark geophone locations. Bottom: Cross section of modeled velocity structure along Line V.

Fig. 22 shows the predicted model arrival times plotted against the observed arrival times. While it is likely that the topography plays a role in the uncertainty of the arrival times, our model can roughly reproduce the two apparent velocities seen in the observed arrival times on forward and reversed shots. This model has a root mean squared error (RMSE) of ~ 4.4 ms. While we were able to create other models that had lower RMSEs, this is still our preferred model because the landslide deposit thickness more accurately reflects our field observation. This model yields a seismic p-wave velocity (V_p) for the landslide deposit of 574 m/s.

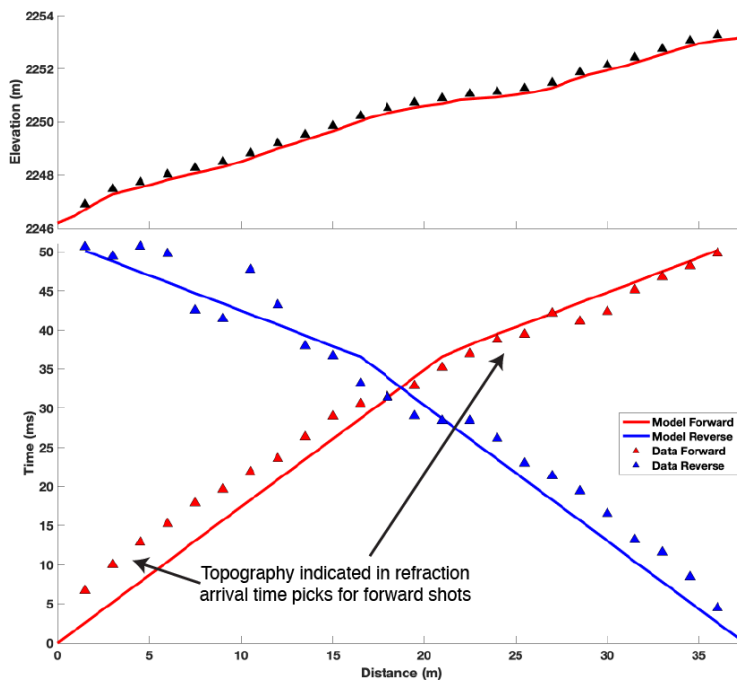


Fig. 22. Top: Elevation profile along geophone array along Line V. Black triangle mark geophone locations. Bottom: Observed and model predicted travel times for direct and refracted arrivals along Line V.

5.3.1.2. LINE A (Fig. 23)



Fig. 23. Photo looking N55E down the lower part of Line A, as it traverses an old borrow area adjacent to access road (both visible on Fig. 21). Line B overlaps the area shown in foreground.

Additionally, the velocities derived from this model were also consistent with a model of the refracted arrival times for the southwestern-most segment of the geophysics line, Line A. Like Line V, Line A has varying topography but is relatively planar. Refraction modeling for this line was used to generate the cross section show in Figure 24. This model yields a V_p of 599 m/s, in close agreement with the model for Line V. The model for Line A doesn't account for any possible vertical offset on an underlying fault, but even as a rough approximation, it is useful in affirming our V_p estimate from Line V. The velocity values obtained from these models were used to generate static elevation corrections for the reflection profiles for Lines A, B, and C, as well as create time to depth conversions using a V_p of 580 m/s.

Static elevation corrections were performed on Lines A, B and C relative to the lowest elevation shot/receiver position on the respective line. In the corrected shot gathers, the time axis on the seismograms was adjusted to account for both the elevation of the shot and the elevation of each receiver, relative to the lowest elevation shot using the V_p velocity of 580 m/s to convert the elevation differences to time differences.

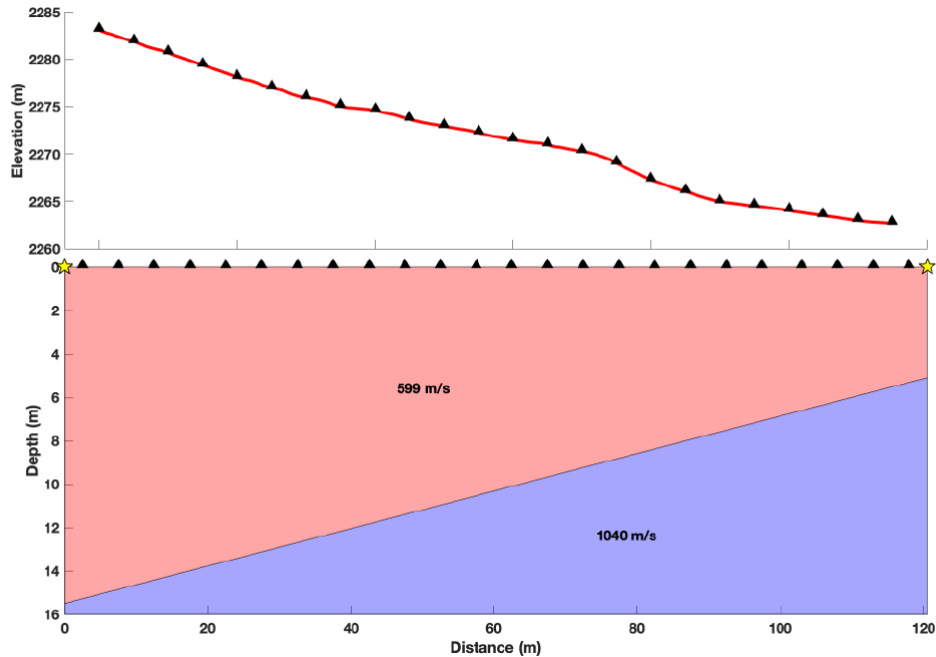


Fig. 24. Top: Elevation profile along geophone array for Line A. Black triangle mark geophone locations. Bottom: Observed and model predicted travel times for direct and refracted arrivals.

5.3.2 Reflection Lines

For simplicity and computational speed, we used a common offset gather (COG) to display and interpret the reflection data. In a COG, a seismic section is displayed using shot/receiver pairs that are separated by the same horizontal distance. This produces a reflection image directly from static corrected data without using computationally expensive move out corrections or migrations associated with other types of reflection data processing. The primary downside to this method is we do not get any signal to noise enhancements of the reflected arrivals that are gained by common midpoint stacking or other more sophisticated types of seismic processing. We also lose accuracy in the locations of our structures as we are plotting the selected seismograms at the midpoints between the shot and receiver locations and assuming that all ray paths are near vertical. Because there is no signal to noise enhancement of reflected phase in a COG, other seismic phases such as ground roll will align neatly and can be misinterpreted as a reflection. COG creates images where reflecting structures maybe less apparent or poorly positioned, resulting in increased opportunities for misinterpretation.

By inspection of the static corrected shot gathers, we determined that an optimum window for reflected arrivals occurred on 15 and 20 m offsets. Figures 25 to 27 show static corrected shot gathers along Lines A, B and C, respectively. These figures highlight the suspected reflected arrivals that were used to determine the optimum window and associated offset.

For each line we create common offset gathers using both a 15 m and a 20 m offset. In addition to two offset lengths, for each length we also used two offset directions. Meaning that, for a 15 m offset, we created a gather for when the receiver was at a 15 m greater distance along the profile than then shot (i.e. shots are left of the receivers on the cross section, or a forward shot), and a gather for when the shot was at a 15 m greater distance than the receiver (i.e. a reverse shot). The COG images are presented in the following sections with light blue rectangles

indicating approximate locations of inferred faults as well as the topographic profiles of the lines.

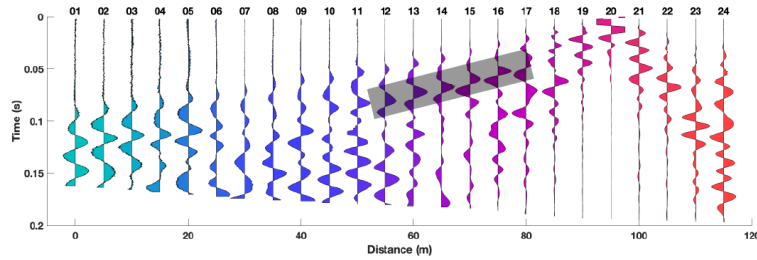


Fig. 25. Static corrected shot gather for Line A with shot location at 95 m corresponding to the location of geophone 20. Grey box shows reflected arrivals for offsets ranging from 15-40 m.

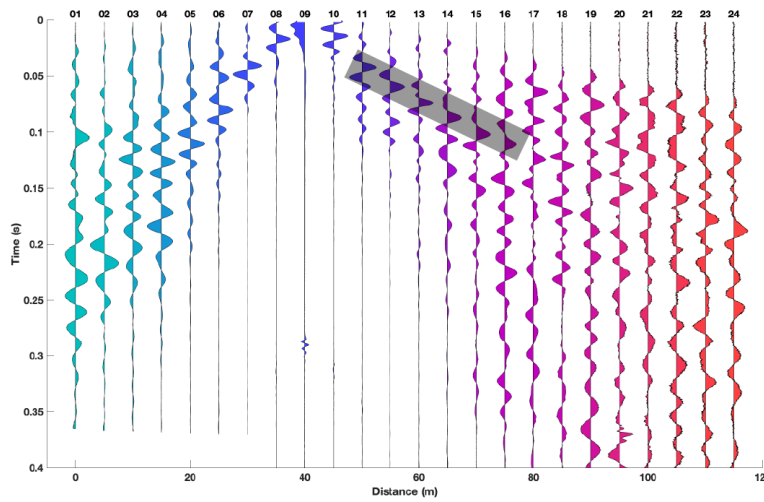


Fig. 26. Static corrected shot gather for Line B with shot location at 40 m corresponding to the location of geophone 9. Grey box shows reflected arrivals for offsets ranging from 10-35 m.

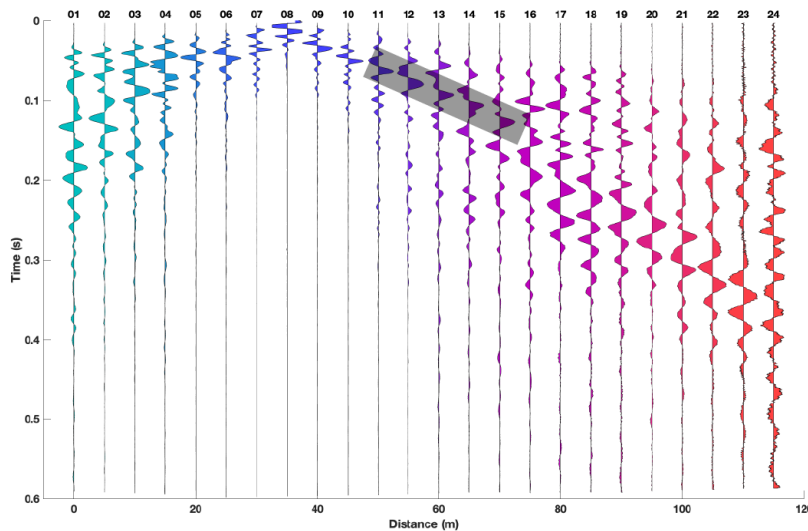


Fig. 27. Static corrected shot gather for Line C with shot location at 35 m corresponding to the location of geophone 8. Grey box shows reflected arrivals for offsets ranging from 15-35 m.

5.3.2.1. LINE A

Figs. 28-30 show the COG for Line A. Fig. 28 shows the forward shot with a 15 m offset. We have marked suspected reflecting surfaces with solid black lines and a more unconvincing reflector with a dashed line. The initial observation that stand out is that we appear to have a change in dip angle of the reflecting surface that occurs very near an inferred fault location . There also appears to be another change in the reflector dip angle near 65 m distance, although at distances greater than 65 m the reflector is much more poorly defined.

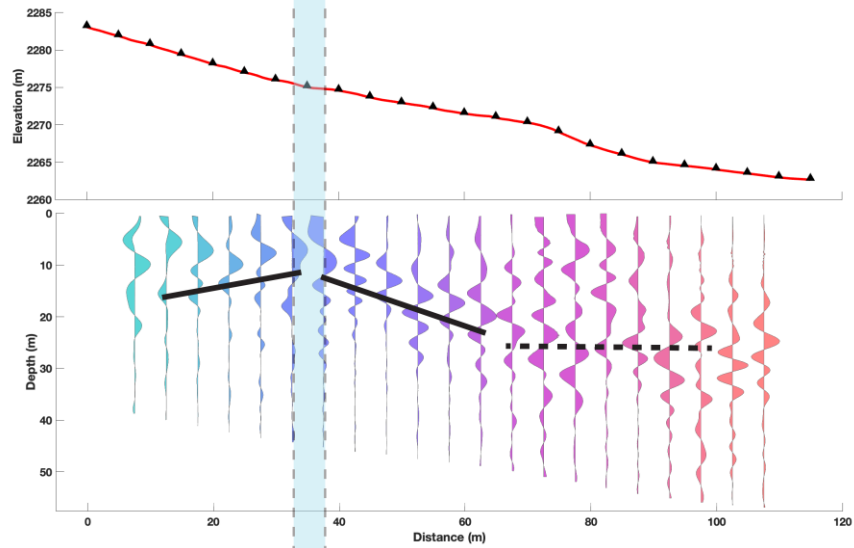


Fig. 28. Line A: 15 m COG with forward shots. Blue shaded region represent approximate location of inferred Ute Pass Fault. Black lines show possible reflections.

In Fig. 29, the same line and offset distance, but for the reverse shot, we see some of the same features, however the reflecting surface is much more poorly defined at distances less that ~20 m. This makes a change in dip angle at the approximate fault location less convincing. However, there is a more pronounced change and dip angle around 55 m distance which suggests that this maybe a robust feature of the reflector, and reprocessing the data on this line with stacking and migration maybe more insightful.

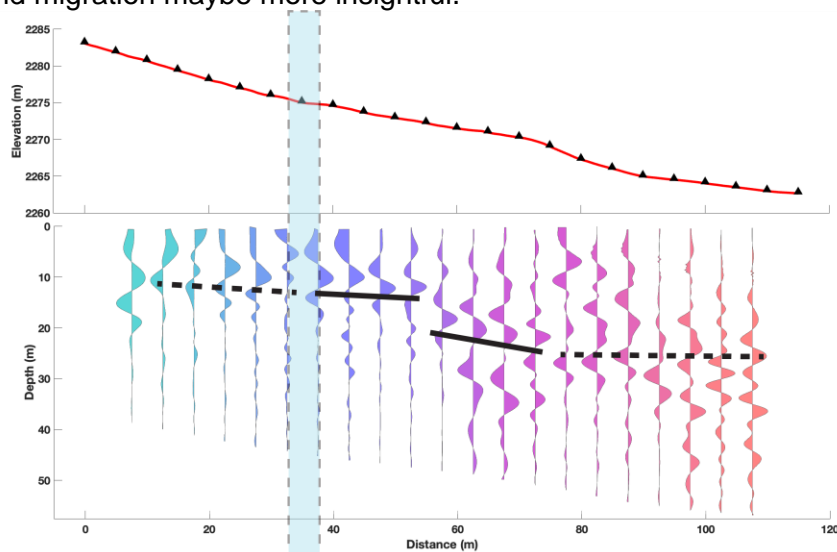


Fig. 29. Line A: 15 m COG with reverse shots. Blue shaded region represent approximate location of inferred Ute Pass Fault. Black lines show possible reflections.

Fig. 30 shows the reverse shot with a 20 m offset. Note that with a greater offset, all reflectors will appear later (visually, lower) in the COG plots since there is no correction for the greater horizontal travel distance. In this figure, we see a more continuous reflector passing through the inferred fault location at ~35 m. But similar to the previous two plots, the reflector becomes much less pronounced at distances greater than about 55 m.

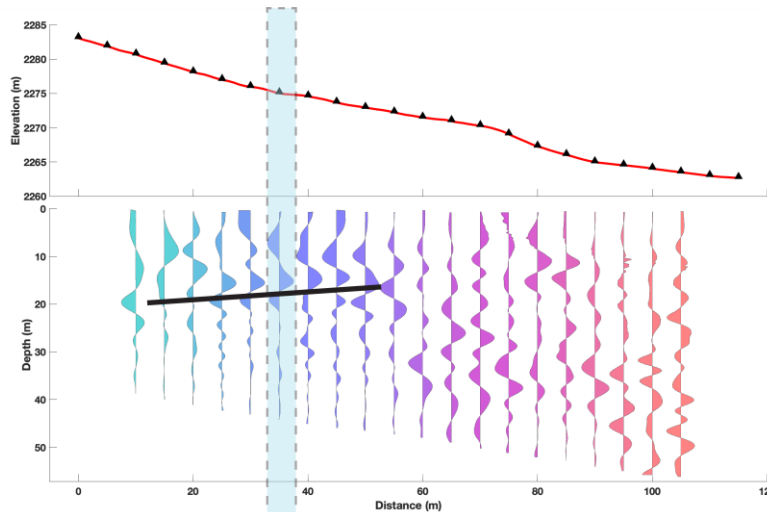


Fig. 30. Line A: 20 m COG with reverse shots. Blue shaded region represent approximate location of inferred Ute Pass Fault. Black lines show possible reflections.

5.3.2.2. LINE B

COGs from Line B are shown in Figs. 31 and 32. In Fig. 31, which shows the 15 m offset with a reversed shot, there is some indication of a reflector starting around ~40 m and going on to greater distances. 40 m is also near the location of an inferred fault. However, there's also some indication of that reflector and distances less than 40 m therefore it's difficult to say definitively that there is a change in the in reflecting surface occurring at the inferred fault location. Unfortunately, the forward shot for the 15 m offset (Fig. 32) isn't much help as there is barely, if any, traceable reflecting surfaces.

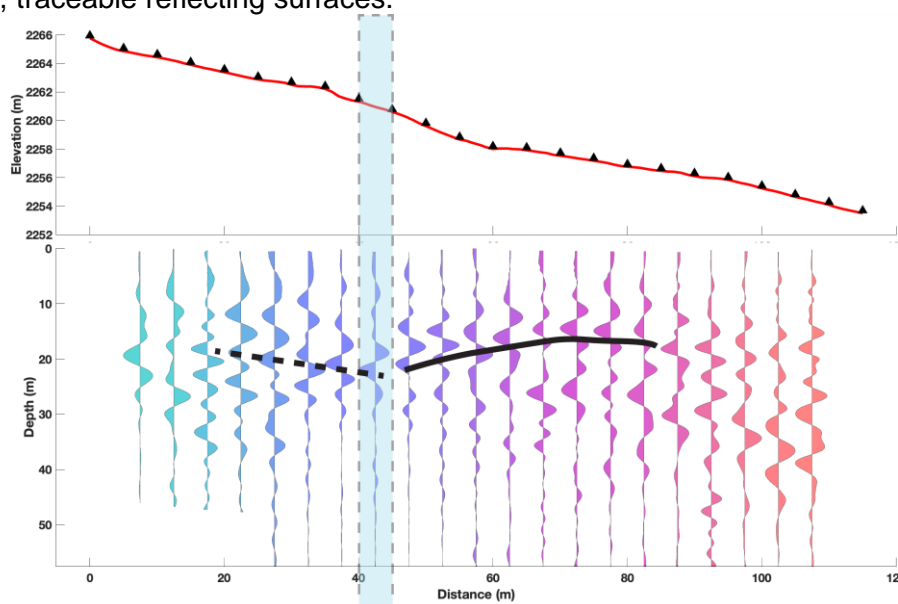


Fig. 31. Line B: 15 m COG with reverse shots. Blue shaded region represent approximate location of inferred Ute Pass Fault. Black lines show possible reflections.

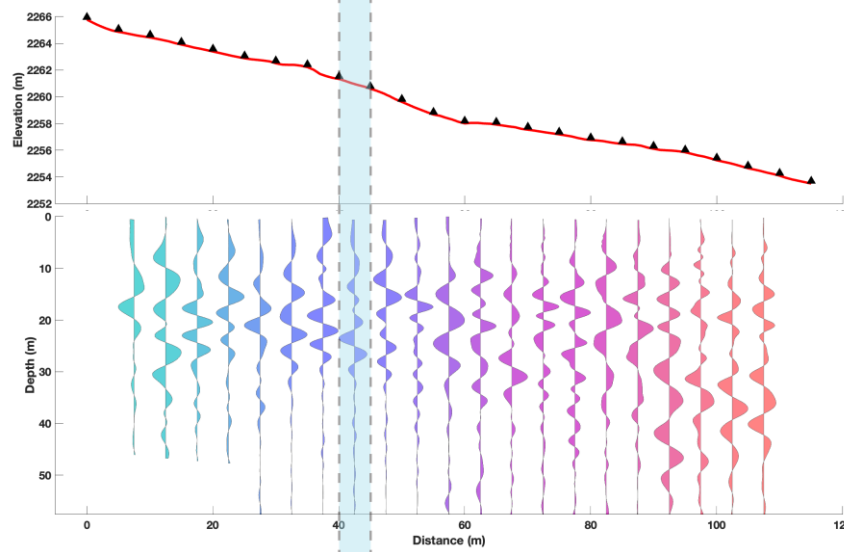


Fig. 32. Line B: 15 m COG with forward shots. Blue shaded region represent approximate location of inferred Ute Pass Fault. There aren't any convincing reflections in this image.

5.3.2.3. LINE C

The image from Line C shows some of the more convincing reflectors in the sets of COGs, shown in Figs. 33-36. Line C also has the most complex topography, and in the 15 m offset shots, it often appears that the dip angles of the reflectors are correlated to the surface topography. This may be due to over or under correcting in the elevation statics, but it may also be a real feature. More sophisticated processing in the future could shed light on this question. Fig. 33 shows the forward shot with 15 m offsets. Again, change in dip angles are located very near inferred fault locations near 50 and 70 m . This is even more so the case in Fig. 34 which shows to reverse shot. At the 20 m offsets, the reflectors are less pronounced, and the possible changes in dip angle seem to occur closer to 60 m distances, between the inferred fault locations. This must be at least partly due to the lower horizontal resolution that comes from having a greater offset distance.

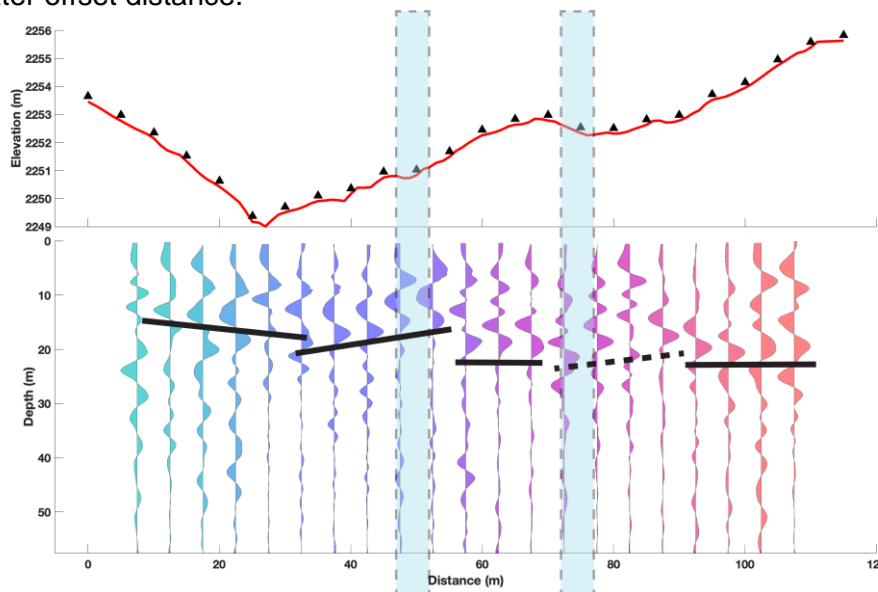


Fig. 33. Line C: 15 m COG with forward shots. Blue shaded region represent approximate location of inferred Ute Pass Fault. Black lines show possible reflections.

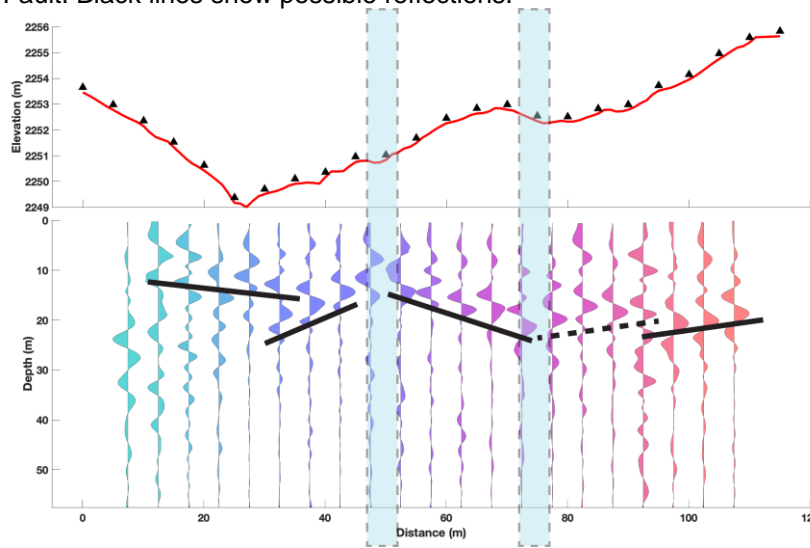


Fig. 34. Line C: 15 m COG with reverse shots. Blue shaded region represent approximate location of inferred Ute Pass Fault. Black lines show possible reflections.

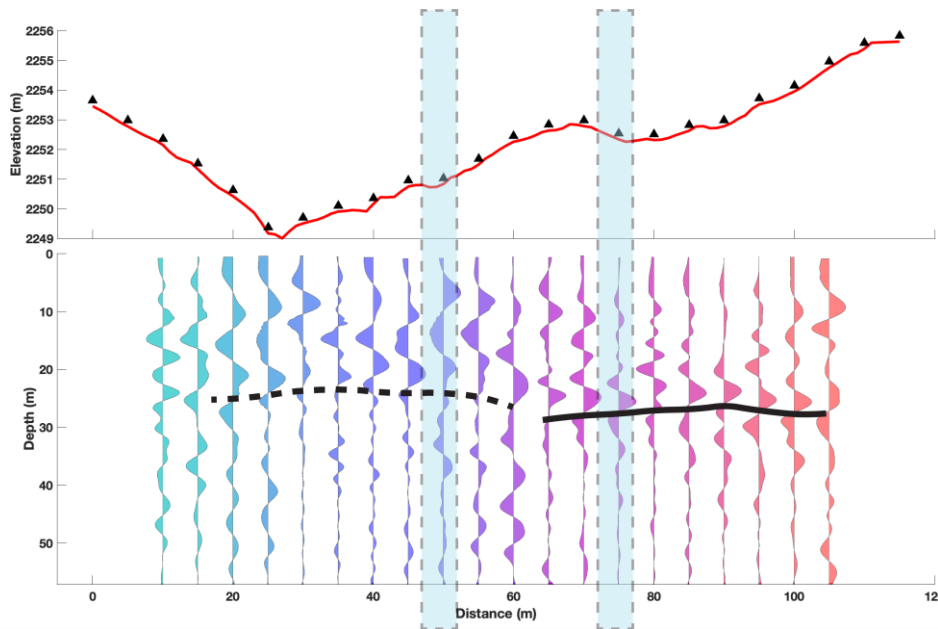


Fig. 35. Line C: 20 m COG with forward shots. Blue shaded region represent approximate location of inferred Ute Pass Fault. Black lines show possible reflections.

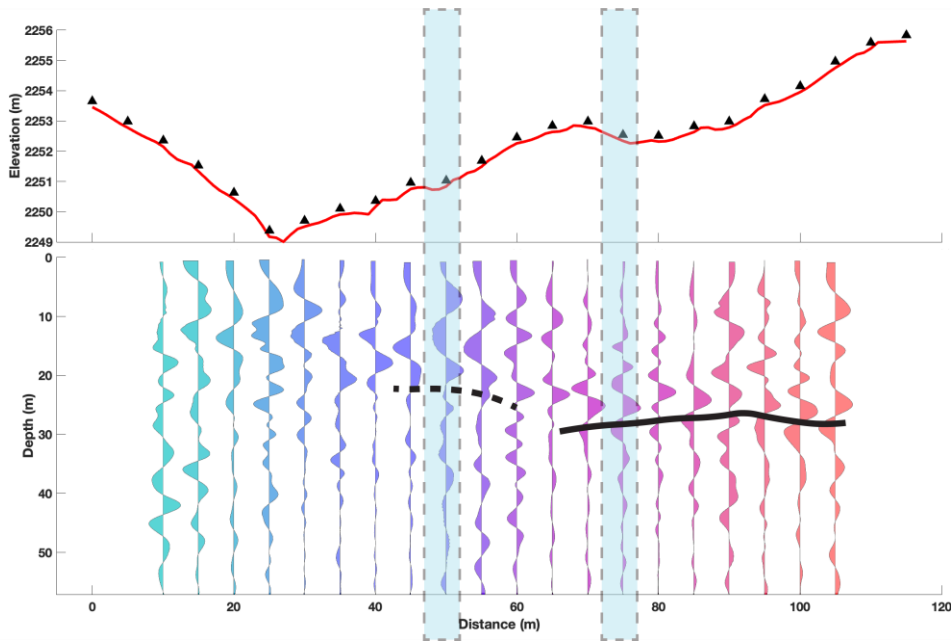


Fig. 36. Line C: 20 m COG with reverse shots. Blue shaded region represent approximate location of inferred Ute Pass Fault. Black lines show possible reflections. This line has the deepest reflections, ca. 29 m below ground surface.

Throughout the three lines, the reflector that we are presuming is from the underlying bedrock arrives at .05-.08 s on the 15 m offset COGs. Based on our refraction velocity modeling, this implies that the landslide deposits are around 12-20 m thick.

5.4 Reconciling Geophysical Interpretation with Surface Geology

Seismic lines A, B, and C indicate that the French Creek landslide deposit is ca. 12-20 m thick, thickening towards the NE end of the lines. In contrast, the contact of the Qls deposit over Pikes Peak granite mapped by Morgan et al. (2004) lies 45 m to 75 m below the top of the Qls deposit. This suggests that the lower 2/3 of the Qls polygon mapped is actually boulder colluvium shed down the slopes from the true, in-situ landslide deposit that is only 12-20 m thick. Such colluviation is to be expected for two reasons. First, even if the landslide came down onto a flat valley floor, the post-slide incision of French Creek (on the N slide margin) and an unnamed creek (on the S slide margin) created steep sideslopes for large boulders to travel down by colluvial processes. Second, the landslide deposit probably came down onto a complex pre-existing topography in the bottom of Fountain Creek. This is indicated in Fig. 37.

We infer that the thickening of the slide deposit to the NE represents slide materials filling up the pre-slide paleochannel of Fountain Creek. A straight-line projection of the modern channel beneath the landslide suggests that the pre-slide channel axis may be beneath the center of seismic Line C.

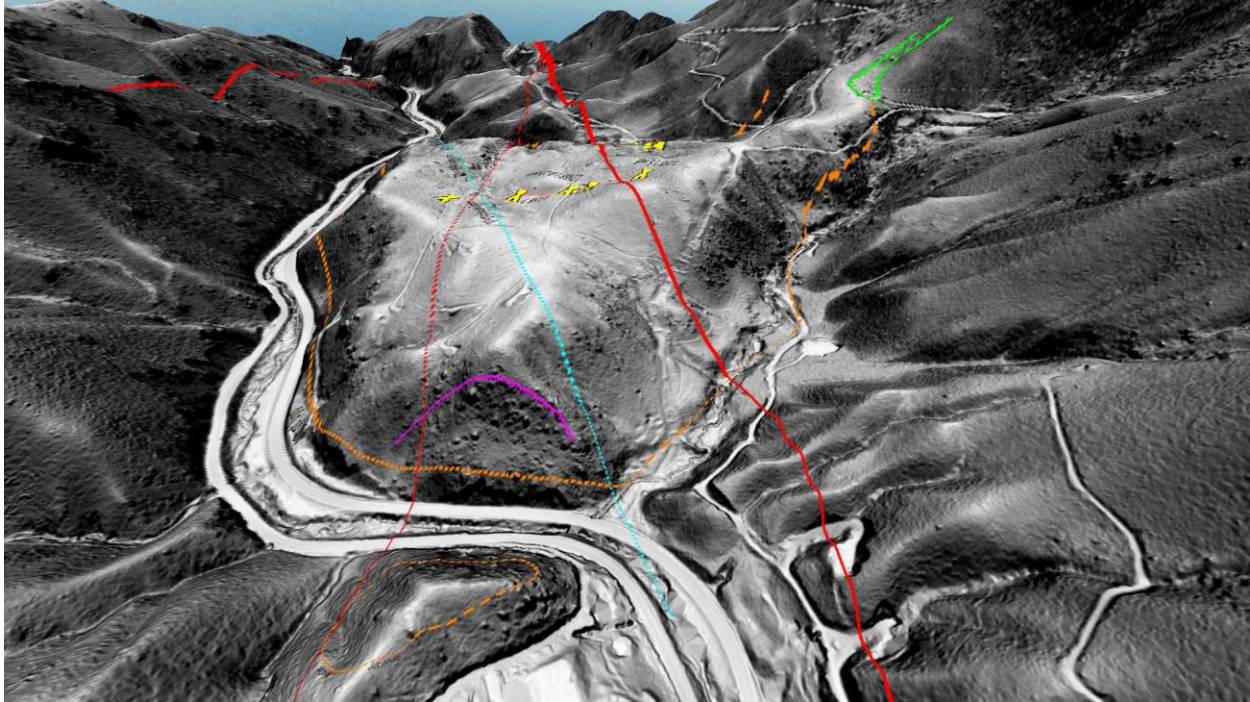


Fig. 37. Oblique lidar view looking SE down Fountain Creek, with the French Creek slide at center. Red lines, UPF fault traces; orange lines, the Qs/Ypp contact; blue line, the projected course of the pre-slide channel axis of Fountain Creek. The implication is that the slide completely filled the pre-existing channel of Fountain Creek and climbed up the opposite valley wall (orange polygon at lower left), where the Qs deposit preserved today is >8-9 m thick. Yellow X's show endpoints of contiguous seismic Lines A, B, and C, with C at left.

Fig. 38 attempts to reconstruct the pre- and post-slide topography, given the available geological and geophysical data. Stage 1 shows the elevations of geologic contacts today, as mapped by Morgan et al. (2004). Stage 2 assumes that the current Qs/Ypp contact facing Fountain Creek is the bottom of the true landslide deposit as originally emplaced. This results in a landslide thickness of ~50 m, which contradicts the seismic interpretation. Stage 3 assumes that the true landslide thickness is ~15 m, and that the slope facing Fountain Creek is covered with colluvial boulders in a much thinner layer. It further assumes that the pre-slide channel of Fountain Creek was at the same elevation as the top of bedrock on either valley wall today. Stage 4 reconstructs the landslide thickness resulting from the Stage 3 assumptions. This results in a maximum slide thickness of 35 m where it filled up the pre-slide valley. It further requires that in the past 35 kyrs, Fountain Creek has eroded away the 35 m of landslide deposits and incised an additional 25 m into Pikes Peak granite. The latter seems less likely than the former.

Stage 5 assumes that the pre-slide channel of Fountain Creek in bedrock was the same elevation as today. In that scenario the landslide deposit would be 60 m thick in the valley, all of which was removed by erosion in the past 35 ka. However, it does not require any post-35 ka incision into bedrock.

Stages 4 and 5 are difficult to reconcile with a proposed pre-slide paleochannel being along the straight-line projection shown in Fig. 37. There should not have been two contemporaneous, parallel paleochannels. If the pre-slide paleochannel was in a more central location and completely buried by the slide, then the entire modern incised valley of Fountain Creek was created in the past 35 ka, by erosion of ~35 m of slide debris and 25 m of granite bedrock. This could be accomplished in theory, but would require the spillover point for Fountain Creek (i.e., the low point on the landslide surface) to be located where Fountain Creek is today. However, the top of the preserved landslide deposit today has a low point near the projected straight-line (blue line in Fig. 37), and then begins to gain elevation as it approaches Fountain Creek. Given that geometry, it is hard to imagine that the spillover occurred where Fountain Creek is today.

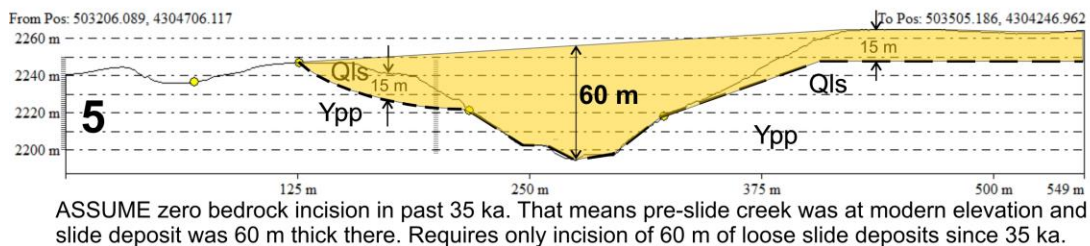
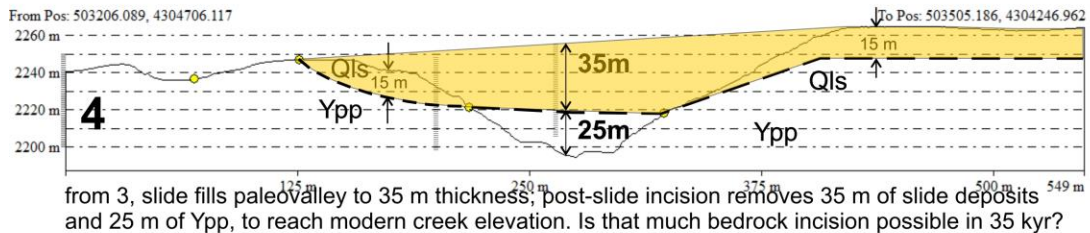
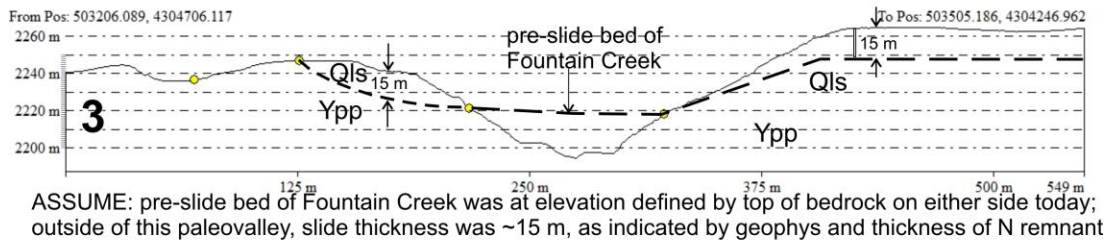
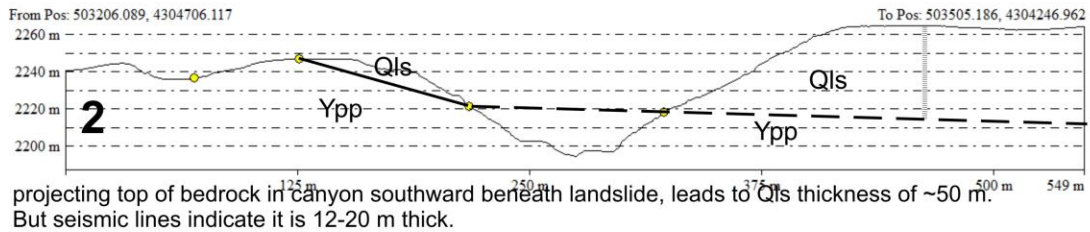
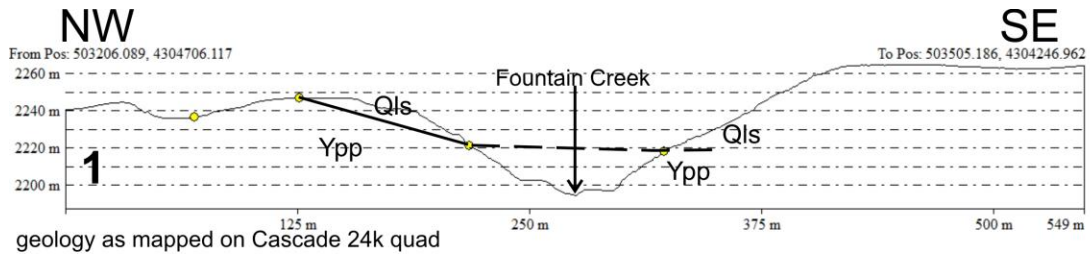


Fig. 38. Conceptual cross-sections of the French Creek slide deposit and the pre-slide valley of Fountain Creek. Stage 1 is earliest, Stage 5 is latest.

The evolution of Fountain Creek and its post-slide erosion would be easier to envision if the slide were older than 35 ka. This would allow more time for Fountain Creek to erode away tens of meters of landslide boulders and granite bedrock. At this time two confirmatory luminescence samples are being processed from the basal contact of the Qls deposit in an area closer to the head of the landslide. If these two ages also cluster near 35 ka, then the analysis shown in Fig. 38 will stand. Conversely, if the two ages come out much older (say, 150 to 300 ka), then Fig. 38 will be revised.

6. CONCLUSIONS

For this project we examined two of the most promising localities for preserving evidence for Quaternary faulting on the UPF. The first site was the splay fault and accompanying scarp across a Verdos-age pediment at the southern end of the UPF. This site was cited by Kirkham and Rogers (1981) as having the best geomorphic & stratigraphic evidence for post-Verdos (<600 ka) but pre-Slocum (>250 ka) fault movement. We interpret Kirkham and Rogers' "tilted block of alluvium" as an unfaulted, post-Verdos paleochannel filled with dipping colluvial strata, underlain by horizontal Verdos channel gravels. Thus, it is not compelling evidence for post-Verdos faulting. The base of the pediment gravels was examined in the field across the mapped fault trace and did not appear to be faulted. Alluvium thickness was essentially identical on both sides of the fault. In contrast, the seismic lines do show some anomalies. The inferred alluvium-bedrock contact reflector cannot be traced beneath the center of the surface scarp, although it exists on either side. Disruption of this reflector could represent pre-Quaternary faulting of the Pierre Shale, however. Overall, there is no compelling evidence for Quaternary faulting at this site.

The second site was the massive rockslide at French Creek in the Central section of the UPF. The landslide deposit is full of house-sized boulders of Pike's Peak granite, which subsequent to the original deposit emplacement, have raveled down the post-slide sideslopes many tens of meters. Thus the true contact between the basal landslide deposit and granite bedrock is covered almost everywhere, and only visible in one or two artificial cuts. Due to a lack of good exposures, it was not possible to assess Quaternary faulting based on surface mapping. Seismic lines did show some reflectors (probably the Q1s/Ypp contact), and on four of the seismic lines breaks in reflectors occurred beneath mapped fault traces (Line A, Figs. 28, 29; Line B, Fig. 31; Line C, Fig. 34). On the other five lines there were either no breaks in reflectors, or if there were, they did not lie beneath mapped faults.

It was hoped that seismic sections might show shallow reflectors vertically offset at shallow (<5 m) depths, which could then be exposed by a deep paleoseismic trench. But the only consistent reflector occurred at depths of 12 to 20 m, too deep to trench. And although there were breaks in the main reflector, there were no clear vertical offsets of a single, good reflector. So a more advanced geophysical campaign would have to be mounted to see reflectors at the resolution needed. Even that may be futile, however, because the landslide deposit is apparently not stratified, being composed of house-sized boulders in a finer matrix. So it might be very difficult to see offsets in such massive deposits at the bottom of a trench, even if trenching were possible. We saw hundreds of boulders at the surface that were large enough to stop any attempt at trenching.

It is just as important to note what we did NOT observe in this study. In all our lidar mapping, we never saw a linear scarp crossing a Holocene or late Pleistocene deposit (Pinedale or Bull Lake equivalent) that was not clearly erosional (such as a terrace riser). Even on the oldest geomorphic surfaces mapped in the area, such as the Miocene-Pliocene Divide paleovalley deposit, there are no surface scarps along the mapped faults. This is true even where the fault trace offsets paleovalley gravels. In places along these faults there is sometimes vertical relief, but half of the time the relief is opposite to the movement direction of the fault, which indicates the relief is from differential erosion, not from direct faulting.

7. ACKNOWLEDGMENTS

This study would not have been possible without the support and landowner permission granted by:

Northern Section: Town of Woodland Park Planning Department (Robyn Brown, Sally Riley, David Burgess, Lor Pelligrino).

Central Section: Colorado Springs Utilities (Brian McCormick); Manitou Springs Water (Mike Cobb)

Southern Section: Golden Eagle Ranch LLC (R.W. Steer)

8. REFERENCES

Berglund, H.T., Sheehan, A.F., Murray, M.H., Roy, M., Lowry, A.R., Nerem, R.S. and Blume, F., 2012, Distributed deformation across the Rio Grande rift, Great Plains, and Colorado Plateau: *Geology*, 40(1): 23-26.

CGS, 2013, Hazus-MH: Earthquake Event Report; Region Name, Ute Pass M7; Earthquake Scenario, Ute Pass fault 7.0: unpublished hazard report, Colo. Geol. Surv., Denver, CO, June 07, 2013, 21 p.

Carroll, C.J. and Crawford, T.A., 2000, Geologic map of the Colorado Springs quadrangle, El Paso County, Colorado: Colo. Geol. Surv., Open-File Map 00-3, scale 1:24,000.

Dickson, P.A., Kewer, R.P. and Wright, J.E., 1986, Regional fault study, central Colorado Front Range, Colorado, in Rogers, W.P. and Kirkham, R.M. (eds.), *Colorado Seismicity and Tectonics —A 1986 Update*: Colo. Geol. Surv. Special Pub. 28, p. 172-185.

Dyman, T.S. and Charpentier, R.R., 1992, Measured sections of the Cambrian Sawatch Quartzite and Peerless Formation, and the lower part of the Ordovician Manitou Formation, Manitou Springs area, Front Range of Colorado: USGS Open-File Rept. 92-718, 6 p., 1 Plate.

Epis, R. C, and Chapin, C. E., 1975, Geomorphic and tectonic implications of the post-Laramide, late Eocene erosion surface in the southern Rocky Mountains, in Curtis, B. F., ed., *Cenozoic history of the southern Rocky Mountains*: Geol. Soc. America Mem. 144, p. 45-74.

Epis, R. C, and others, 1976a, Petrologic, tectonic, and geomorphic features of central Colorado: Colorado School Mines Prof. Contr. 8, p. 301-322.

Geotechnical Advisory Committee (ed.), 1985, Geologic and Seismotectonic Investigations, East-Central Front Range, Colorado, Second Interim Report: Denver Water Department, Denver, CO, July 1985, 161 p.

Geotechnical Advisory Committee, 1986, Geologic and Seismotectonic Investigations, East-Central Front Range, Colorado, Summary Report: Denver Water Department, Denver, CO, January 1986, 117 p.

Harms, J. C, 1959, Structural geology of the eastern flank of the southern Front Range, Colorado: Univ. Colorado Ph.D. Thesis, 165 p.

Harms, J. C., 1964, Structural history of the southern Front Range: *Mtn. Geologist*, v. 1, p. 93-101.

Harza Engineering Company, 1985, Report A, Regional Fault Study, *in* Geotechnical Advisory Committee (ed.), *Geologic and Seismotectonic Investigations, East-Central Front Range, Colorado*, Second Interim Report: Denver Water Department, Denver, CO, July 1985, 71 p. plus Map Folio.

Himmelreich, J.W. Jr and Noe, D.C., 1999, Map of Areas Susceptible to Differential Heave in Expansive, Steeply Dipping Bedrock, City of Colorado Springs, Colorado: Colorado Geological Survey, Map Series MS-32, Scale: 1:24,000.

Keller, J.W., Siddoway, C.S., Morgan, M.L., Route, E.E., Grizzell, M.T., Sacerdoti, R., and Stevenson, A., 2004, Geologic Map of the Manitou Springs Quadrangle, El Paso and Teller Counties, Colorado: Colorado Geological Survey, Open-File Report OF-03-19, scale 1:24,000.

Kirkham, R.M. and Rogers, W.P., 1981, Earthquake potential of Colorado: *Colo. Geol. Surv. Bull.* 43, 171 p.

Kolb, C.R., 1975, Geologic control of sand boils along Mississippi River levees: Misc. Paper S-75-22, US Army Engineer Waterways Experiment Station, Vicksburg, MS, Final Report, August 1975, 29 p.

Kupfer, D. H., and others, 1968, The Rocky Mountain frontal fault: *Internat. Geol. Cong.*, 23rd, Prague, Sec 3, p. 313-327.

Leonard, M., 2010 Earthquake Fault Scaling: Self-Consistent Relating of Rupture Length, Width, Average Displacement, and Moment Release: *Bull. Seismol. Soc. Amer.*, v. 100, p. 1971-1988.

Morgan, M., 2015, Colorado's potentially hazardous Quaternary faults, in Briggs, R. and Gold, R. (conveners), Basin and Range Province, Seismic Hazards Summit III: *Utah Geol. Surv. Misc. Pub.* 15-5, p. 66-88.

Morgan, M., 2018, Update and Issues Facing Earthquake Research in Colorado, in *Utah Geol. Surv.*, 2018 Basin and Range Province Earthquake Working Group (BRPEWG) Meeting, Thursday, February 15, 2018; p. 67-80.

Morgan, M.L., Siddoway, C.S., Rowley, P.D., Temple, J., Keller, J.W., Archuleta, B.H., and Himmelreich, J.W., 2004, Geologic Map of the Cascade Quadrangle, El Paso County, Colorado: Colorado Geological Survey, Open-File Report OF03-18, scale 1:24,000.

Murray, K.D., Murray, M.H. and Sheehan, A.F., 2019, Active deformation near the Rio Grande Rift and Colorado Plateau as inferred from continuous global positioning system measurements. *Jour. Geophys. Res.-Solid Earth*, 124 (2): <https://doi.org/10.1029/2018JB016626>

Rowley, P, Himmelreich, J.W., Kupfer, D.H., and Siddoway, C.S., 2004, Geologic Map of the Cheyenne Mountain Quadrangle, El Paso County, Colorado: Colorado Geological Survey, Open-File Report OF02-05, scale 1:24,000.

Temple, Jay, Madole, Rich, Keller, J.W., and Martin, Dawn, 2007, Geologic Map of the Mount Deception Quadrangle, Teller and El Paso Counties, Colorado: Colorado Geological Survey, Open-File Report OF-07-07, scale 1:24,000.

Scott, G.R. and Wobus, R.A., 1973, Reconnaissance geologic map of Colorado Springs and vicinity, Colorado: USGS Map MF-482, scale 1:62,500.

Taylor, R.B., 1975a, Neogene tectonism in south-central Colorado, in Curtis, B. F., Cenozoic history of the southern Rocky Mountains: Geol. Soc. America Mem. 144, p. 179-226.

Tweto, O., 1976a, Preliminary geologic map of Colorado: U.S. Geol. Survey Misc. Field Studies Map MF-788.

Wells, D. L. and Coppersmith, K.J., 1994 New empirical relationships among magnitude, rupture length, rupture width, rupture area, and surface displacement: Bull. Seismol. Soc. Amer., v. 86, p. 974-1002

White, J.L., and Wait, T.C., 2003, Colorado Springs landslide susceptibility map, El Paso County, Colorado: Colorado Geological Survey, Map Series MS-42, Scale: 1:24,000.

Widmann, B.L., Kirkham, R.M. and Rogers, W.P., 1998, Preliminary Quaternary Fault and Fold Map and Database of Colorado: Colo. Geol. Surv. Open-File Report 98-8, 330 p. Unruh, J.R.,

Wong, I.G., Hitchcock, C.S., Bott, J.D.J., Silva, W.J., and Lettis, W.R., 1994, Seismotectonic evaluation, Pueblo Dam, Fryingpan-Arkansas Project, south-central Colorado: U.S. Bureau of Reclamation, 134 p.

APPENDIX 1

Preliminary Luminescence Age Report

Table 1: Single Aliquot Regeneration, optically-stimulated luminescence (SAR-OSL) ages on quartz grains from Ute Pass, Colorado (09/16/2021).

Field number/ Depth (m)	BG Lab number	Grain size (μm)	Equivalent Dose (De) (Gy) ^b	Over- dispersion (%) ^c	U (ppm) ^d	Th (ppm) ^d	K ₂ O (%) ^d	H ₂ O (%)	Cosmic Dose Rate (mGray/yr) ^e	Dose Rate) (mGray/yr)	SAR-OSL age (yr) ^f	
UPF-1/9.15	5101	6/11	355-500	>210	NA	7.20 ± 0.01	36.2 ± 0.01	4.63 ± 0.01	15 ± 5	0.128 ± 0.013	6.52 ± 0.21	> 32,200
UPF-2/9.45	5102	25/30	150-250	248.52 ± 13.82	25 ± 4	7.28 ± 0.01	39.9 ± 0.01	4.50 ± 0.01	15 ± 5	0.125 ± 0.012	7.06 ± 0.38	35,180 ± 2590
UPF-3/1.75	5103											
UPF-4/1.35	5104											

^aAliquots measured, used to define De population by the Central Age Model or the Minimum Age Model (Galbraith and Roberts, 2012)

^bEquivalent dose calculated on a pure quartz fraction with ultra-small aliquots with 20-80 grains/aliquot and analyzed under blue-light excitation (470 ± 20 nm) by Single Aliquot Regeneration protocols (SAR; Murray and Wintle, 2003; Wintle and Murray, 2006). Equivalent dose (De) was calculated by Minimum age model (Galbraith and Roberts, 2012) ^c Overdispersion values reflects precision beyond instrumental errors; values of ≤ 20% (at 1 sigma limit) indicate low dispersion in equivalent dose values and defines a unimodal distribution. Values > 20% are associated with mixed equivalent dose signature reflecting multiple grain populations or partial solar resetting.

^dU, Th, Rb and K content analyzed by inductively-coupled plasma-mass spectrometry by ALS Laboratories, Reno, NV.

^eincludes also a cosmic dose rate calculated from parameters in Prescott and Hutton (1994) and includes soft components (Peng and Forman, 2019).

^fSystematic and random errors calculated in a quadrature at one standard deviation by the Luminescence Dating and Age Calculator (LDAC) at

<https://www.baylor.edu/geosciences/index.php?id=962356> (Peng and Forman, 2019) Datum year is AD 2010.

APPENDIX 2A
Previous Work on the UPF- **Kirkham and Rogers, 1981**

“The Ute Pass fault zone (fault number 144) extends from south of Colorado Springs, where it bounds the east flank of Cheyenne Mountain, northward through Woodland Park to the vicinity of Deckers. Fault characteristics change significantly along its length. At its south end east of Cheyenne Mountain, the fault is a west-dipping reverse fault with dips as low as 30° (Epis and others, 1976a). Northward, the fault steepens in dip and at Woodland Park the fault zone consists of several nearly vertical faults that form a graben. Total fault displacement is on the order of a few thousand meters (Kupfer and others, 1968; Harms, 1959, 1964). At least 300 m of Neogene movement is indicated by offset of the late Eocene erosion surface and overlying late Tertiary deposits (Epis and Chapin, 1975; Taylor, 1975a; Tweto, 1976a).

Several features suggestive of Quaternary activity are developed along the fault east of Cheyenne Mountain. A prominent scarp is developed in Verdos Alluvium along a bedrock fault in Sec. 30, T15S, R66W (Scott and Wobus, 1973). The nature of this feature is not known with certainty, but a tectonic origin is supported by the tilted block of Verdos Alluvium exposed in a roadcut in E1/2 SE1/4 sec. 25, T.15S., R.67W., on strike with the prominent scarp. Several subtle, anomalous lineaments are apparent on aerial photographs of Secs. 1, 12, and 13, T15S, R67W. Many of the lineaments are marked by discontinuous scarps in a large sheet of rockfall debris. It is difficult to explain these colinear scarps in rockfall debris by any mechanism other than fault rupture.

Scott and Wobus (1973) believe that the large rockfall event on the east flank of Cheyenne Mountain may have been initiated by earthquake shaking during the Yarmouth(?) interglacial period. Such an earthquake could have resulted from movement on the Ute Pass fault. If the scarps preserved in the rockfall debris are of tectonic origin, then the Ute Pass fault may have moved at least twice during the Quaternary. One movement is required to produce the catastrophic rockfall event, and a second movement to explain the scarps in the rockfall debris.

Highly deformed beds of oxidized, reworked grus are exposed along a small creek in SE1/4 of sec. 23, T.14S, R.67W. Bedding is folded into a series of small folds with a maximum amplitude of about 15 cm. Mechanisms other than fault movement could explain the observed deformation (i.e. mass movement, subsidence, periglacial frost action), but a tectonic origin cannot be ruled out. Many small exposures along the mountain front reveal Precambrian rocks in vertical or near vertical contact with Quaternary deposits. Some of these contacts may be the result of fault offset.

Evidence of Quaternary movement on the Ute Pass Fault is not definitive. In view of the many pieces of circumstantial evidence, however, it is likely that the fault has moved at least once and possibly twice during the Quaternary, probably during the Yarmouth interglacial period or early in the Illinoian glacial period. Slocum Alluvium does not

appear to be offset by the fault, hence there probably has been no appreciable movement since Illinoian or Sangamon time.”

APPENDIX 2B
Previous Work on the UPF- Allen, 1984

Allen, C.R., 1984, DESIGN EARTHQUAKES FOR THE PROPOSED TWO FORKS PROJECT, INTERIM LETTER REPORT; REPORT J, in GEOTECHNICAL ADVISORY COMMITTEE, GEOLOGIC AND SEISMOTECTONIC INVESTIGATIONS, EAST-CENTRAL FRONT RANGE, COLORADO, INTERIM REPORT by DENVER WATER DEPARTMENT, DENVER, COLORADO 80254, AUGUST, 1984).

*"The nearest other faults on which Kirkham and Rogers (1981) have suggested evidence of Quaternary displacement are the Rampart Range and Ute Pass faults, based in turn on the work of Scott (1970) and Scott and Wobus (1973). In both cases, the areas of suggested Quaternary displacement are more than 50 km from the site, although the northerly extensions of the same faults extend to within 20 km of the site, according to the map of Kirkham and Rogers (1981). Several things should be noted: (1) The **Ute Pass fault** does not break Slocum alluvium, so that "there probably has been no appreciable movement since Illinoian or Sangamon time" (Kirkham and Rogers, 1981), more than 130,000 years ago; (2) At the locality near the Air Force Academy described by Scott (1970), the Rampart Range fault cuts Douglass Mesa gravels (equals Verdos alluvium), thought to be about 600,000 years old (Bryant et al., 1981). However, younger Quaternary units elsewhere overlying the fault are shown as unbroken on the maps of Scott and Wobus (1973) and Bryant et al. (1981), although most of these units are probably Holocene and latest Pleistocene in age. (3) No hint of late Quaternary fault scarps could be seen during my helicopter survey along the northern extensions of the two faults, nor have any of which I am aware been suggested by other authors. (4) The 1:250,000 geologic map of Bryant et al. (1981) shows several northerly splays and branches of the Ute Pass and Rampart Range faults which could be considered to come closer to the site than indicated by Kirkham and Rogers (1981). However, it should be noted that the Bryant et al. map is a compilation of earlier mapping, mostly done at larger scales (e.g., Peterson 1964), and an important cartographic simplification has made "solid-line" faults out of all "dashed-line" (approximately located or inferred) faults on the original large scale maps. Thus the plethora of solid lines on the 1:250,000 map does not adequately portray the various degrees of geological confidence in mapping faults during the original field work, and an undue sense of accuracy may be implied to the unwary reader. By picking appropriate branch points on the map, in fact, one can follow a solid line almost completely across the map from north to south, yet I doubt that anyone would really claim that a single earthquake could credibly be associated with such a fault rupture. Similarly, I doubt that it is credible that an earthquake centered near Colorado Springs, for example, could be associated with rupture extending past the Two Forks damsite on the Kennedy Gulch fault, although solid-line faults can be found on the Bryant et al. map to connect the two areas. (I don't mean, incidentally, to be critical of Bryant et al.; this cartographic procedure evidently represents current U. S. Geological Survey policy.)"*

APPENDIX 2C

Previous Work on the UPF- **text from Harza Engineering Company, 1985**

Harza Engineering Company, 1985, REGIONAL FAULT STUDY, SECOND INTERIM REPORT, REPORT A, in GEOTECHNICAL ADVISORY COMMITTEE, GEOLOGIC AND SEISMOTECTONIC INVESTIGATIONS, EAST-CENTRAL FRONT RANGE, COLORADO; DENVER WATER DEPARTMENT, DENVER, COLORADO 80254, JULY, 1985, 70 p.

Quadrangles (and map numbers following) mapped by Harza on the Ute Pass Fault; listed from north to south:

Kassler (16)

Devils Head (20)

Deckers (19)

Westcreek (23)

Dakan Mountain (24)

Mount Deception (27)

Woodland Park (30)

Cascade (31)

Manitou Springs (34)

Colorado Mountain (36)

Cheyenne Mountain (36)

“General

The Ute Pass fault, as shown by Bryant and others (1981), is about 57 mi long, extending from Stevens Gulch in the north (16, A-3) to Cheyenne Mountain in the south (36, A-3). Discussion of this fault is divided into three segments: a southern segment that trends about N.40°W. from Cheyenne Mountain to Crystola (30, D-2); a central segment trending about N.15°W. to Rainbow Falls (23, E-4); and a northern segment trending north and N.15°E. to Stevens Gulch.

The southern and central fault segments, as used here, have been mapped as a complex zone of multiple faulting and comprise a major structure of the southern Front Range. The southern segment curves around the east flank of Cheyenne Mountain (35, 36) and up the strongly linear valley of Fountain Creek (30, 31, 34). This segment, in part, forms the boundary fault between the crystalline rocks of the Front Range Uplift and Phanerozoic sedimentary rocks of the piedmont. The central segment trends along the west side of the Manitou Park half-graben and separates the Pikes Peak granite, on the west, from down-faulted sedimentary rocks, on the east. The northern fault segment, as shown by Trimble and Machette (1979), Bryant and others (1981) and others, does not appear on early maps but is shown as a continuation of the central and southern segments by Harms (1959, 1965). This segment follows moderately developed linear valleys of Sugar Creek, Bear Gulch, Stevens Gulch and other minor drainages and crosses the Pikes Peak granite-metamorphic contact north of Moonridge (20, A-1).

Literature Review

Geologic literature available for the central and southern segments of the Ute Pass fault is extensive, ranging from early publications of Hayden (1874), Crosby (1895), George (1913), Finlay (1916), Bloesch (1919), Bucher (1933), and Roy (1940), to more recent mapping and interpretations of Harms (1959, 1965), Grose (1960), Kupfer and others (1968), Scott and Wobus (1973), Epis and Chapin (1975), Wobus and Scott (1977), and others. These publications reflect the controversy and the evolution of thought that has surrounded structural interpretations of this complex zone since it was first investigated. These interpretations have

ranged from one of relatively simple, vertical to east-dipping normal faulting (Finlay, 1916), to one of west-dipping, predominantly reverse faulting described in most recent publications. Exposures of the fault are rare and the nature of the reverse faulting remains subject to interpretation. Most authors ascribe steep to vertical dips to the multiple faults in the central segment, along the half-graben, while wide variations in dip, that range from 30° to 80° west, are described by Kupfer and others (1968) and other authors in the southern segment.

Geologic literature available for the northern segment of the fault is less extensive than in the south. This part of the fault is shown as a single trace with several splays based, in part, on mapping and interpretations of Harms (1959, 1965) and Johnson (1961). Harms (1959) infers the northern fault segment to be a west-dipping reverse structure for most of its length based on the occurrence of sandstone dikes. Johnson (1961), however, reported left-lateral offset of the metamorphic contact that could be due to either strike-slip displacement or to dip-slip displacement of a non-vertical contact. Detailed geologic mapping of the northern end of the fault is available from Scott (1963a).

The central and southern segments of the Ute Pass fault, as used in this report, are categorized as "potentially active" by Kirkham and Rogers (1981, fault number 144).

Results of Investigations

Northern Segment (16, A-3 to 23, E-4)

From its northern end (16, A-3) to Moonridge (20, A-1) the mapped fault trace is located in metamorphic rocks and follows the linear valleys of Stevens Gulch and part of Bear Creek. The mapped trace generally is covered by thin colluvium, talus, and alluvium, although flat, with sporadic outcrops, of sandstone dike are fairly common. Conclusive evidence of shearing was not observed, although Johnson (1961) describes a poorly exposed crushed zone in the area, also noted by Scott (1963a). The fault is covered by recent alluvium for about 1.5 mi north of Moonridge.

At Moonridge, Johnson (1961), and most subsequent authors, show about 2700 ft of left-lateral offset of the metamorphic-granite contact along the fault. This offset is readily confirmed and faulting is indicated by extensive iron-staining and fracturing exposed in road cuts. Several northwest trending fault splays also are mapped by Scott (1963a), crossing the contact east of Moonridge (16, A-5 and B-5). Several hundred ft of left-lateral offset of the contact is shown along one, although bedrock is poorly exposed and no evidence of either the fault traces or the offset was observed in the present study.

South of Moonridge for a distance of about 6 mi, the main fault trace occurs in or adjacent to a linear part of Sugar Creek valley. A zone of fracturing and iron-staining up to about 800 ft wide is mapped in the northern part of this section (Trimble and Machette, 1979) and is intermittently exposed in road cuts. Further south (19, E-4), fractured, iron-stained and locally slickensided granite in a zone up to about 200 ft wide is well exposed in road cuts and locally elsewhere. Sandstone dikes also were observed in the southern part of this section. Although not specifically examined, no evidence of several fault splays mapped in this area were observed during the reconnaissance.

From Sugar Creek to Rainbow Falls (23, E-4) the fault is mapped as two branches which divide and then rejoin further south. The two fault branches follow minor drainage channels and topographic saddles and were not examined. Harms (1959) notes sandstone dikes locally in this area.

Central Segment (23, E-4 to 30, D-2)

The central segment of the Ute Pass fault is mapped as a complex zone, variably including 2 or 3 faults, along the western boundary of the Manitou Park half-graben. Relatively detailed mapping is available in this area (i.e. Harms, 1959), and the present study concentrated on evaluating recency of movement. Nonetheless, most of this fault segment was examined in the study and the data collected are in substantial agreement with published reports, as described below.

The several branches of the Ute Pass fault in this segment are poorly exposed, the easternmost traces generally being covered by Quaternary fan and alluvial deposits, and the westernmost traces by alluvium and colluvium. Two parallel fault traces are mapped along the northern part of the half-graben. One of these passes through a narrow topographic saddle near Quinlan Gulch (27, A-2) and, although not exposed, is closely located by the proximity of steeply west-dipping sedimentary rocks on the east, to granite, on the west. From this location south to the Woodland Park area (27, B-5), the fault zone is mapped with three principal traces which are characterized in sporadic outcrops, by sandstone dikes (27, B-3), fault breccia (27, B-3) and heavy iron-staining (17, B-4). Harms (1959) reports extensive sandstone dikes along parts of the westernmost fault in this section not covered in the present study. West of Woodland Park (27, B-5 to 30, C-1), sandstone dikes also are prominently exposed in a zone up to 1000 ft wide. Detailed geologic mapping of most of this area, and south to Crystola (30, E-2), is available from Wobus and Scott (1977) and indicates complex faulting, numerous sandstone dikes and displacement of Tertiary gravels. Most of these features are readily confirmed.

In addition to the principal fault traces in the central segment, as discussed above, a significant northwesterly trending splay occurs near Westcreek (23, E-4 to 23, D-3), that apparently connects the Ute Pass to the Oil Creek faults. The southeast end of this splay near the Ute Pass fault (23, E-4), is exposed by heavy iron-staining and severe fracturing in road cuts and quarries. Near the northwest end of the splay, (23, D-3), a zone of fault breccia and gouge is exposed in an abandoned mine. A colluvial deposit, exposed in a pit, appears to be offset either by the splay or the main Oil Creek fault.

These locations are described further in the section on the Oil Creek fault.

Southern Segment (30, D-2 to 36, A-3)

Detailed geologic mapping is available for the structurally complex southern segment of the Ute Pass fault zone, and the present study concentrated on evaluating cited evidence for Quaternary movement. Although iron-staining and fracturing were noted in several locations (i.e. 31, A-4), and sandstone dikes are described by Hayden (1874) and subsequent authors, the fault traces in general are obscured or difficult to reach. Cited evidences for recency of movement are discussed in the following section.

Recency of Fault Movement

The central and southern segments of the Ute Pass fault, as referred to in this report, are categorized as "potentially active" by Kirkham and Rogers (1981). It is listed as their fault number 144 with documented evidence of Tertiary movement and circumstantial evidence of Quaternary movement. The northern segment is not noted as potentially active.

Tertiary (Neogene) displacement is indicated by about 985 ft of offset of the late Eocene erosion surface and of Tertiary gravels documented by Epis and Chapin (1975), Taylor (1975)

and Tweto (1976) in the southern fault segment. Displacement of Tertiary gravel deposits is clearly indicated by Wobus and Scott (1977) near Woodland Park.

Quaternary displacement, as cited by Kirkham and Rogers (1981), is based largely on evidence reported by Scott and Wobus (1973) on the eastern and southern flanks of Cheyenne Mountain. This evidence, described as circumstantial, is strongly suggestive of Illinoian or Yarmouth movement and includes: 1) a scarp in the Verdos Alluvium over a bedrock fault; 2) a tilted block of the alluvium along the strike of the same fault; 3) discontinuous linear scarps in a large rockfall deposit; 4) deformed, oxidized, reworked grus; and 5) exposures of Precambrian rocks in near vertical contact with Quaternary deposits. No evidence of Quaternary movement is referenced north of the Cheyenne Mountain area (36) and Kupfer and others (1968) further conclude that post-Laramide movement has not occurred along this fault, based on the continuity of the Cretaceous Pierre shale across part of the fault.

In the present study, reconnaissance was performed in the Cheyenne Mountain and other areas to locate possible indications of Quaternary movement. However, it quickly became apparent that extensive study would be required to adequately assess the evidence, owing to the complex bedrock and Quaternary geology, poor exposures, and restricted access. These studies could not be performed within the scope of this study and, because the area is at the extreme limits of the region of interest, no further work is recommended at this time. Elsewhere along the Ute Pass fault, no indication of Quaternary movement was observed or is reported. Quaternary deposits cover parts of the fault but generally are intermittent, thin and only of Holocene age. Although apparently undisturbed, these are of little value in determining most recent movement. Older (Pleistocene) Quaternary fans, also apparently undisturbed, occur in the Manitou Park half-graben. These are not recommended for further study because they probably are too thick to trench to rock, most likely are unstratified and difficult to date, and because the underlying fault traces cannot be located with reasonable accuracy.”

APPENDIX 2D
Previous Work on the UPF- **Annotated fault maps from
Harza Engineering Company, 1985**

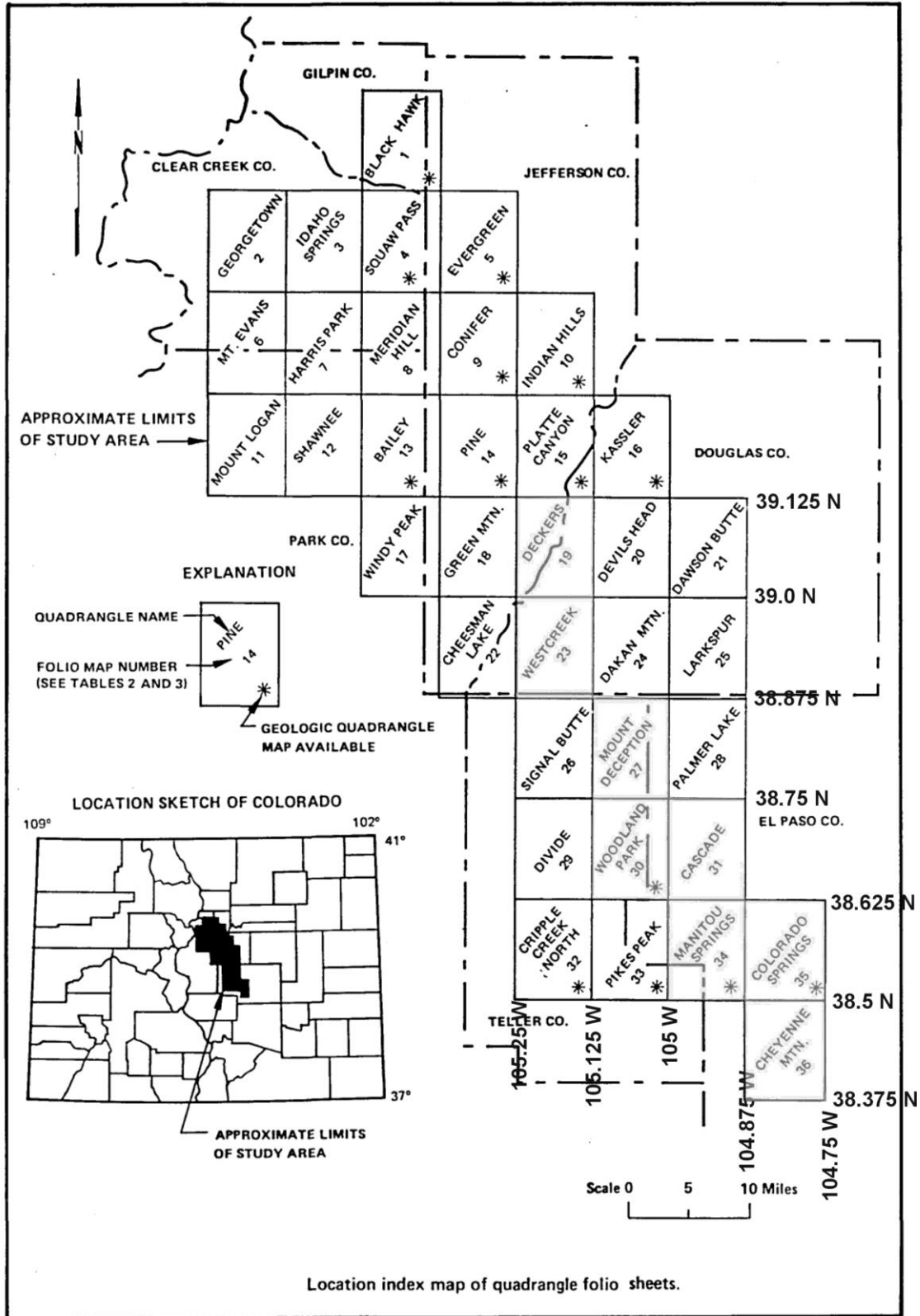
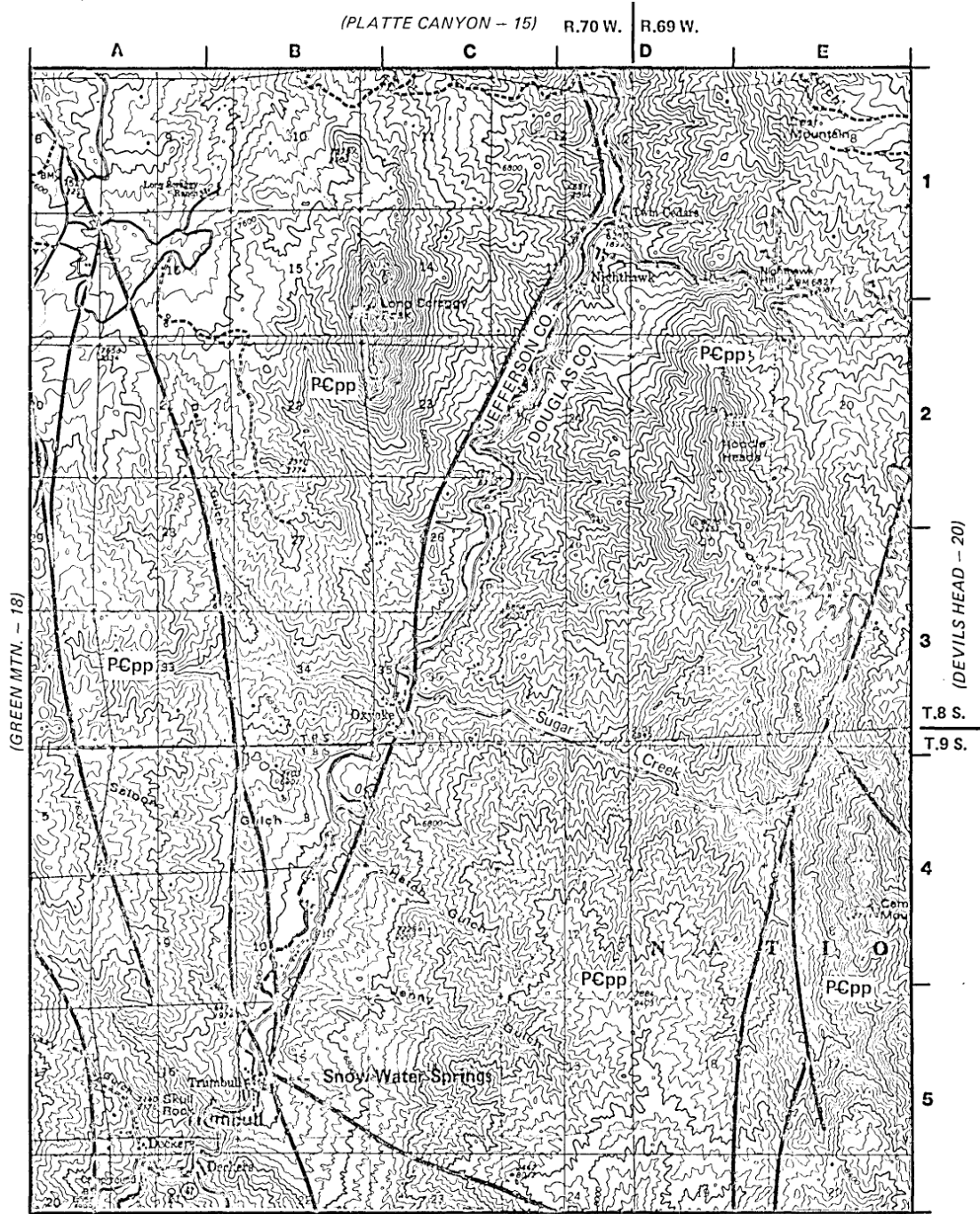


Fig. 3D-1. Index map of quadrangles mapped by Harza, 1985. The UPF (shaded quads) extends from the bottom right quad (Cheyenne Mtn., no. 36) to the quad at center (Deckers, no. 19).

7.5' QUADRANGLES SHOWING PARTS OF UTE PASS FAULT ZONE
No. 19, Deckers

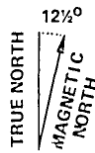


SCALE 0 1 2 MILES

SCALE 0 5000 10000 FEET

CONTOUR INTERVAL 80 FEET

SEE EXPLANATION FOR NOTES, SYMBOLS
AND MAP LOCATION

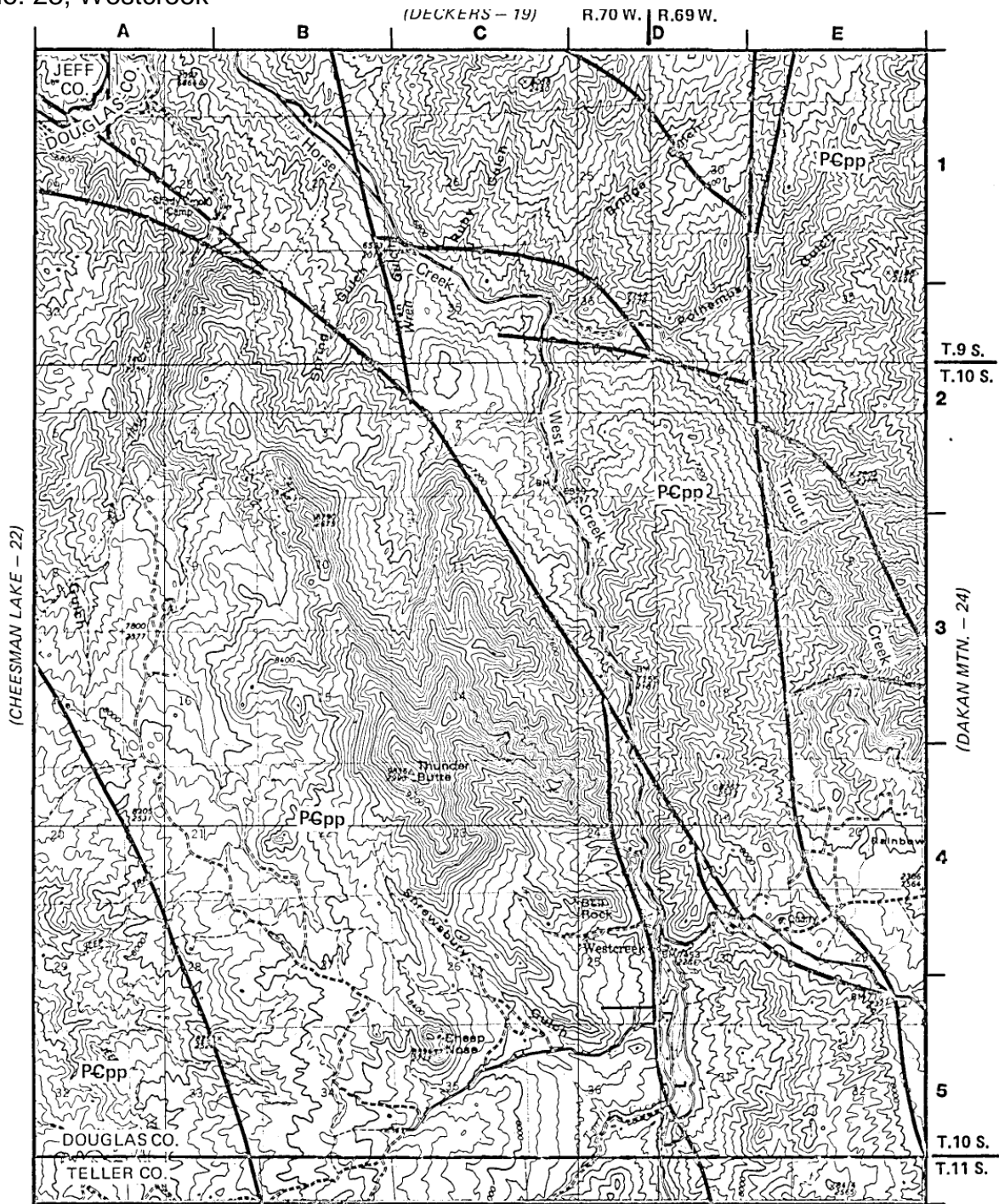


EAST SLOPE STORAGE PROJECT
GEOLOGY—APRIL 1985

REGIONAL FAULT STUDY FOLIO

No. 19
DECKERS

No. 23, Westcreek



SCALE 0 1 2 MILES

SCALE 0 5000 10000 FEET

CONTOUR INTERVAL 80 FEET

SEE EXPLANATION FOR NOTES, SYMBOLS AND MAP LOCATION



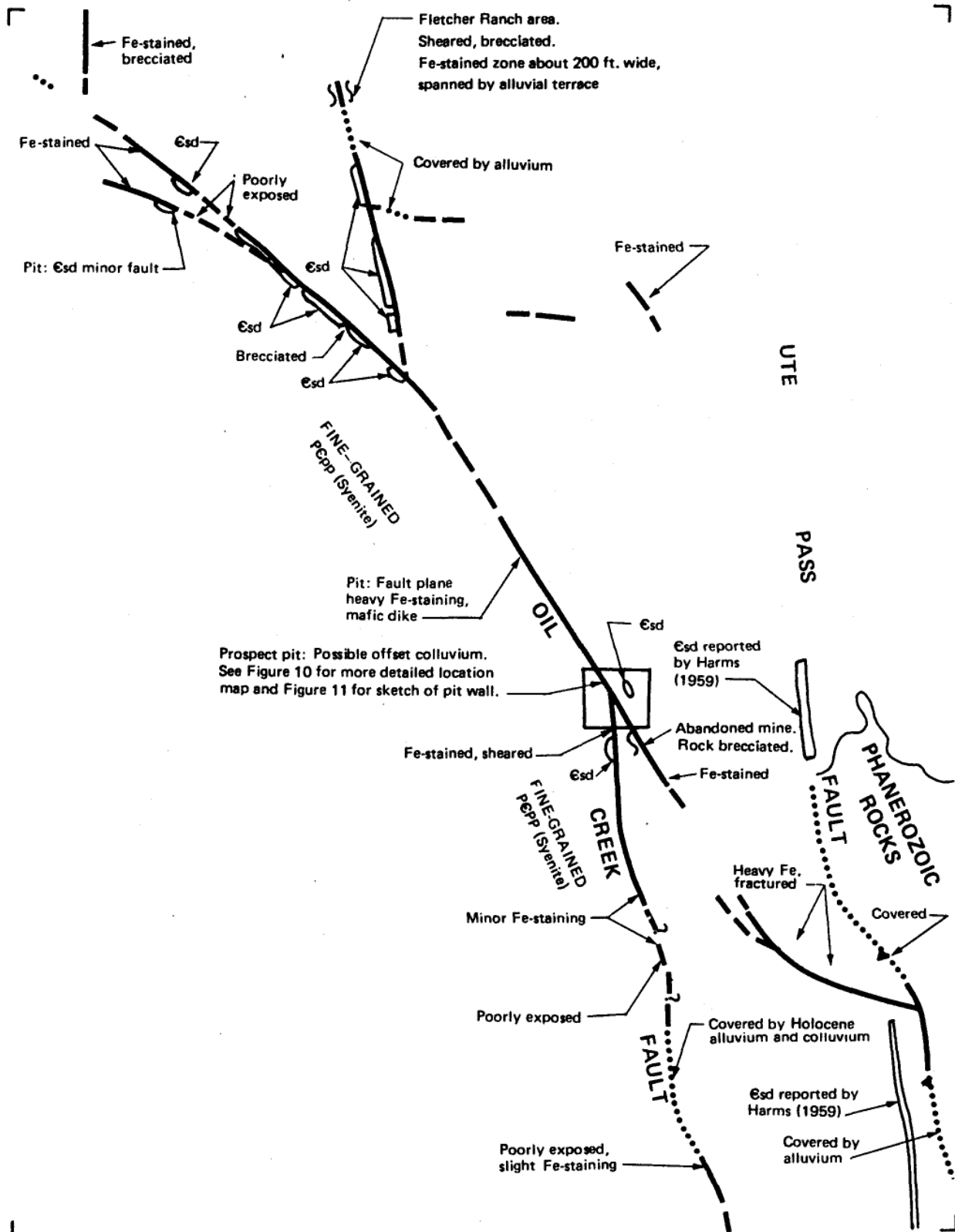
(SIGNAL BUTTE - 26)

EAST SLOPE STORAGE PROJECT
GEOLOGY—APRIL 1985

REGIONAL FAULT STUDY FOLIO

No. 23
WESTCREEK

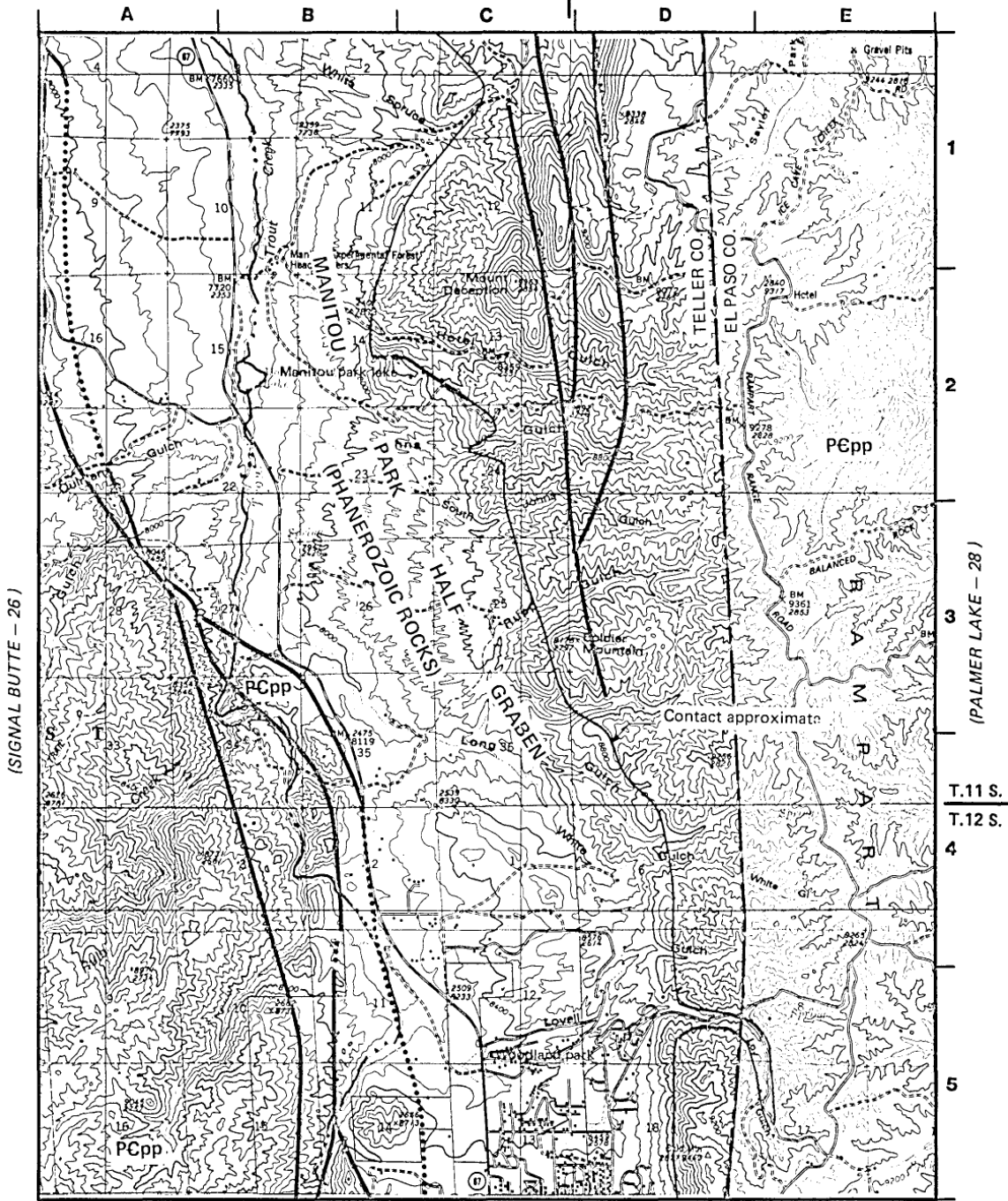
No. 23, Westcreek



No. 27, Mt. Deception

(DAKAN MTN. 24)

R.69 W. R.68 W.



SCALE 0 1 2 MILES (WOODLAND PARK - 30)

SCALE 0 5000 10000 FEET

CONTOUR INTERVAL 80 FEET

SEE EXPLANATION FOR NOTES, SYMBOLS AND MAP LOCATION



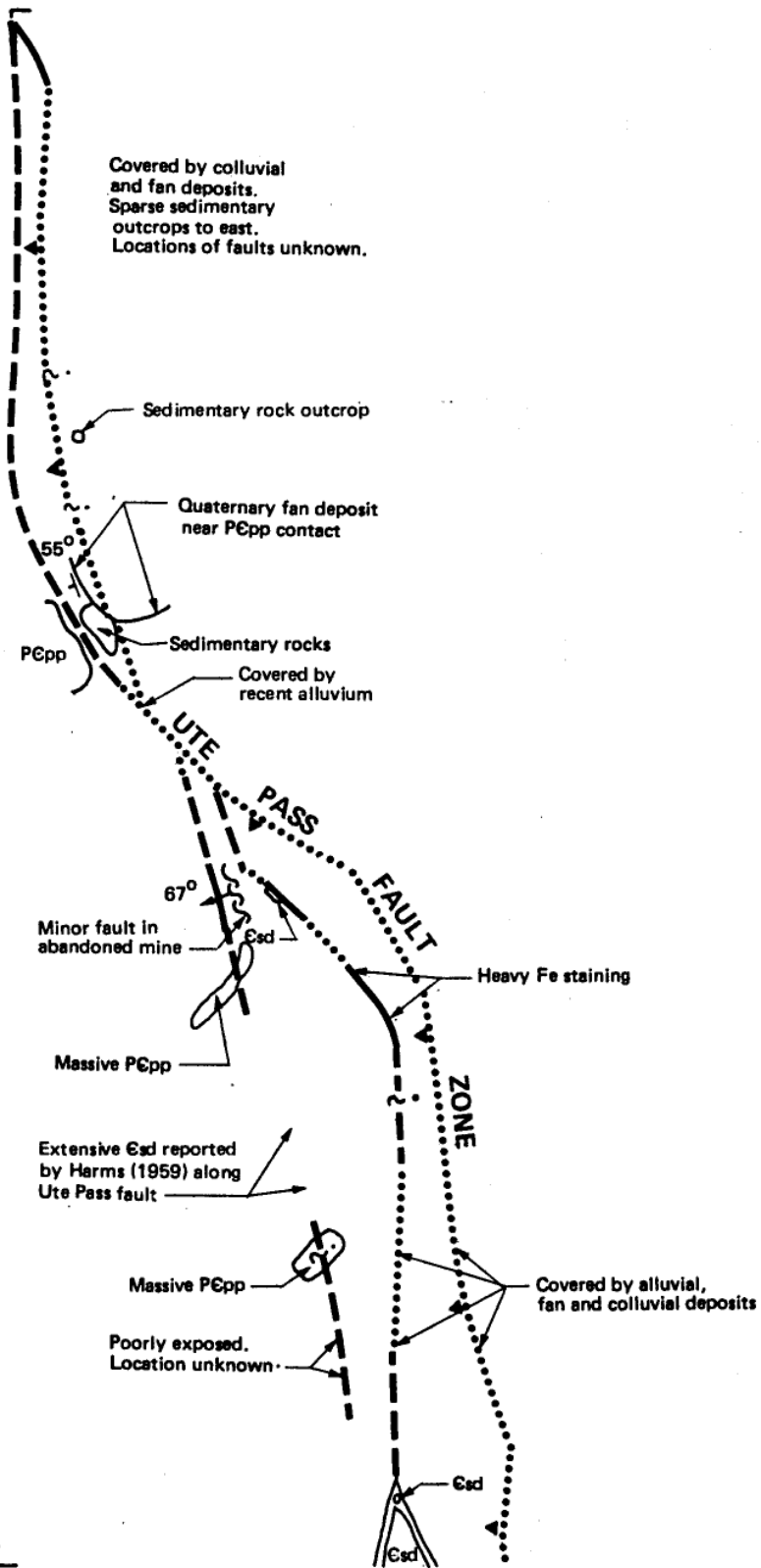
EAST SLOPE STORAGE PROJECT
GEOLOGY—APRIL 1985

REGIONAL FAULT STUDY FOLIO

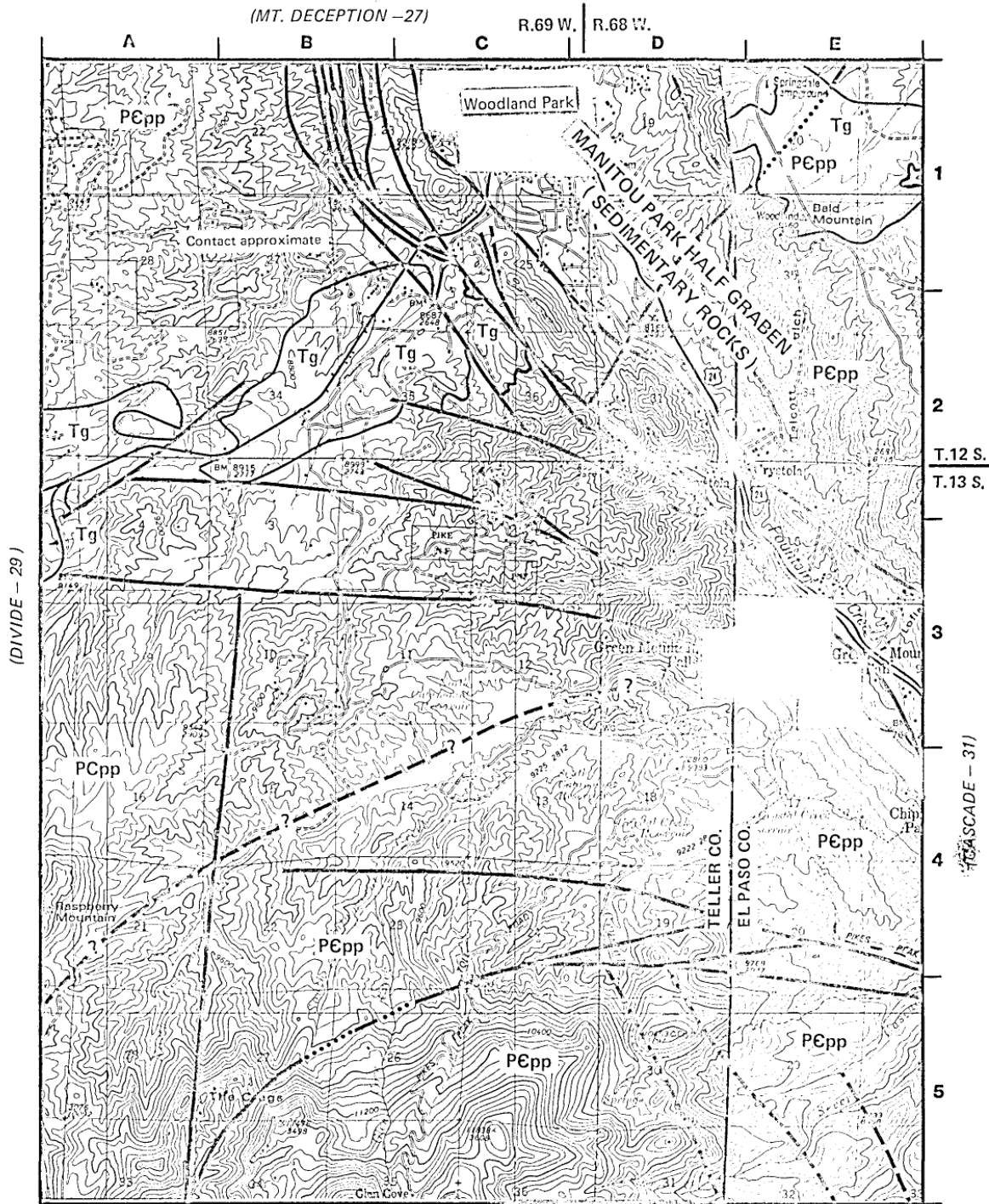
No. 27

MOUNT DECEPTION

No. 27, Mt. Deception



No. 30, Woodland Park



SCALE 0 1 2 MILES

SCALE 0 5000 10000 FEET

CONTOUR INTERVAL 80 FEET

SEE EXPLANATION FOR NOTES, SYMBOLS AND MAP LOCATION

(PIKES PEAK - 33)



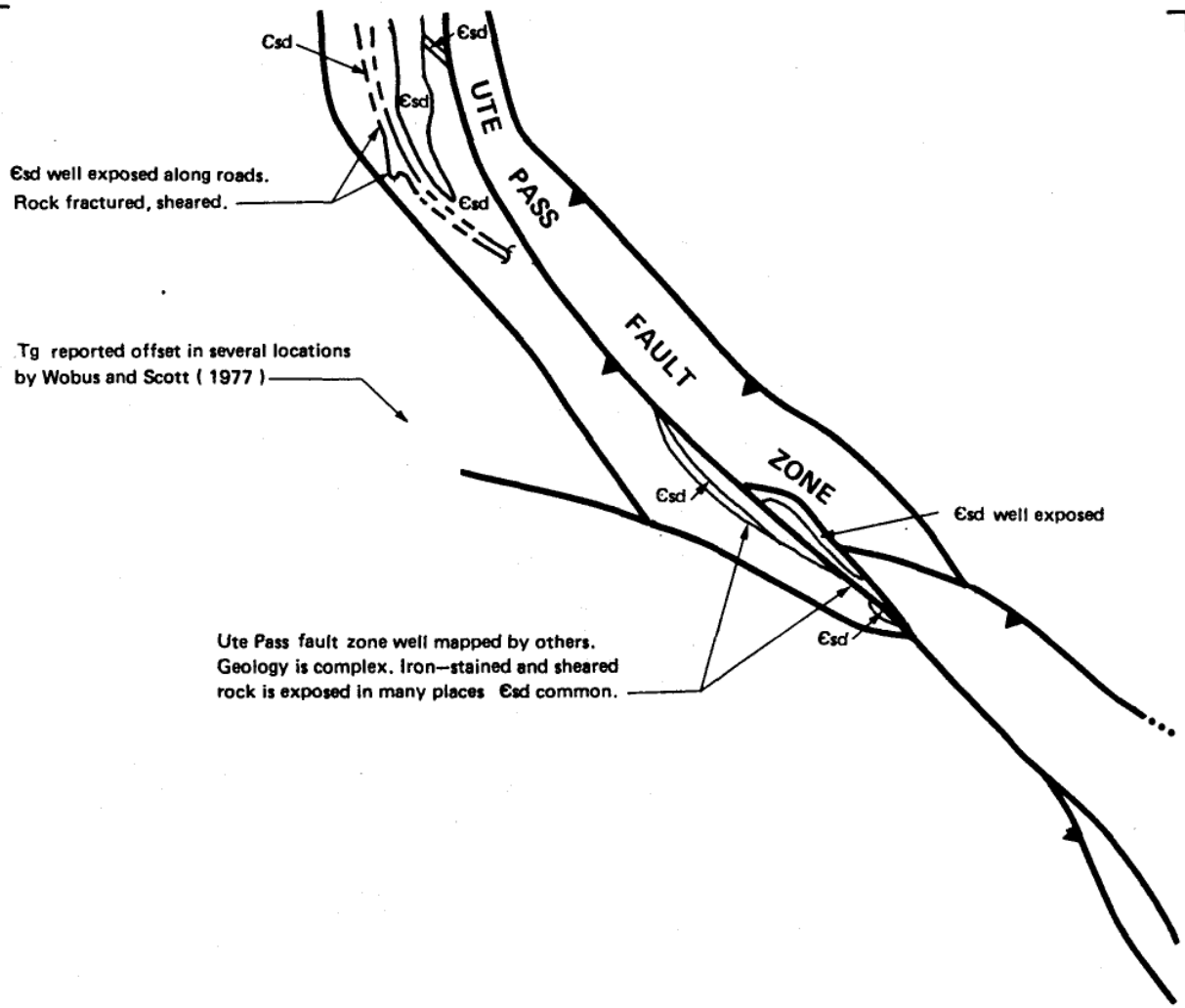
EAST SLOPE STORAGE PROJECT
GEOLOGY-APRIL 1985

REGIONAL FAULT STUDY FOLIO

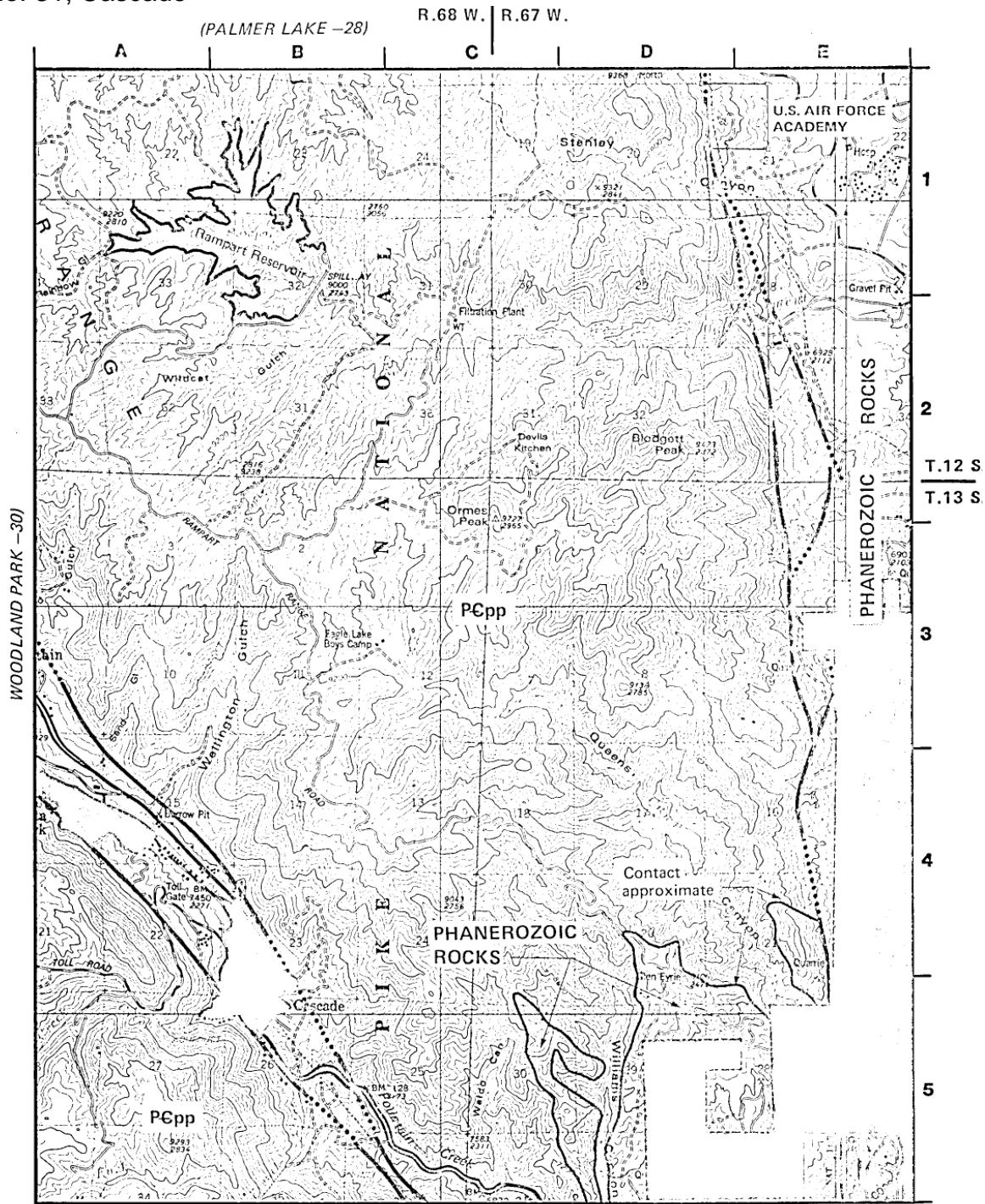
No. 30

WOODLAND PARK

No. 30, Woodland Park



No. 31, Cascade



SCALE 0 1 2 MILES

SCALE 0 5000 10000 FEET

CONTOUR INTERVAL 80 FEET

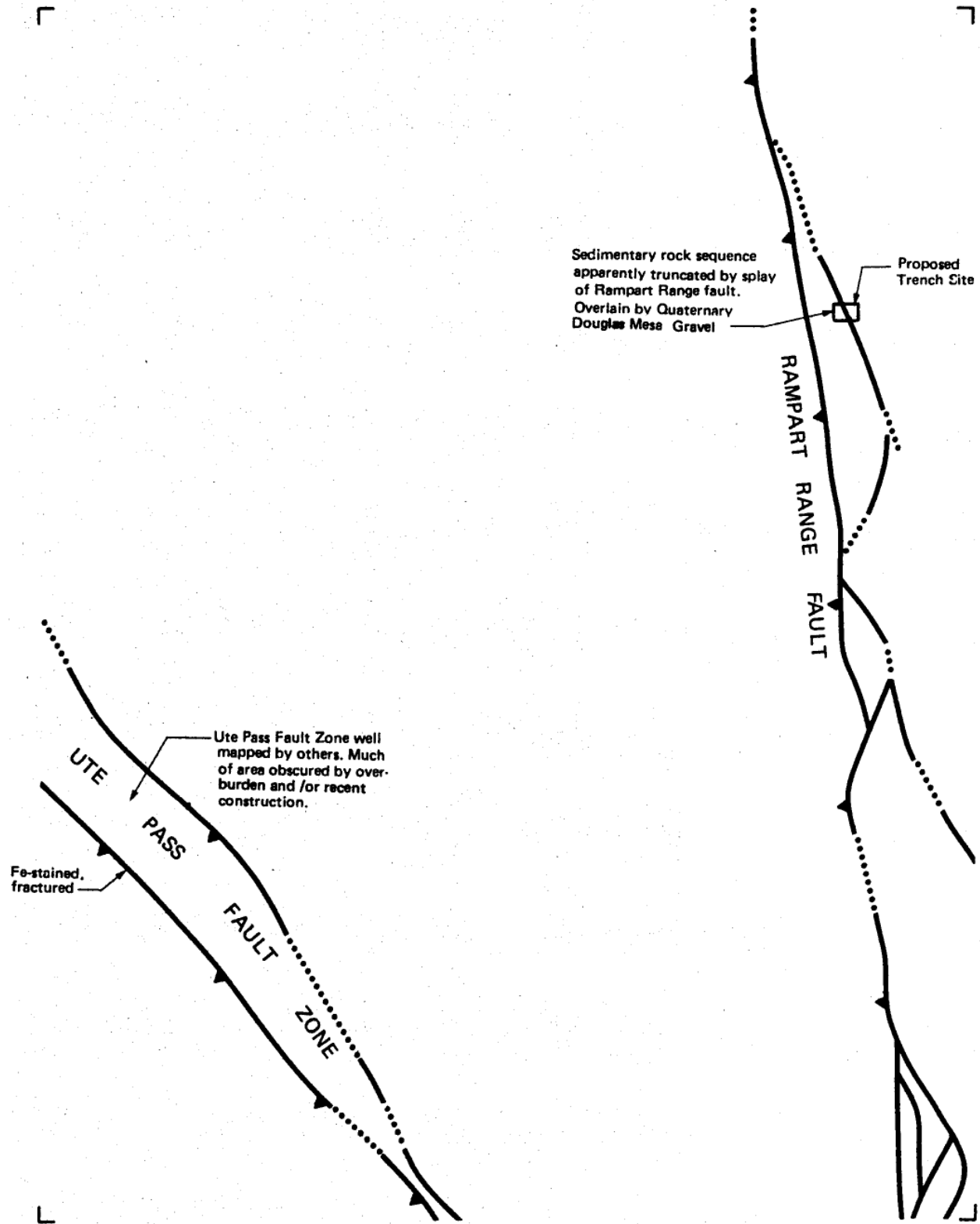
SEE EXPLANATION FOR NOTES, SYMBOLS AND MAP LOCATION



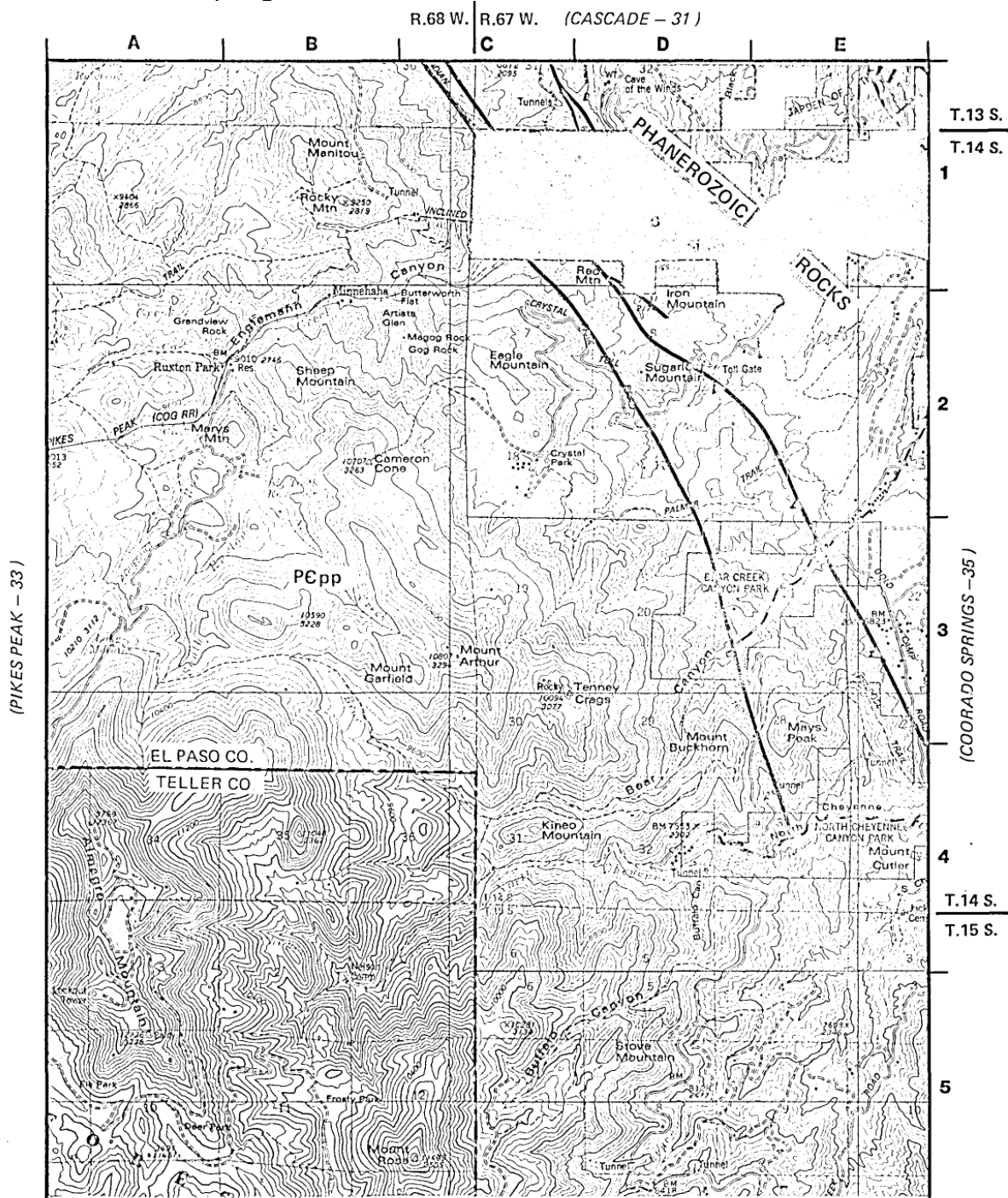
EAST SLOPE STORAGE PROJECT
GEOLOGY—APRIL 1985

REGIONAL FAULT STUDY FOLIO
No. 31
CASCADE

No. 31, Cascade

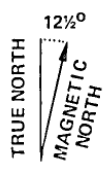
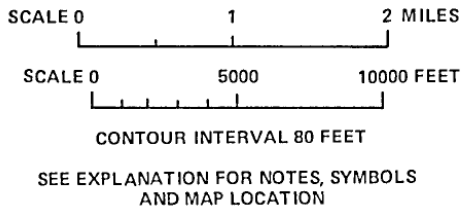


No. 34, Manitou Springs



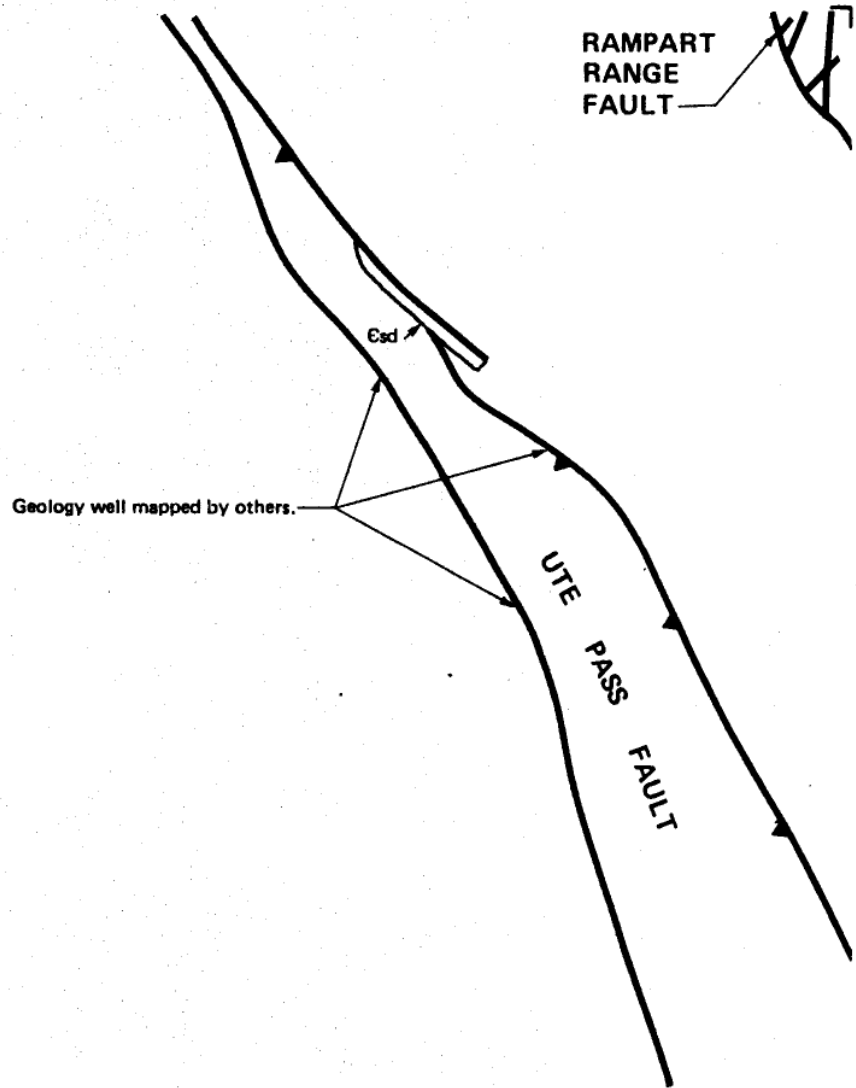
(PIKES PEAK - 33)

T.13 S.
T.14 S.
1
2
3
4
T.14 S.
T.15 S.
5
(COORADO SPRINGS - 35)

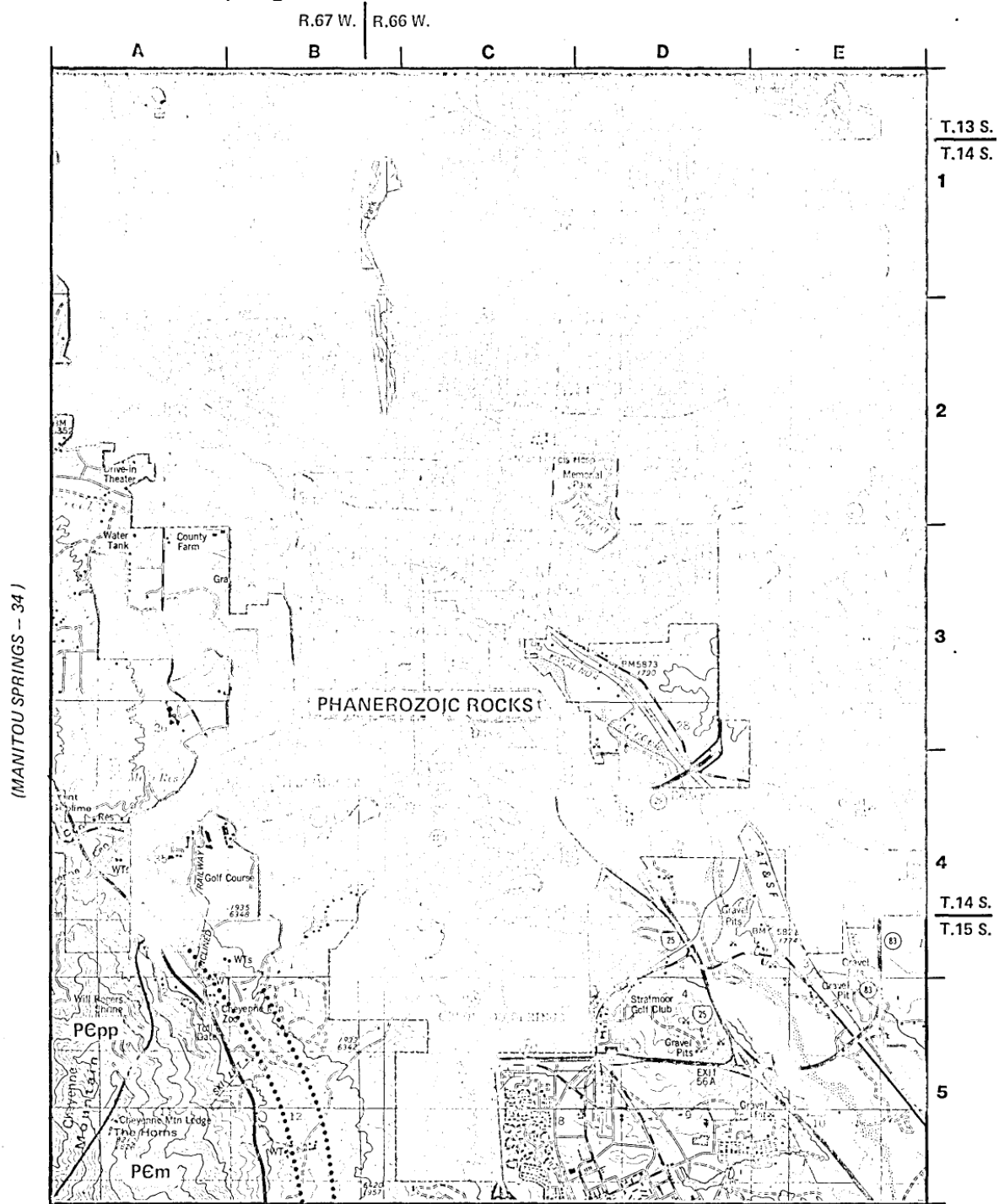


EAST SLOPE STORAGE PROJECT
GEOLOGY—APRIL 1985
REGIONAL FAULT STUDY FOLIO
No. 34
MANITOU SPRINGS

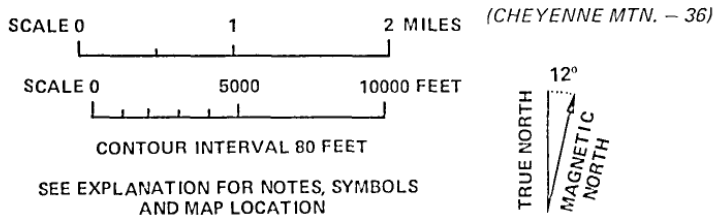
No. 34, Manitou Springs



No. 35, Colorado Springs

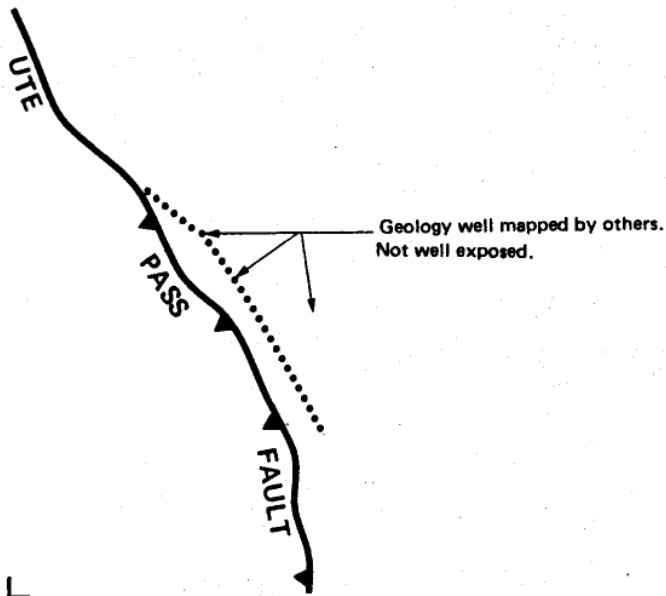


(MANITOU SPRINGS - 34)



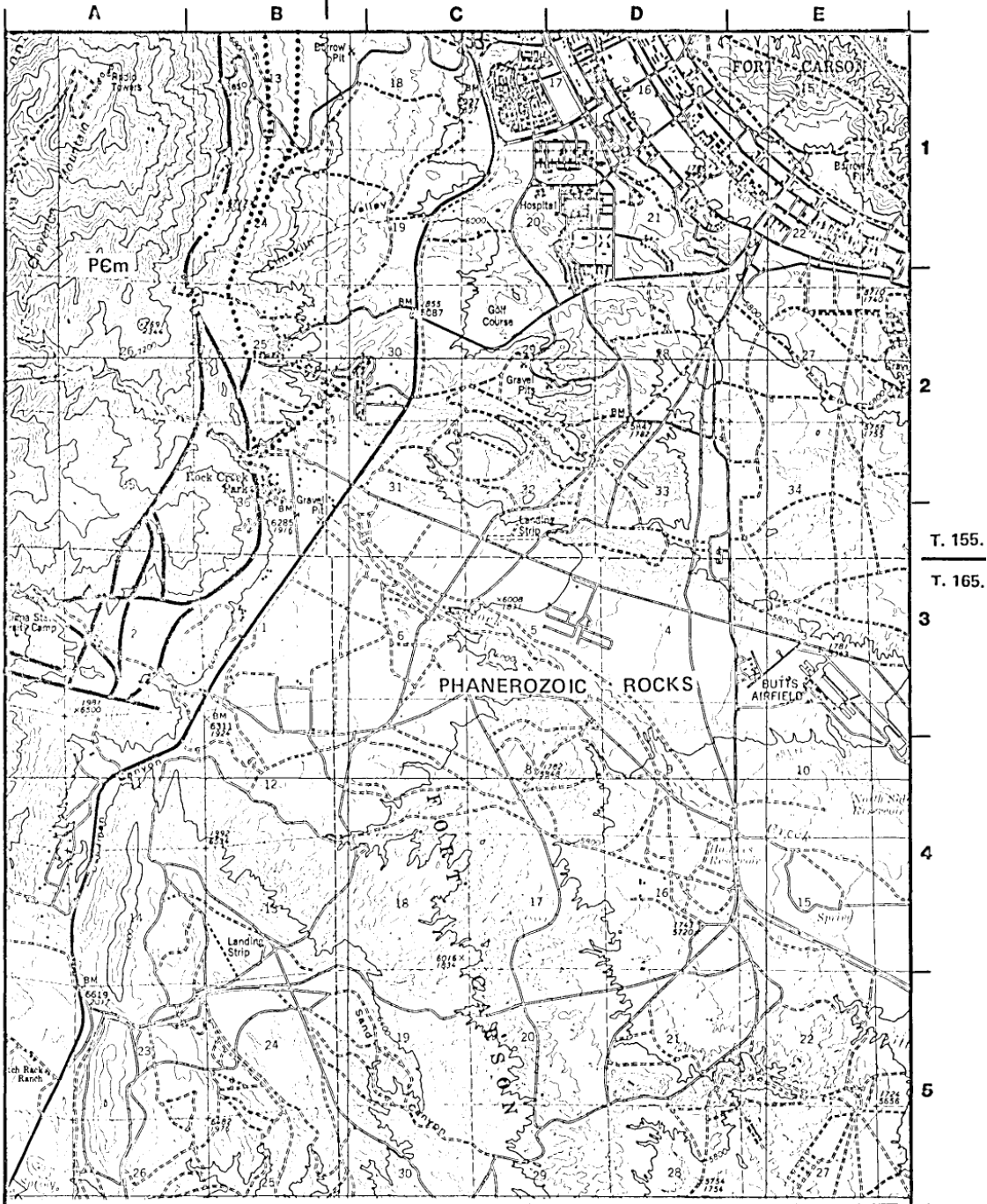
EAST SLOPE STORAGE PROJECT
 GEOLOGY-APRIL 1985
 REGIONAL FAULT STUDY FOLIO
No. 35
 COLORADO SPRINGS

No. 35, Colorado Springs



No. 36, Cheyenne Mountain

R. 67 W. R. 66 W. (COLORADO SPRINGS - 35)



SCALE 0 1 2 MILES

SCALE 0 5000 10000 FEET

CONTOUR INTERVAL 80 FEET

SEE EXPLANATION FOR NOTES, SYMBOLS AND MAP LOCATION



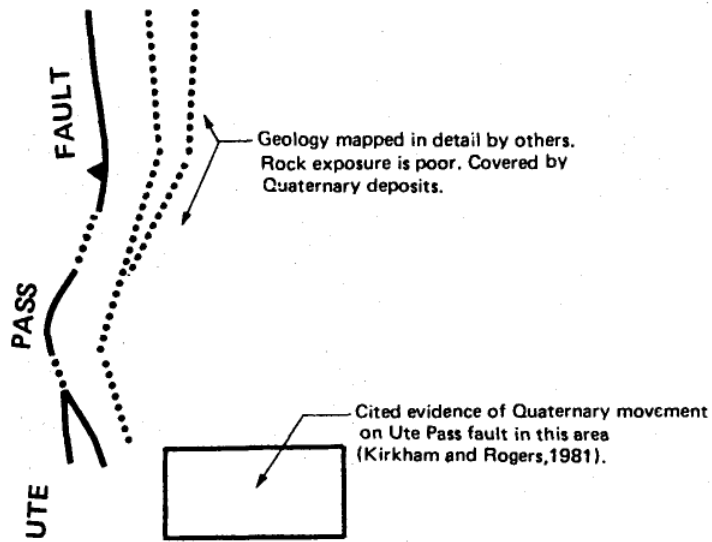
EAST SLOPE STORAGE PROJECT
GEOLOGY—APRIL 1985

REGIONAL FAULT STUDY FOLIO

No. 36

CHEYENNE MOUNTAIN

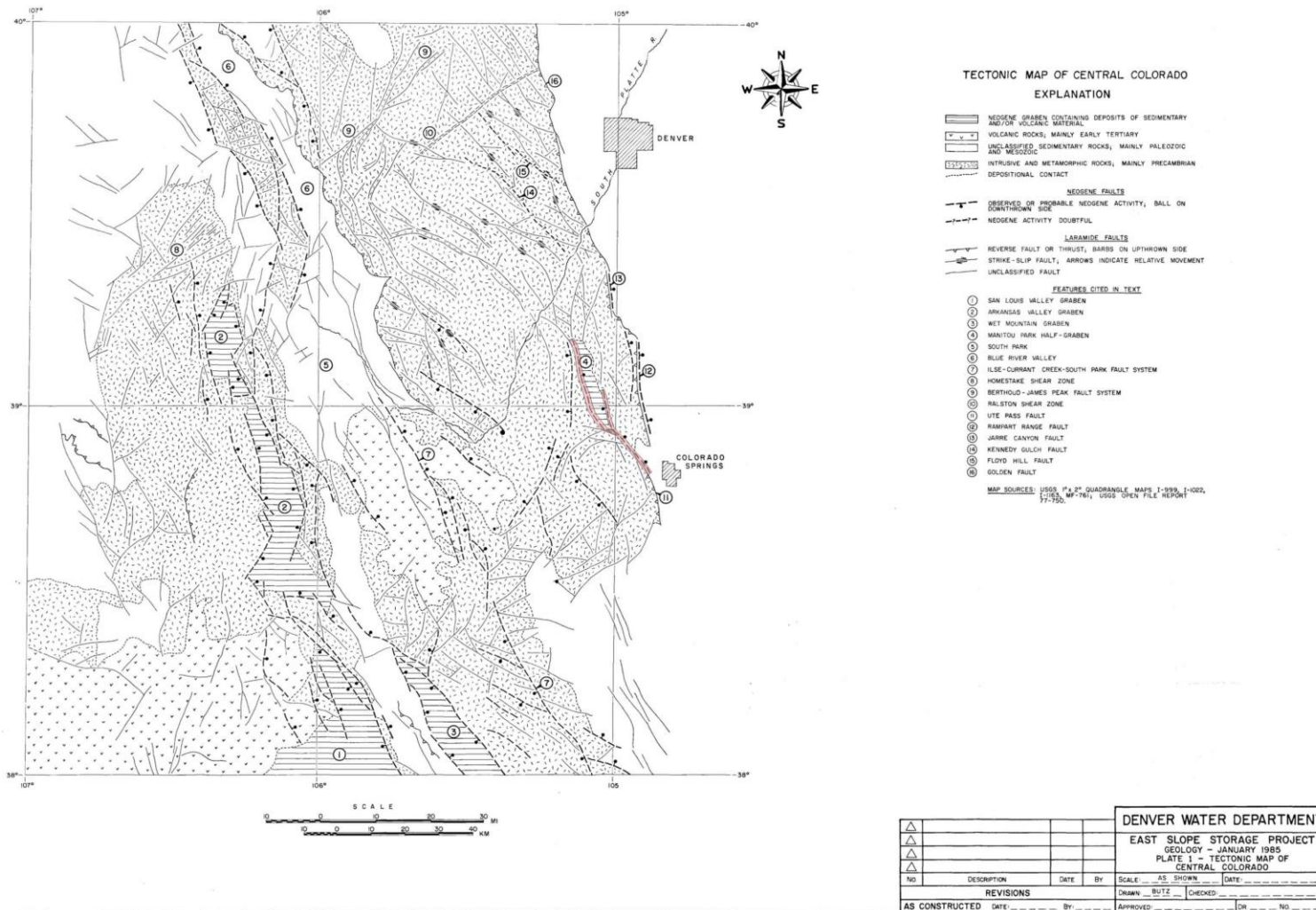
No. 36, Cheyenne Mountain



APPENDIX 2E

Previous Work on the UPF-Text from Geotechnical Advisory Committee, 1985, Part 4

p. 2; "Gravity faulting also affected the southern part of the Front Range, notably in the Manitou Park half-graben [circled 4 on map, at center right margin] along the Ute Pass fault, which had been a reverse fault in Laramide time." The part of UPF reactivated in the Neogene is shaded pink. The map authors show the southern section of the UPF to be a Laramide thrust fault, NOT reactivated in Neogene, in contrast to the interpretation of Kirkham and Rogers (1981).



APPENDIX 2F

Previous Work on the UPF-Text from Geotechnical Advisory Committee, 1986

p. iii; *"The three major fault trends in the Front Range are: 1) a N50°E trend represented by the Homestake shear zone, the Berthoud-James Peak system and the Ralston shear zone; 2) a N50°-60°W trend represented by the Kennedy Gulch, Floyd Hill and related faults; and, 3) a N1U°-25°W trend represented by the Use-Currant Creek-South Park system, and faults along both sides of the Blue River Valley. All three trends were reactivated during the Laramide, the northeast and northwest trends being affected by strike-slip movements mainly in early Laramide, and the north-northwest trend by reverse dip-slip movement in later Laramide time. Neogene activity was restricted largely to normal (gravity) movement along N10°-25°W trending faults. This Neogene gravity faulting has been described in the southern part of the Front Range along the Ute Pass fault (Manitou Park half-graben) and along the Rampart Range and Jarre Canyon faults at the east margin of the Front Range north of Colorado Springs."*

p. vi; *"Ute Pass fault - Evidence for Quaternary movement is described as circumstantial. Most of the fault trace north of Woodland Park is overlain by undisturbed Pleistocene fan deposits and Holocene colluvium and alluvium. No evidence of Quaternary movement was found.*

Oil Creek fault - Tertiary movement on this fault has been postulated on the basis of displaced Miocene-Pliocene gravels in the Divide area. Quaternary movement along the fault is difficult to evaluate because of a paucity of datable soil units. Pleistocene glacial deposits overlie part of the fault trace in the south and are not disturbed by faulting, establishing that the latest movement occurred at least 125,000 years ago. Further north near Westcreek, a splay of the fault is crossed in two locations by well-preserved, multiple terrace deposits that are unbroken.

New evidence of Quaternary faulting was found in an abandoned exploratory mine pit overlying a projected northward extension of the Oil Creek fault. The displaced colluvial deposits are probably at least 600,000 years, based on their geomorphic position. Can we do OSL on these?

The Divide earthquake of 1979 is reported in the literature as associated with the Oil Creek fault. There is no evidence to support this association; epicenters in this region are known to occur randomly with no association with faults."

p. 28; *"d. Ute Pass Fault. Cited evidence for Tertiary and Quaternary movement on the Ute Pass fault is restricted to the southern part of the fault, between Woodland Park and Cheyenne Mountain. Neogene movement, based on reported offset of the Eocene erosion surface and Tertiary gravel deposits, is not disputed in this study. Evidence for Quaternary movement is described as "circumstantial", and has not been established undisputably. The evidence is based on locations near Cheyenne Mountain which were not fully evaluated in the 1984 field study. However, most of the fault trace north of Woodland Park was examined, and no evidence of Quaternary movement was observed. Parts of the fault in these areas are overlain by undisturbed Pleistocene fan deposits and Holocene colluvium and alluvium."*

"e. Oil Creek Fault. Tertiary movement on this fault has been postulated based on displaced Miocene-Pliocene gravels in the Divide area. This offset was not confirmed in the present study, but offset along splays to the east could not be disputed and late Neogene movement should be assumed. Quaternary movement on the fault is difficult to evaluate owing to a paucity of

datable soil units. Pleistocene glacial deposits (Pinedale and Bull Lake moraines) overlie part of the trace in the south and are not disturbed by faulting, establishing the most recent movement in that area as pre-Bull Lake (i.e. at least older than 125,000 years old). However, further north, near Westcreek, a remanent colluvial deposit appears to be offset by the fault, or a splay. This deposit, although not readily dated, is postulated to be early Quaternary in age based mainly on geomorphic evidence obtained in this study. In the same general area, another fault splay is spanned in two locations by well-preserved multiple terrace deposits that are not offset. The terraces are tentatively dated as pre-Bull Lake in age. The Divide earthquake of 1979 has been attributed by some to the Oil Creek fault (see Report P in Third Interim Report).”

APPENDIX 2G

Previous Work on the UPF-*Text from Wm. Lettis & Assoc., 1994;* *Pueblo Dam study for US Bureau of Reclamation*

“3.1.8 Ute Pass Fault

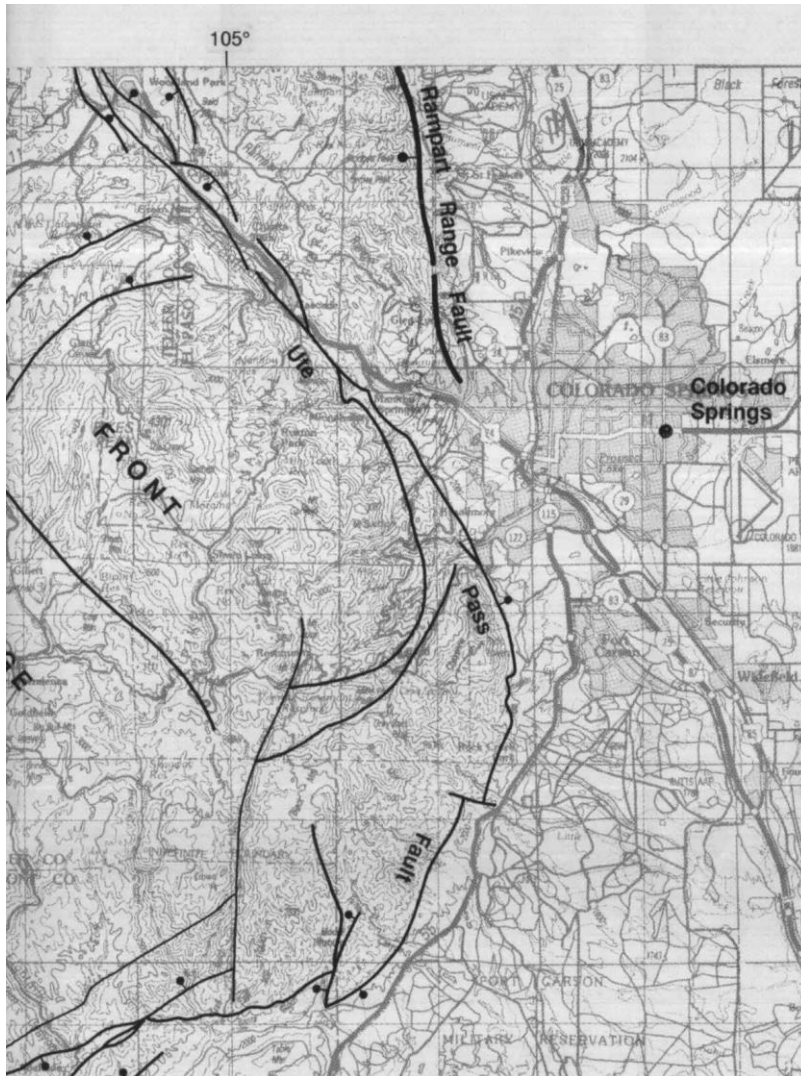
The Ute Pass fault is a 91-km-long, north-south- to northwest-southeast-striking fault in the eastern Front Range between the cities of Denver and Colorado Springs (Plate 2). The Ute Pass fault displaces Tertiary gravel deposits and a late Eocene erosion surface that is extensively preserved throughout the eastern Front Range (Scott, 1975; Denver Water Department [DWD], 1986). Surface investigations reveal that the central and northern parts of the fault are overlain by unfaulted late Pleistocene and Holocene deposits (DWD, 1986), thus providing evidence of no late Quaternary activity. The southern part of the Ute Pass fault consists of: (1) a 32-km-long, approximately north-south-striking segment that lies along the bedrock piedmont of the Front Range south of Colorado Springs; and (2) an approximately 25-km-long northwest-striking segment that turns away from the mountain front near Colorado Springs and strikes into the interior of the mountains where it joins the main mapped trace of the fault (Plate 1). The closest approach of the Ute Pass fault (southern end) to Pueblo Dam is 41 km. We performed air photo analysis, aerial reconnaissance, and limited field investigations to assess late Quaternary activity on the southern part of the Ute Pass fault.

The north-south-striking segment of the Ute Pass fault south of Colorado Springs coincides with the mapped trace of a west-dipping Laramide thrust fault (Trimble and Machette, 1979). Airphoto analysis shows that this trace of the fault is marked by discontinuous tonal and vegetation lineaments, saddles across ridges, and locally by a prominent east-facing bedrock scarp. Streams draining east from the Front Range that cross the fault are flanked by late Pleistocene and Holocene terraces. No deformation of late Pleistocene or Holocene terraces was observed during airphoto analysis and aerial reconnaissance. Field investigations conducted near Rock Creek (Plate 2) confirm the presence of an abrupt east-facing bedrock scarp along the mapped fault trace, and small saddles along ridges that are crossed by the fault. Stream bank exposures show, however, that the top of the bedrock can be traced continuously across the mapped fault trace and is observed to underlie late Quaternary fluvial deposits at shallow depth east of the fault. We conclude that the bedrock scarp is a result of differential erosion between the bedrock and Quaternary fluvial deposits. The small ridge-crest saddles probably result from headward erosion of small intermittent streams incised along the contact between the bedrock and Quaternary fluvial deposits. We observed no scarps or anomalous geomorphic features in the fluvial deposits east of the bedrock scarp.

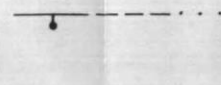
We also conducted field reconnaissance along the northwest-striking part of the Ute Pass fault west and north of Colorado Springs. The fault trace is marked by a prominent southwest-facing escarpment. Numerous late Pleistocene and Holocene alluvial fans cross the fault and do not exhibit scarps or other anomalous topographic breaks. In most places, the fault is draped with colluvium. The colluvium forms unbroken, graded slopes across the escarpment. Based on the evidence for no faulting of the late Quaternary fans, terraces and colluvial slopes, we conclude that the southwest-facing escarpment is a faultline scarp.

Based on these observations, and based on evidence for no middle Pleistocene or younger activity on similar faults in the interior Front Range such as the Kennedy Gulch and Floyd Hill faults (DWD, 1986), we conclude that the southern part of the Ute Pass fault is

not active.”



LEGEND

-  Active or potentially active faults; ball on downthrown block (dashed where approximately located, dotted where concealed)
-  Tertiary faults; ball on downthrown block (dashed where approximately located, dotted where concealed)
-  Probable Laramide-Age faults, age of last movement older than late Pleistocene (dashed where concealed)
- A** Detailed study site area described in text